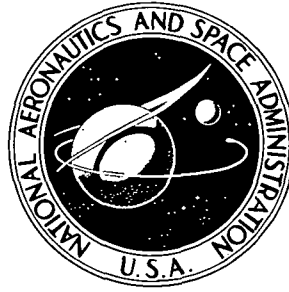


**NASA CONTRACTOR  
REPORT**



**NASA CR-2924**

**NASA CR-2924**

**COMPUTATIONAL TECHNIQUES  
FOR SOLAR WIND FLOWS  
PAST TERRESTRIAL PLANETS -  
THEORY AND COMPUTER PROGRAMS**

*Stephen S. Stahara, Denny S. Chaussee,  
Barbara C. Trudinger, and John R. Spreiter*

*Prepared by*  
**NIELSEN ENGINEERING & RESEARCH, INC.**  
Mountain View, Calif. 94043

*for*

**NATIONAL AERONAUTICS AND SPACE ADMINISTRATION • WASHINGTON, D. C. • NOVEMBER 1977**

1. Report No. NASA CR- 2924		2. Government Accession No.		3. Recipient's Catalog No.	
4. Title and Subtitle Computational Techniques for Solar Wind Flows Past Terrestrial Planets - Theory and Computer Programs				5. Report Date November 1977	
				6. Performing Organization Code	
7. Author(s) Stephen S. Stahara, Denny S. Chaussee, Barbara C. Trudinger, and John R. Spreiter				8. Performing Organization Report No. NEAR TR 140	
				10. Work Unit No.	
9. Performing Organization Name and Address Nielsen Engineering & Research, Inc. 510 Clyde Avenue Mountain View, California 94043				11. Contract or Grant No. NASW-2945	
				13. Type of Report and Period Covered Contractor Report June 1976-July 1977	
12. Sponsoring Agency Name and Address National Aeronautics and Space Administration Washington, D.C. 20546				14. Sponsoring Agency Code	
				15. Supplementary Notes	
16. Abstract <p>Theoretical analysis and the development of user-oriented computer programs were carried out for the purpose of developing computational techniques for predicting the interaction of the solar wind with terrestrial planets. The procedures are based on a single-fluid, steady, dissipationless, magnetohydrodynamic model and are appropriate for the calculation of axisymmetric, supersonic, super-Alfvénic solar wind flow past both magnetic and nonmagnetic planets. The actual calculations are implemented by an assemblage of computer codes organized into one program. These include finite-difference codes which determine the gas-dynamic solution, together with a variety of special-purpose output codes for determining and automatically plotting both flow field and magnetic field results.</p> <p>Theoretical results obtained using these procedures are reported for a variety of solar wind conditions and different obstacle shapes. Comparisons are made with previous results, and new results are presented for a number of solar wind flows. The computational programs developed under this work have been documented and are presented in a general user's manual included as part of this report.</p>					
17. Key Words (Suggested by Author(s)) Solar Wind Flows Finite-Difference Computations Steady Flow Magnetosphere Ionosphere			18. Distribution Statement  UNCLASSIFIED-UNLIMITED  Cat. 92		
19. Security Classif. (of this report) UNCLASSIFIED		20. Security Classif. (of this page) UNCLASSIFIED		21. No. of Pages 133	22. Price* \$6.00

## TABLE OF CONTENTS

<u>Section</u>	<u>Page No.</u>
LIST OF ILLUSTRATIONS	iv
LIST OF TABLES	v
SUMMARY	1
INTRODUCTION	1
LIST OF SYMBOLS	3
ANALYSIS	7
General Considerations	7
Mathematical Representation of Solar Wind-Magneto/Ionosphere Interaction	8
Magnetic Planet - Determination of the Magnetosphere Boundary	11
Nonmagnetic Planet - Determination of the Ionosphere Boundary	16
Calculation of the Gasdynamic Flow Properties	19
Calculation of the Magnetic Field	26
RESULTS AND DISCUSSION	29
CONCLUDING REMARKS	32
APPENDIX A - COMPUTER PROGRAM USER'S MANUAL	34
APPENDIX B - LISTING OF COMPUTER PROGRAM	73
REFERENCES	107
TABLE 1	110
FIGURES 1 THROUGH 15	113

## LIST OF ILLUSTRATIONS

### Figure

- 1 Comparison of the equatorial and principal meridian traces of the magnetosphere boundary as provided by the simplified theory of equation 16.
- 2 Illustration of ionopause shapes for various values of the ionosphere scale height to shock standoff distance ratio  $H/R_0$ .
- 3 Comparison of former and present computational procedures for determining the gasdynamic flow properties of solar wind-magneto/ionopause interactions.
- 4 Illustration of the components of the three-dimensional magnetic field.
- 5 Comparison of flow properties predicted by the present implicit method with other techniques and experiment for supersonic flow past a sphere;  $M_\infty = 4.926$ ,  $\gamma = 1.4$ .
- 6 Comparison of implicit and inverse methods for shock shape and sonic line location, and density distribution along bow shock and magnetosphere boundary for  $M_\infty = 8$ ,  $\gamma = 5/3$  flow past the rotated equatorial trace of the magnetopause.
- 7 Bow wave and sonic line locations for various supersonic flows past the rotated equatorial trace of the magnetopause with  $\gamma = 5/3$ .
- 8 Bow shock location for solar wind flow with  $M_\infty = 8$ ,  $\gamma = 5/3$  past various ionopause shapes.
- 9 Bow shock and embedded shock locations for solar wind flow with  $M_\infty = 5$ ,  $\gamma = 5/3$  past the rotated principal meridian of the magnetosphere.
- 10 Magnetopause pressure coefficients for the principal meridian magnetopause shapes shown in figure 9.
- 11 Variation of shock stand-off distance with oncoming Mach number and ratio of specific heats for various magneto/ionopause traces as determined by the present implicit procedure.
- 12 Shock shapes for various supersonic flows past the rotated equatorial trace of the magnetopause; combined near (blunt body) and far (marching) solutions.
- 13 Shock shapes for  $M_\infty = 8$ ,  $\gamma = 5/3$  flow past an ionopause shape with  $H/R_0 = 0.1$ ; combined near (blunt body) and far (marching) field solutions.

LIST OF ILLUSTRATIONS (CONTINUED)

Figure

- 14 Streamline, density, and velocity maps for  $M_\infty = 8.0$ ,  $\gamma = 5/3$  flow past the rotated equatorial trace of the magnetopause; combined blunt body and marching flow field.
- 15 Contours and field line locations of the in-plane magnetic field components  $(B/B_\infty)_\perp$  and  $(B/B_\infty)_\parallel$  for  $M_\infty = 8$  and  $\gamma = 5/3$  flow past the rotated equatorial trace of the magnetopause.
- A.1 Card input for sample case.
- A.2 Abbreviated output for sample case.
- A.3 Plot output for sample case.

LIST OF TABLES

Table

- 1 Ordinates of various magneto/ionopause shapes.

COMPUTATIONAL TECHNIQUES FOR SOLAR  
WIND FLOWS PAST TERRESTRIAL PLANETS  
- THEORY AND COMPUTER PROGRAMS

by Stephen S. Stahara, Denny S. Chaussee,  
Barbara C. Trudinger, and  
John R. Spreiter\*  
Nielsen Engineering & Research, Inc.

SUMMARY

Theoretical analysis and the development of user-oriented computer programs were carried out for the purpose of developing computational techniques for predicting the interaction of the solar wind with terrestrial planets. The procedures are based on a single-fluid, steady, dissipationless, magnetohydrodynamic model and are appropriate for the calculation of axisymmetric, supersonic, super-Alfvénic solar wind flow past both magnetic and nonmagnetic planets. The actual calculations are implemented by an assemblage of computer codes organized into one program. These include finite-difference codes which determine the gasdynamic solution, together with a variety of special-purpose output codes for determining and automatically plotting both flow field and magnetic field results.

Theoretical results obtained using these procedures are reported for a variety of solar wind conditions and different obstacle shapes. Comparisons are made with previous results, and new results are presented for a number of solar wind flows. The computational programs developed under this work have been documented and are presented in a general user's manual included as part of this report.

INTRODUCTION

The gasdynamic and magnetohydrodynamic calculations of solar wind flow around magnetic and nonmagnetic planets that Spreiter et al. (refs. 1-8) carried out some years ago have been and continue to be widely used in the interpretation of data measured in space around the Earth and other planets. The objective at the time those calculations were made, was to

---

\*Professor, Department of Applied Mechanics, Stanford University.  
Consultant, Nielsen Engineering & Research, Inc.

provide some theoretical results based on a fluid rather than particle description of the flow that might be compared with measurements in space to determine the applicability of such a description. During the intervening years, the usefulness and accuracy of those results have become so well established that they are currently being used, for instance, as one of the ways in which the magnetic field of a planet such as Mercury or Mars is estimated from measurements of fly-by or orbiting spacecraft.

In such applications, the previous calculations leave much to be desired. They have been carried out for only a limited set of conditions such as obstacle shape, oncoming Mach number, angle between free-stream flow and magnetic vectors, etc., and are presented in archival publications only in the form of plots from which results for other conditions must be determined by scaling and interpolation. The usefulness of the present theoretical model, therefore, would be considerably enhanced if similar but more detailed results for the specific conditions measured by a spacecraft would be provided by the application of a documented, user-oriented, economical computer code.

That objective has been successfully accomplished in the work reported here. Based upon the identical theoretical model employed previously (refs. 1-8), and discussed in more detail below, a new more versatile means of solution far superior in efficiency and generality to the former method is now available. Current advances in computational methods have been incorporated in these programs and, in fact, an entirely new blunt body code based on a recently published algorithm was developed to determine the flow field in the region surrounding the nose of the obstacle. The new methods confirm previous results and are readily applicable to additional cases involving different geometries and flow conditions. The entire procedure is fully automated and provides detailed flow field and magnetic field properties in a convenient output format. An automatic plotting capability for generating report-quality plots is also included.

LIST OF SYMBOLS

a	speed of sound, $(\gamma p/\rho)^{1/2}$
$a_e$	planetary radius of earth, $6.37 \times 10^8$ cm
A	Alfvén speed, $(B^2/4\pi\rho)^{1/2}$
$\bar{A}$	Jacobian matrix associated with IMP code, equal to $\partial \hat{E}/\partial \hat{U}$
$\vec{B}$	magnetic field vector
$B_{eq}$	strength of Earth's magnetic field at geomagnetic equator, equal to 0.312 gauss
$\bar{B}$	Jacobian matrix associated with IMP code, equal to $\partial \hat{F}/\partial \hat{U}$
$C_p$	specific heat at constant pressure
$C_v$	specific heat at constant volume
D	geometric distance to magnetosphere nose, equal to $a_e (f^2 B_{eq}^2 / 2\pi K \rho_\infty V_\infty)^{1/6}$
e	internal energy, eq. (5)
E	column matrix defined by eq. (29)
$\hat{E}$	column matrix associated with IMP code, equal to $(\xi_T U + \xi_X E + \xi_R F)/J$
f	constant associated with tangential component of Earth's magnetic dipole field at magnetopause location
F	column matrix defined by eq. (29)
$\hat{F}$	column matrix associated with IMP code, equal to $(\eta_T U + \eta_X E + \eta_R F)/J$
$\vec{F}$	column matrix defined by eq. (34)
g	acceleration due to gravity
G	column matrix defined by eq. (29)
$\vec{G}$	column matrix defined by eq. (34)
h	enthalpy, eq. (6)
H	local scale height of atmosphere, $\bar{R}T/\mu g$
$H_t$	total enthalpy, eq. (35)
$\vec{H}$	column matrix defined by eq. (34)
J	Jacobian matrix, eq. (30)



LIST OF SYMBOLS (Continued)

K	constant defined by eq. (14)
$\Delta \ell$	vector length of elemental magnetic flux tube
M	local Mach number, $ \tilde{V} /a$
$M_A$	local Alfvén Mach number, $ \tilde{V} /A$
p	pressure
q	magnitude of velocity vector, eq. (36)
Q	dummy parameter
r	spherical radial distance
R	cylindrical radial distance
$\bar{R}$	gas constant, $8.315 \times 10^7$ ergs/gm $^\circ$ K
$R_i$	spherical radius of ionopause, eq. (25)
$R_m$	spherical radius of magnetopause, eqs. (16-18)
$R_o$	spherical distance from center of planet to ionopause nose
S	entropy
$\Delta S$	incremental distance along streamline
T	time
(u,v,w)	velocity components associated with the (X,R, $\omega$ ) coordinate directions, respectively
U	column matrix defined by eq. (29)
$\hat{U}$	column matrix associated with IMP code, equal to U/J
$\tilde{U}$	column matrix defined by eq. (34)
$\tilde{V}$	velocity vector
x	axial distance from center of planet measured positive upstream
X	axial distance from center of planet measured positive downstream
$\beta$	spherical polar angle, measured with respect to planet center, from subsolar point with respect to undisturbed solar wind direction; varies from 0 in upstream direction to $\pi$ in downstream direction; eq. (25)
$\gamma$	ratio of specific heats

LIST OF SYMBOLS (Continued)

$\delta_s$	local angle of bow shock wave
$(\delta_\xi, \delta_\eta)$	second-order difference operators in $(\xi, \eta)$ direction
$\eta$	transformation variable; eqs. (27), (37)
$\theta$	polar angle measured with respect to north geomagnetic pole, eq. (15)
$\Lambda$	quantity defined by eq. (26)
$\mu$	nondimensionalized mean molecular mass, equal to 1/2 for ionized atomic hydrogen
$\xi$	transformation variable, eqs. (27), (37)
$\rho$	density
$\tau$	transformed time, eq. (27)
$\phi$	geomagnetic longitude, eq. (16)
$\psi$	angle between outward normal to magneto/ionosphere boundary and oncoming undisturbed solar wind, eq. (12)
$\omega$	azimuthal angle in axis-normal plane, eq. (33)

Subscripts

n	normal direction
P	arbitrary point on streamline
R	reference quantity
t	tangential direction
o	reference quantity at subsolar point
1	conditions upstream of a discontinuity
2	conditions downstream of a discontinuity
$\infty$	upstream undisturbed quantity
(" , $\perp$ , n)	parallel, perpendicular, and normal magnetic field components as defined in eq. (42)

**Page  
Intentionally  
Left Blank**

## ANALYSIS

### General Considerations

An overall description of solar wind flow past terrestrial planets, including an account of the principal features of the interplanetary solar wind and a description of the physical basis of the continuum fluid model are provided in references 3 and 6. Although details of those accounts won't be repeated here, several specific points relevant to the present work will be reviewed.

The fundamental assumption underlying the theoretical analysis of large-scale features of the interaction of the solar wind with terrestrial planets is that the average bulk properties of the flow can be described adequately by the continuum equations of magnetohydrodynamics for a single-component, perfect, dissipationless (perfect electrically conducting, inviscid, nonheat-conducting) gas. Theoretical justification of this point has not yet been established, and proof remains essentially qualitative at present. The primary justification for use of the continuum fluid model is the outstanding agreement of the qualitative results predicted on this basis with those actually measured in space. It appears that the continuum model is capable of accounting both for many of the details as well as the broad features of the observations.

The primary emphasis on development of the continuum model has been on steady flow past the Earth (refs. 3, 4), a planet with a strong magnetic field. Initial applications to nonmagnetic planets have also been made (ref. 5). These particular applications are the ones toward which this study is directed.

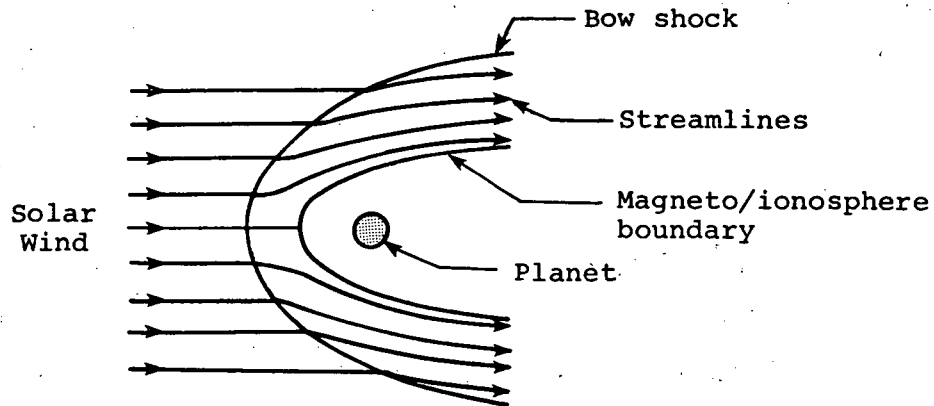
The following subsection provides the mathematical basis of the interaction of the solar wind with planetary magneto/ionospheres. The governing differential equations as well as relations for discontinuities present in the flow are discussed. The next two subsections provide the determination of the magnetosphere and ionosphere boundary shapes. The following two subsections discuss the calculation of the gasdynamic and magnetic field properties.

## Mathematical Representation of Solar Wind- Magneto/Ionosphere Interaction

The differential equations governing the motion of the solar wind are the magnetohydrodynamic equations for steady flow of a dissipationless perfect gas and can be written as follows

$$\left. \begin{aligned}
 \nabla \cdot \rho \vec{v} &= 0 \\
 \rho (\vec{v} \cdot \nabla) \vec{v} + \nabla p &= -(1/4\pi) \vec{B} \times \text{Curl } \vec{B} \\
 \text{Curl} (\vec{B} \times \vec{v}) &= 0 \\
 \text{div } \vec{B} &= 0 \\
 (\vec{v} \cdot \nabla) S &= 0 \\
 S - S_0 &= C_v \ln \frac{p/p_0}{(\rho/\rho_0)^\gamma}
 \end{aligned} \right\} \quad (1)$$

and apply in the region exterior to the magneto/ionosphere boundary, as shown in the sketch below.



In these equations,  $\rho$ ,  $p$ ,  $S$ , and  $\vec{v}$  refer to the density, pressure, entropy, and velocity of the gas,  $\vec{B}$  denotes the magnetic field, and  $\gamma = C_p/C_v$  is the ratio of specific heats, equal to 5/3 for a monatomic gas. The temperature  $T$  is related to the pressure and density by the equation of state for a perfect gas

$$p = \rho \bar{R} T / \mu \quad (2)$$

in which  $\bar{R} = (C_p - C_v)\mu = 8.315 \times 10^7$  ergs/gm $^\circ$ K is the universal gas constant, and  $\mu$  is the mean molecular mass nondimensionalized so that  $\mu = 16$  for atomic oxygen. For fully ionized hydrogen,  $\mu$  is thus 1/2. The magnetic field  $\vec{B}$  is expressed in terms of gaussian units.

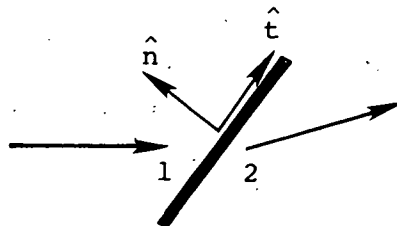
We note that it is fully equivalent and convenient for some purposes to replace the entropy equation  $(\vec{V} \cdot \vec{\nabla})S = 0$  in equation (1) by the following energy equation:

$$\text{div}[\rho \vec{V} (\frac{1}{2} V^2 + h) + \vec{V} B^2 / 4\pi - (\vec{B} \cdot \vec{V}) \vec{B} / 4\pi] = 0 \quad (3)$$

Because of the omission of dissipative terms in equation (1), surfaces of discontinuity, such as the bow shock and the magneto/ionosphere boundary indicated in the sketch above, may develop in the flow. Across these surfaces, continuous solutions of the dissipationless differential equations cease to exist. The flow is no longer governed solely by the differential equations (1), but must be supplemented by additional considerations. Mass, momentum, magnetic flux, and energy must be conserved across these surfaces, and these conditions lead to the following relations which relate quantities on the two sides of any such discontinuity:

$$\left. \begin{aligned} [\rho V_n] &= 0 \\ [\rho V_n V_t + (p + B^2/8\pi) \hat{n} - B_n B_t / 4\pi] &= 0 \\ [B_n V_t - B_t V_n] &= 0 \\ [B_n] &= 0 \\ [\rho V_n (h + V^2/2) + V_n B^2 / 4\pi - (\vec{B} \cdot \vec{V}) B_n / 4\pi] &= 0 \end{aligned} \right\} \quad (4)$$

Here,  $(\hat{n}, \hat{t})$  denote unit vectors normal and tangential to the discontinuity surface, as sketched below,



The basis for important simplifying approximations to the governing tangential discontinuity conditions

$$\begin{aligned} v_n = B_n = [p + B^2/8\pi] = 0 \\ [v_t] \neq 0; [B_t] \neq 0; [\rho] \neq 0 \end{aligned} \quad (9)$$

which apply at the Earth's magnetosphere boundary are that the gas pressure  $p$  is much less than the magnetic pressure  $B^2/8\pi$  in the confined region interior to the magnetopause, and that  $p$  is much greater than  $B^2/8\pi$  in the exterior flow region around the forward part of the magnetopause. Consequently, the boundary condition to be satisfied by the exterior flow at the magnetopause can be satisfactorily approximated by the limiting case of the tangential discontinuity conditions in equation (9) in which there is a vacuum ( $p = \rho = 0$ ) on one side, and no magnetic field on the other. Thus, the condition  $[p + B^2/8\pi] = 0$  becomes

$$(B^2/8\pi)_{\text{mag}} = (p)_{\text{flow}} \quad (10)$$

while the equations governing the magnetic field interior to the magnetopause are

$$\text{div } \vec{B} = 0, \text{ Curl } \vec{B} = 0 \quad (11)$$

Furthermore, it has been shown (refs. 3, 6) that the gas pressure of the flow on the forward portion of the magnetosphere boundary -  $(p)_{\text{flow}}$  in equation (10) - can be approximated adequately by the Newtonian formula

$$p = p_{\text{st}} \cos^2 \psi \quad (12)$$

Here,  $\psi$  is the angle between the outward normal to the magnetosphere boundary and the flow direction of the oncoming undisturbed solar wind, and  $p_{\text{st}}$  is the stagnation or ram pressure exerted on the nose of the magnetosphere and is given by

$$p_{\text{st}} = K \rho_{\infty} V_{\infty}^2 \quad (13)$$

In this relation,  $K$  is a constant usually taken as one, but whose actual value is

$$K = \frac{1}{\gamma} \left[ \frac{(\gamma + 1)(\gamma - 1)}{\gamma - (\gamma - 1)/2M_\infty^2} \right]^{\frac{1}{\gamma - 1}} \quad (14)$$

For the high Mach number flows typical of solar wind conditions,  $K$  approaches 0.844 for  $\gamma = 2$  and 0.881 for  $\gamma = 5/3$ . The important implication associated with the introduction of the Newtonian approximation is that the calculation of the shape of the magnetosphere boundary decouples from the calculation of the external flow.

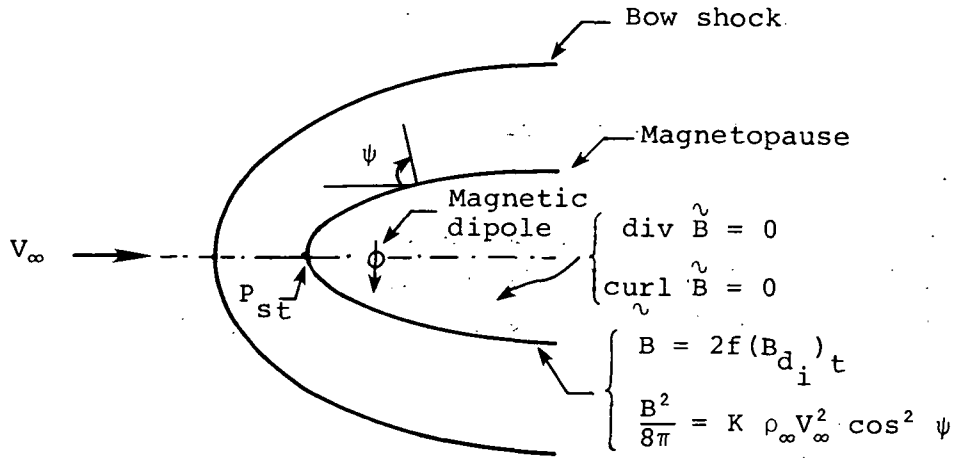
Implementation of the above analysis requires a representation of the Earth's magnetic field. This is provided with sufficient accuracy for the present application by a magnetic dipole located at the center of the Earth and given by

$$\vec{B} = -B_{eq} (a_e/r)^3 (\sin \theta \hat{e}_\theta + 2 \cos \theta \hat{e}_r) \quad (15)$$

where  $B_{eq} = 0.312$  gauss is the strength of the field at the geomagnetic equator,  $a_e = 6.37 \times 10^8$  cm is the radius of the Earth,  $r$  is the geocentric distance, and  $\theta$  is the polar angle measured with respect to the north geomagnetic pole which is at  $78.6^\circ$  north latitude and  $70.1^\circ$  west longitude. The problem for determining the magnetopause and the distortion of the confined geomagnetic field is then reduced to finding a solution of equations (11) which has the dipole singularity equation (15) at the origin, and which satisfies the tangential discontinuity conditions  $B_n = 0$  and  $B^2/8\pi = K\rho_\infty V_\infty^2 \cos^2 \psi$  at the unknown location of the magnetopause. This problem is identical to the classical steady-state Chapman-Ferraro problem (ref. 10) specified over four decades ago, and based on particle rather than continuum concepts. Even at this stage, however, the problem still remains sufficiently complex that only a few numerical solutions have been carried out (refs. 11-13) at the present time. An early approximation which has proven quite successful in providing accurate magnetopause shapes (refs. 9, 12, 14) is to replace the  $B_n = 0$  condition with the condition that the magnetic-field intensity at the magnetosphere boundary is equal to  $2f$  times the tangential component of the Earth's dipole field, where  $f$  is a constant usually taken as unity (refs. 15-17).



The final mathematical statement for the free-boundary problem for the shape of the magnetosphere boundary, then, is summarized in the sketch below:



This formulation leads to the following partial differential equation for the geocentric distance  $r$  to the magnetopause for the case in which the dipole axis is perpendicular to the solar-wind flow (ref. 18)

$$\left[ \frac{1 + 3 \cos^2 \theta}{R_m^6} \left( \frac{1}{R_m \sin \theta} \frac{\partial R_m}{\partial \phi} \right)^2 + \frac{1}{R_m^6} \left( \sin \theta + \frac{2 \cos \theta}{R} \frac{\partial R_m}{\partial \phi} \right)^2 \right] = \left[ \sin \phi \sin \theta - \frac{\sin \phi \cos \theta}{R_m} \frac{\partial R_m}{\partial \theta} - \frac{\cos \phi}{R_m \sin \theta} \frac{\partial R_m}{\partial \phi} \right]^2 \quad (16)$$

where  $R_m = r/D$ ,  $D = a_e (f^2 B_{eq}^2 / 2\pi K \rho_\infty V_\infty^2)^{1/6}$  is the geocentric distance to the magnetosphere nose,  $\phi$  is the geomagnetic longitude measured with respect to a line through the origin that is normal to both the dipole axis and the free-stream direction, and is equal to  $\pi/2$  when directed in the upstream direction, and  $3\pi/2$  when directed downstream.

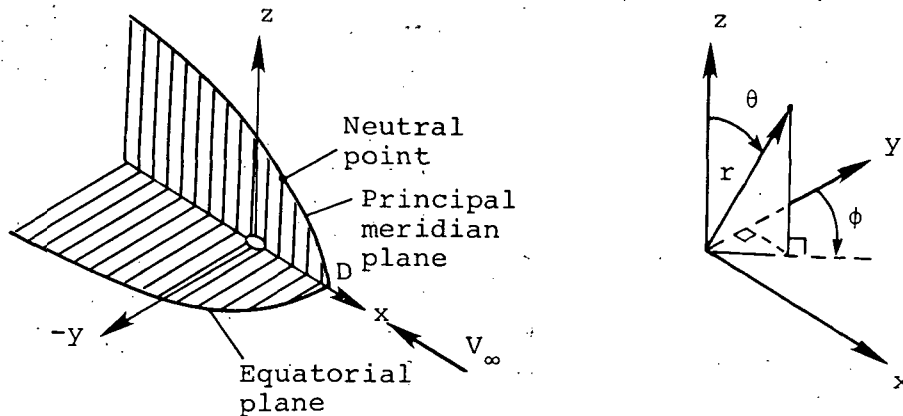
A considerable simplification occurs if attention is confined to either the geomagnetic equatorial plane or the principal meridian plane defined by the dipole axis and the direction of the incident solar wind. These equations are; in the equatorial plane ( $\theta = \pi/2$ ,  $\partial R_m / \partial \theta = 0$ )

$$\frac{dR_m}{d\phi} = R_m \left( \frac{R_m^6 \sin \phi \cos \phi + \sqrt{R_m^6 - 1}}{R_m^6 \cos^2 \phi - 1} \right) \quad \pi/2 \leq \phi \leq \frac{3\pi}{2} \quad (17)$$

and in the principal meridian plane ( $\phi = \pm \pi/2$ ,  $\frac{\partial R}{\partial \phi} = 0$ )

$$\frac{dR_m}{d\theta} = (R_m \tan \theta) \frac{R_m^3 \mp 1}{R_m^3 \pm 2} \quad -\pi/2 \leq \theta \leq \frac{\pi}{2} \quad (18)$$

A sketch of the traces of the magnetosphere boundary in the equatorial and principal meridian planes is provided below together with the spherical ( $r, \theta, \phi$ ) coordinate system. We note in particular that the



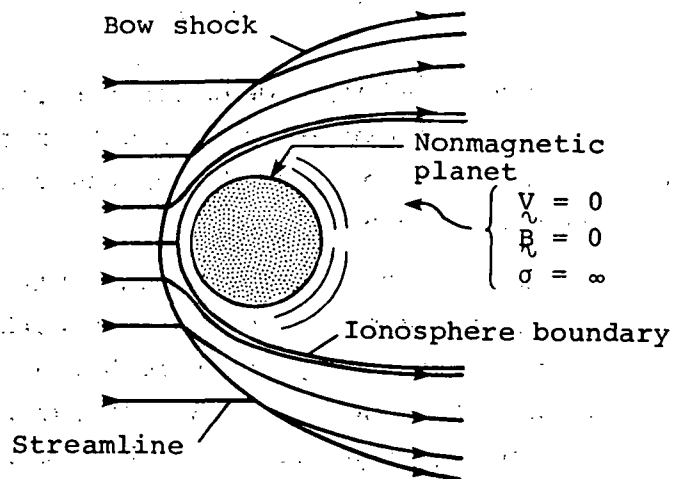
shape of the equatorial trace is a smooth curve, while that of the principal meridian contains a pronounced dent at the location of the neutral point where the magnetic field vanishes in the ideal theory. In all of the reported work to date (refs. 1-4, 6, 8) concerning flow fields past the magnetosphere, the magnetopause has been approximated by an axisymmetric shape obtained by rotating the equatorial trace of the boundary about the longitudinal axis. That this provides a very good approximation to the actual three-dimensional shape is shown in figure 1 which displays in more detail the comparison of the equatorial and principal meridian traces of the magnetopause as calculated by equations (17) and (18), respectively. Also shown on the principal meridian trace is a dashed line which forms a tangent surface across the cusped neutral point region, and which represents the free-streamline surface which will

most likely appear in nature (ref: 19). We note that all three of these shapes are quite close to one another so that the rotated equatorial trace provides a satisfactory approximation to the three-dimensional shape. Furthermore; it has been shown (ref. 3, 13) that higher-order approximations to the Chapman-Ferraro problem for the magnetosphere shape are in reasonable agreement with the approximate shape given by the solution to equation (16).

Consequently, the boundary shape of the magnetosphere for which the majority of results are presented here is the rotated equatorial trace given by equation (17). That shape has been incorporated in the associated computer codes developed herein as the default shape for magnetosphere calculations. Tabulated ordinates ( $Y_m/D$  - vs.  $-x/D$ ) for the equatorial trace are provided in Table 1 where  $Y_m$  is the cylindrical radial coordinate of the profile.

#### Nonmagnetic Planet - Determination of the Ionosphere Boundary

The determination of the ionosphere boundary initiates from the assumptions that the ionosphere, or at least the outer part of it that participates in the interaction with the solar wind, is idealized as a spherically symmetric and hydrostatically supported plasma having infinite electrical conductivity, effectively bound to the planet and incapable of mixing with the solar wind, as indicated in the sketch below:



This interior plasma is separated from the flowing solar plasma by a tangential discontinuity across which the same relations, given previously by equations (9) for the analogous problem for a magnetic planet, must hold. The assumption of hydrostatic support implies a quiescent ionosphere in which the bulk motions of the gas with respect to the planet are sufficiently small ( $V_{\infty} = 0$ ) that equilibrium exists between the pressure gradient and gravity, viz.

$$\frac{dp}{dr} = -\rho g \quad (19)$$

where  $p$  and  $\rho$  are the gas pressure and density,  $r$  is the radial distance measured from the center of the planet, and  $g$  is the acceleration due to gravity. The variation of  $g$  is inversely proportional to  $r^2$ , so that  $g = g_s (r_s/r)^2$  where the subscript  $s$  denotes values at the surface of the planet. Since the density  $\rho$  is related to the pressure according to the perfect gas law equation (2), equation (19) can be integrated to yield

$$p = p_R \exp\left(-\int_{R_R}^r \frac{dr}{H}\right) \quad (20)$$

where  $p_R$  is the pressure at some reference radius  $R_R$  and  $H$  is the local scale height of the atmosphere given by  $H = RT/g$ . If  $H$  is regarded as constant; that is, if variations of  $g$  and  $T$  with  $r$  are neglected, equation (20) can be integrated directly to yield

$$p = p_R \exp\left(-\frac{r - R_R}{H}\right) \quad (21)$$

In view of uncertainties associated with measurements of the atmospheric properties of Venus and Mars, the variation of  $p$  with  $r$  as given by equation (21) was adopted in previous solar wind/ionosphere applications (ref. 5) and has also been used herein.

In the present application, it is also evident that the gas pressure  $p$  is much larger than the magnetic pressure  $B^2/8\pi$  on both sides of the ionopause. Therefore, the discontinuity pressure balance relation  $[p + B^2/8\pi] = 0$  of equation (9) reduces to a simple equality between the ionospheric pressure given by equation (21) and the static pressure of the flowing solar plasma adjacent to the ionopause. Introducing as in the magnetosphere application the Newtonian approximation equation (12) for

the static pressure of the flowing plasma on the exterior boundary of the ionosphere, we arrive at the following equation for the pressure balance at the ionopause  $R_i$ :

$$p_{st} \cos^2 \psi = K \rho_{\infty} V_{\infty}^2 \cos^2 \psi = p_R \exp \left( - \frac{R_i - R_R}{H} \right) \quad (22)$$

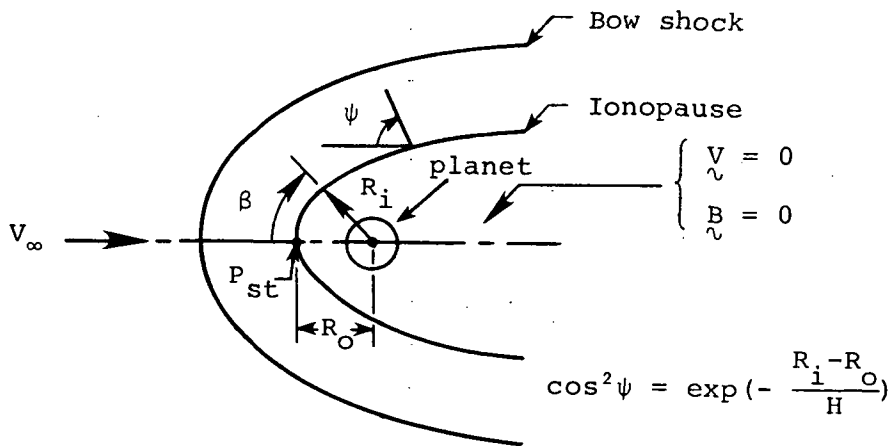
It is convenient to choose as the reference radius and location the stagnation point on the ionopause; that is,  $R_R = R_O$  where  $R_O$  is the distance from the center of the planet to the nose of the ionopause. This implies that

$$p_R = p_O = K \rho_{\infty} V_{\infty}^2 \quad (23)$$

and that at all points along the ionosphere boundary

$$\cos^2 \psi = \exp \left( - \frac{R_i - R_O}{H} \right) \quad (24)$$

The final mathematical statement of the free-boundary problem for determining the shape of the ionosphere boundary then is summarized in the sketch below:



By relating the local angle  $\psi$  to the slope of the ionopause, the following ordinary differential equation results for the ordinates of the ionosphere boundary

$$\frac{dR_i}{d\beta} = R_i \left[ \frac{\sin 2\beta - 2\sqrt{\Lambda - \Lambda^2}}{2(\Lambda - \sin^2 \beta)} \right] \quad 0 \leq \beta \leq \pi \quad (25)$$

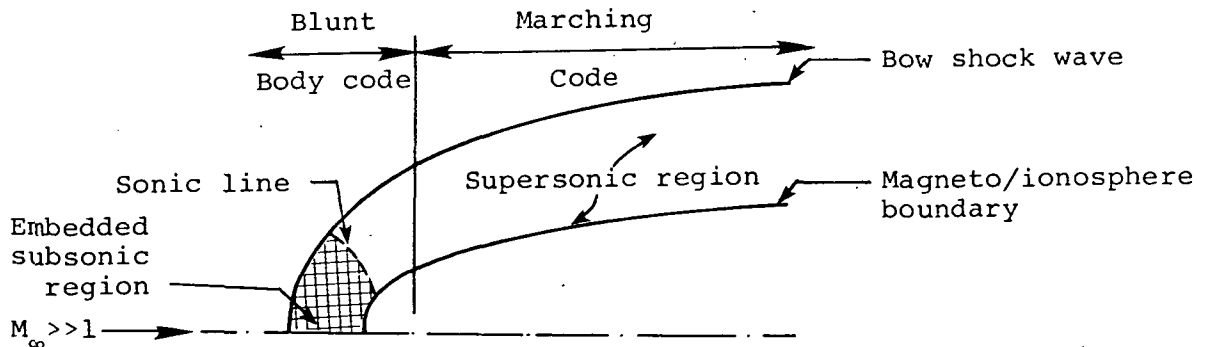
where

$$\Lambda = \exp[-(R_i - R_o)/H] \quad (26)$$

and  $\beta$  is the angle measured from the subsolar point as indicated above. Results for various ionopause shapes obtained by integrating equation (25) for different values  $H/R_o$  in the range  $0.001 \leq H/R_o \leq 1.0$  are provided in figure 2. We note that the range of interest for planetary applications to Venus and Mars appears to be  $0.01 \lesssim H/R_o \lesssim 0.30$  (ref. 5). Tabulated ordinates ( $Y_i/R_o$  vs.  $-X/R_o$ ) are provided in Table 1 for  $H/R_o = 0.01, 0.1, 0.2,$  and  $0.5$ , where  $Y_i = R_i \sin \beta$  is the cylindrical radial coordinate of the ionopause profile.

#### Calculation of the Gasdynamic Flow Properties

Computation of the gasdynamic flow properties consists of determining solutions to the differential equations and discontinuity conservation equations given by equations (7). Because both the downstream tail region (far field) as well as the region in the vicinity of the obstacle nose (near field) are generally of interest in solar wind-magneto/ionopause interactions, the computational methods selected must be capable of determining this entire flow field. In view of the need to carry the flow calculation to an arbitrary downstream distance, the most computationally efficient procedure to employ is to subdivide the flow field into two regions, as indicated in the sketch below:



Illustrated here are the essential features of the high supersonic Mach number flow typical of solar wind flows past terrestrial planets. Of special note is the embedded subsonic pocket, located at the nose of the magneto/ionopause. The presence of this pocket necessitates use of a computational technique capable of treating a mixed subsonic/supersonic flow. Downstream of this region, the flow becomes supersonic and remains so for the convex shapes typical of magneto/ionopause boundaries. In that far field region, a more economical procedure than that used near the nose can be employed.

We note that this subdivision of flow field and use of different solution procedures in each region is common practice for calculating hypersonic blunt-body flows, and was employed in the former solar wind method (ref. 3) as well as in a more recent application to space shuttle re-entry flows (ref. 20). Indicated in figure 3 is a comparison of the former and present computational procedures which illustrates the breakdown of the various solution domains. The previous method treated the nose region by the inverse iteration method, and the remainder of the flow field by the method of characteristics. In light of recent advances, both of those techniques, particularly the inverse method, are now considered dated and inferior to more current methods. In the present study, those two methods have been superseded by: (1) a new axisymmetric implicit unsteady Euler equation solver (IMP) specifically developed under this contract (ref. 21) and which determines the steady state solution in the nose region by a time-marching procedure, and (2) a shock-capturing marching solution (SCT) which spatially advances the solution downstream as far as required by solving the steady Euler equations. As indicated in figure 3, the implicit unsteady Euler equation (IMP) code is used to determine the flow in the region between the stagnation streamline on the symmetry axis and a body-axis normal plane ( $x = \text{constant}$ ) conveniently chosen at the  $\beta = 90^\circ$  ( $x = 0$ ) location. For the magneto/ionopause shapes considered here, purely supersonic flow exists on this plane and the conditions there provide the starting data for the SCT code. The SCT code then marches the solution downstream in axis normal planes to the final specified location.

Obstacle nose solution - implicit unsteady Euler equation (IMP) code.-  
The partial differential equations employed in the implicit (IMP) code are the unsteady axisymmetric versions of the gasdynamic Euler equations given

by equations (7). To implement the calculation, those equations are written in conservation-law form under the generalized independent variable transformation

$$\left. \begin{aligned} \tau &= T \\ \xi &= \xi(T, X, R) \\ \eta &= \eta(T, X, R) \end{aligned} \right\} \quad (27)$$

as follows:

$$\begin{aligned} (U/J)_{\tau} + [(\xi_T U + \xi_X E + \xi_R F)/J]_{\xi} \\ + [(\eta_T U + \eta_X E + \eta_R F)/J]_{\eta} + G = 0 \end{aligned} \quad (28)$$

where

$$U = \begin{pmatrix} \rho \\ \rho u \\ \rho v \\ e \end{pmatrix} \quad E = \begin{pmatrix} \rho u \\ p + \rho u^2 \\ \rho uv \\ (e + p)u \end{pmatrix} \quad (29)$$

$$F = \begin{pmatrix} \rho v \\ \rho uv \\ p + \rho v^2 \\ (e + p)v \end{pmatrix} \quad G = \frac{1}{RJ} \begin{pmatrix} \rho v \\ \rho uv \\ \rho v^2 \\ (e + p)v \end{pmatrix}$$

and the Jacobian

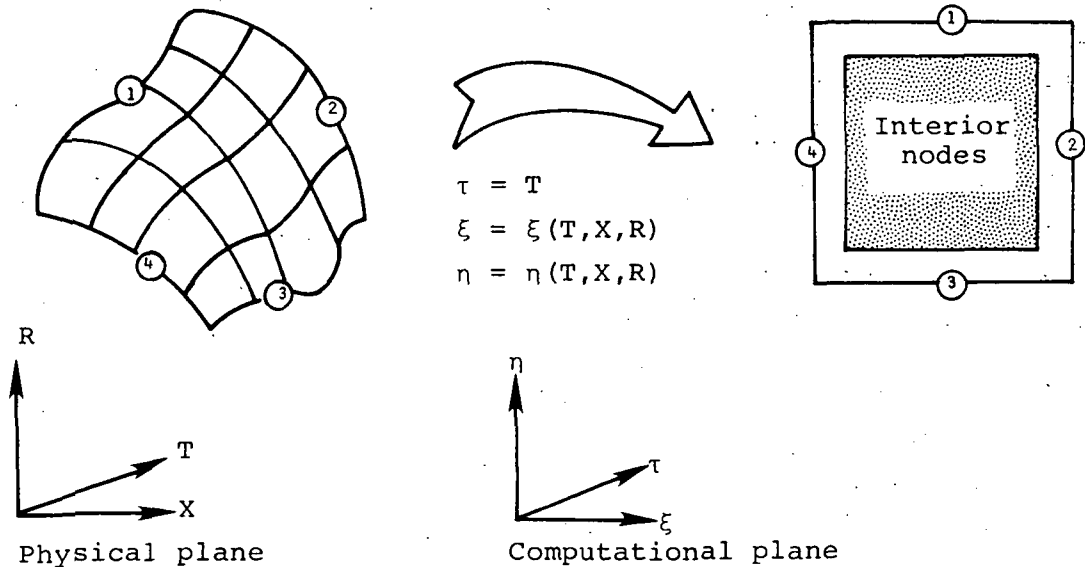
$$J = \xi_X \eta_R - \xi_R \eta_X \quad (30)$$

In equations (27) to (30), T denotes time, X is the axial downstream direction, and R is the cylindrical radial distance; p represents the pressure;  $\rho$  the density; u and v the velocity components in the X and R directions, respectively; and e the total energy per unit volume. The following equation relates the pressure, density, and velocity components to the energy for an ideal gas

$$e = p/(\gamma - 1) + \rho(u^2 + v^2)/2 \quad (31)$$



Using the independent variable transformation equation (27), the physical plane with boundaries 1-4 in  $X, Y, T$  space is mapped into the rectangular computational plane  $\xi, \eta$ , and  $\tau$  space as shown in the sketch below. Generally, at each time step the transformation metrics are not known beforehand and must be determined numerically. Integration step size is established by using the eigenvalues of the Jacobian matrices  $\bar{A}$  and  $\bar{B}$ , where  $\bar{A} = \partial \hat{E} / \partial \hat{U}$ ,  $\bar{B} = \partial \hat{F} / \partial \hat{U}$  and  $\hat{U} = U/J$ ,  $\hat{E} = (\xi_T U + \xi_X E + \xi_R F) / J$ , and  $\hat{F} = (\eta_T U + \eta_X E + \eta_R F) / J$ .



The boundaries, as indicated in the sketch, at which appropriate conditions are imposed on the present problem consist of: (1) the bow shock surface at which the Rankine-Hugoniot relations are satisfied, (2) the downstream outflow boundary where the flow is assumed to be entirely supersonic, (3) the obstacle surface at which a no flow condition in the normal direction is imposed, and (4) the stagnation streamline where symmetry conditions are implemented. Initial flow field conditions are determined by guessing a bow shock shape for the particular blunt obstacle at hand and by prescribing a Newtonian pressure distribution on the body. Since the maximum entropy streamline wets the body, that fact plus the known surface flow direction serve to determine the remainder of the flow properties on the obstacle surface. A linear variation for the flow properties between the bow shock and the obstacle is then prescribed.

This provides the initial flow field which is then integrated in a time-asymptotic fashion until the steady-state solution is obtained.

The basic numerical algorithm used in the IMP code was developed by Beam and Warming (ref. 22) and is second-order accurate, noniterative, and spatially factored. In particular, the "delta form" with Euler time differencing is employed. When applied to equation (28) the algorithm assumes the form

$$(I + \Delta\tau\delta_{\xi}\bar{A}^n)(I + \Delta\tau\delta_{\eta}\bar{B}^n)(\hat{U}^{n+1} - \hat{U}^n) = -\Delta\tau(\delta_{\xi}\hat{E}^n + \delta_{\eta}\hat{F}^n + G) \quad (32)$$

where  $\bar{A}$  and  $\bar{B}$  are the Jacobian matrices,  $I$  is the identity matrix,  $\delta_{\xi}$  and  $\delta_{\eta}$  are second-order, central difference operators,  $U^{n+1} = U(n\Delta\tau)$  and  $\Delta\tau$  is the integration step size.

Equation (32) is solved at the interior points only. It requires two  $4 \times 4$  block tridiagonal inversions at each time step of the integration. The solution procedure is as follows:

1. Define  $\Delta\hat{U} = U^{n+1} - \hat{U}^n$ .
2. Form the right-hand side of equation (32) and store results in the  $\hat{U}^{n+1}$  array.
3. Define  $\bar{U} = (I + \Delta\tau\delta_{\eta}\bar{B}^n)\Delta\hat{U}$  and solve the matrix equation  $(I + \Delta\tau\delta_{\xi}\bar{A}^n)\bar{U} = \hat{U}^{n+1}$  for  $\bar{U}$  storing the result in the  $\hat{U}^{n+1}$  array.
4. Solve the matrix equation  $(I + \Delta\tau\delta_{\eta}\bar{B}^n)\Delta\hat{U} = \hat{U}^{n+1}$  for  $\Delta\hat{U}$ .
5. Obtain the values of  $\hat{U}^{n+1}$  from the relation  $\hat{U}^{n+1} = \Delta\hat{U} + \hat{U}^n$ .
6. Obtain the final solution after applying the smoothing;  $\hat{U}^{n+1} = \hat{U}^{n+1} - (\epsilon/8)S/J$ .

A fourth-order smoothing term  $S$  is usually required to eliminate nonlinear instabilities which may arise since the use of central differences in the spatial directions results in a neutrally stable algorithm.

Downstream solution - shock capturing steady Euler equations (SCT) code. - Since the shock-capturing technique employed has been established previously (refs. 23, 24, 25) only a brief description will be provided here. The steady, full three-dimensional Euler equations are written in cylindrical coordinates in the form:

$$\frac{\partial \tilde{U}}{\partial X} + \frac{\partial \tilde{F}}{\partial R} + \frac{\partial \tilde{G}}{\partial \omega} + \tilde{H} = 0 \quad (33)$$

where

$$\left. \begin{aligned} \tilde{U} &= \begin{pmatrix} \rho u \\ p + \rho u^2 \\ \rho uv \\ \rho uw \end{pmatrix} & \tilde{G} &= \frac{1}{R} \begin{pmatrix} \rho w \\ \rho uw \\ \rho vw \\ p + \rho w^2 \end{pmatrix} \\ \tilde{F} &= \begin{pmatrix} \rho v \\ \rho uv \\ p + \rho v^2 \\ \rho vw \end{pmatrix} & \tilde{H} &= \frac{1}{R} \begin{pmatrix} \rho v \\ \rho uv \\ \rho(v^2 - w^2) \\ 2\rho vw \end{pmatrix} \end{aligned} \right\} \quad (34)$$

Here  $p$  and  $\rho$  represent dimensional pressure and density and  $(u, v, w)$  denote velocity components in the cylindrical coordinate directions  $(X, R, \omega)$ , respectively, where  $X$  is the axial downstream direction,  $R$  is the cylindrical radius in an axis-normal plane, and  $\omega$  is the azimuthal angle measured in the axis-normal plane. This set of equations is closed by the use of energy conservation as provided by the equation for total enthalpy

$$H_t = h(p, \rho) + \frac{q^2}{2} = \text{constant} \quad (35)$$

where

$$q = \sqrt{u^2 + v^2 + w^2} \quad (36)$$

is the magnitude of the velocity vector and  $h(p, \rho)$  is the caloric equation of state.

The equations are then transformed to a computational plane by using the independent variable transformation

$$\begin{aligned} X &= X \\ \xi(X, R, \omega) &= \frac{(R - R_b)}{(R_s - R_b)} \end{aligned} \quad (37)$$

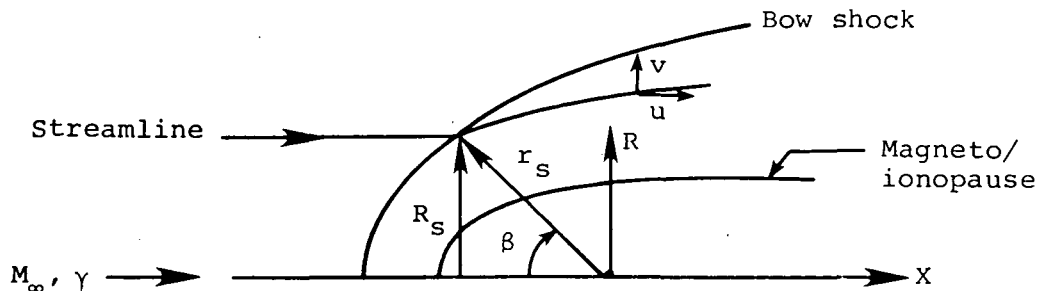
$$\xi(\omega) = f(\omega)$$

where the subscripts (b,s) denote body and shock surfaces, respectively. This change of variable is employed in equation (33) and the result then rearranged into the following conservation law form (refs. 23,24,25).

$$\frac{\partial U}{\partial X} + \frac{\partial F}{\partial \xi} + \frac{\partial G}{\partial \eta} + H = 0 \quad (38)$$

The finite-difference formulation of MacCormack (ref. 26) is used to integrate equation (38) with respect to the hyperbolic coordinate X to yield values of the conservative variable U. This procedure is calculable as long as the flow velocity in the axial (X) direction is greater than the local speed of sound. We note that for the axisymmetric obstacle shapes considered here,  $\partial/\partial\omega = 0$ ; however, the version of the SCT code employed has the capability for treating full three-dimensional geometries.

Streamline and contour calculations.- A number of special purpose subroutines were written to calculate streamlines and contour maps of various flow field properties, and also to provide automated plots of these quantities. The streamlines are determined by integrating trajectories through the known velocity field as this procedure was found to be more accurate than a mass flow calculation. The calculation of a particular streamline is initiated at the point where the streamline crosses the bow shock, as shown below:



At that point, exact values of the streamline slope  $dR_s/dX$  are known in terms of the local shock angle  $\delta_s$  and free-stream quantities according to the relation

$$\frac{dR_s}{dX} = \frac{2 \cdot \cot \delta_s \cdot (M_\infty^2 \sin^2 \delta_s - 1)}{2 + M_\infty^2 (\gamma + 1 - 2 \sin^2 \delta_s)} \quad (39)$$

which is implicit in the blunt-body (IMP) and marching (SCT) code solutions. At other points in the flow field, the local streamline slope is given by the ratio of radial to downstream velocity, i.e.

$$\frac{dR_s}{dX} = \frac{v}{u} \quad (40)$$

and the streamline determination is made by stepwise integration in X of equation (40) according to a modified third-order Euler predictor/corrector method. Two-dimensional linear interpolation from the flow field grid points is employed to obtain the velocity components (u,v) required at the stepwise points along the streamline trajectory. Separate streamline calculations are made for the near field (IMP results) and far field (SCT results) because of the different coordinate systems employed in those two regions.

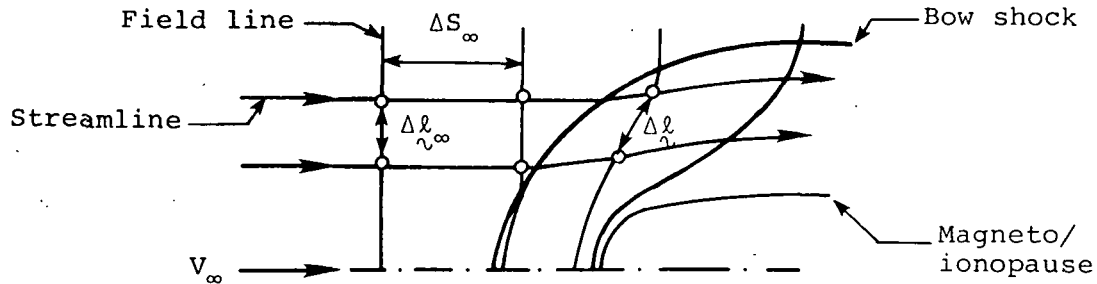
Contours of various flow field quantities are determined for the entire flow field (near field plus far field) by using a modified version of the contour package developed by R. Sorensen at NASA/Ames Research Center. Pertinent details of that package are provided in the user's manual section of this report.

#### Calculation of the Magnetic Field

With the flow properties known from the gasdynamic calculations, determination of the magnetic field  $\vec{B}$  proceeds by integrating equations (8). Those equations are commonly interpreted as indicating the field lines move with the fluid. This leads to a straightforward, although tedious, calculation in which the vector distance from each point on an arbitrarily selected fluid line to its corresponding point on an adjacent field line in the downstream direction is determined by numerically integrating  $\int \vec{v} dt$  over a fixed time interval  $\delta t$ . While that calculation determines the location of the field lines, the intensity of the magnetic field at any point may then be calculated from the relation

$$\frac{|\underline{B}|}{|\underline{B}_\infty|} = \frac{\rho |\Delta \underline{\ell}|}{\rho_\infty |\Delta \underline{\ell}_\infty|} \quad (41)$$

where  $\Delta \underline{\ell}$  is the vector length of a small element of a flux tube. The sketch below clarifies these quantities for the case when the oncoming  $\underline{B}_\infty$  field is perpendicular to the flow:



where the open symbol  $\odot$  denotes locations of points on the streamlines corresponding to a fixed time interval  $\Delta t = \Delta S_\infty / V_\infty$ .

Because of the axisymmetry of the gasdynamic quantities and the linearity of the equations for  $\underline{B}$ , Alksne and Webster (ref. 27) have shown that the magnetic field at any point in the flow field can be calculated by vectorially summing the contributions of the three component fields indicated in figure 4. At any point P, the magnetic field  $\underline{B}_P$  is given by

$$\underline{B}_P = \left( \frac{B_P}{B_\infty} \right)_{\parallel} B_{\infty \parallel} + \left( \frac{B_P}{B_\infty} \right)_{\perp} B_{\infty \perp} + \hat{e}_n \left( \frac{B_P}{B_\infty} \right)_n B_{\infty n} \quad (42)$$

where the subscripts ( $\parallel$ ,  $\perp$ ,  $n$ ) refer respectively to the contributions associated with the components of  $\underline{B}_\infty$  parallel to  $\underline{V}_\infty$ ; perpendicular to  $\underline{V}_\infty$  in the plane that contains the point P, the center of the planet, and the vector  $\underline{V}_\infty$ ; and normal to the latter plane.

For the contribution associated with the parallel component  $B_{\infty \parallel}$ , it has been shown (refs. 28,29) that  $\left( \frac{B_P}{B_\infty} \right)_{\parallel}$  is proportional to  $\rho \underline{V}$  throughout the entire flow field. Consequently, this component can be calculated directly from the gasdynamic solution by the expression

$$\left( \frac{B_P}{B_\infty} \right)_{\parallel} = \frac{\rho_p \underline{V}_p}{\rho_\infty |\underline{V}_\infty|} \quad (43)$$

Similarly, the normal component  $(B_P/B_\infty)_n$  can be shown to be equal to

$$\left( \frac{B_P}{B_\infty} \right)_n = \frac{R_P \rho_P}{R_{P_\infty} \rho_\infty} \quad (44)$$

where  $R_P$  is the radial cylindrical coordinate of the streamline, as indicated in figure 4.

The determination of the contribution  $(B_P/B_\infty)_t$  cannot be made directly from the gasdynamic properties as can the other two components. For this component, recourse must be made to the general computation associated with equation (41). Details of the calculation procedure for  $(B_P/B_\infty)_t$  are provided in the user's manual section of this report.

## RESULTS AND DISCUSSION

In order both to verify the correctness of the procedures developed under this study as well as to demonstrate their flexibility and power for calculating solar wind flows for a variety of conditions, a large number of test cases have been run. A representative sample of the results obtained from those calculations is reported here. Because the implicit blunt-body procedure (IMP code) is new, that code was tested and compared to previously established theoretical methods to substantiate its validity prior to solar wind applications. We have prepared figure 5 to exhibit such a comparison. Here, flow field results predicted by the present implicit method are compared with those of other theoretical techniques and also experimental data for supersonic flow past a sphere with  $M_\infty = 4.926$  and  $\gamma = 1.4$ . The variation of density and Mach number along the stagnation streamline are provided in the two plots on the left, while the variation of surface pressure and shock standoff distance with spherical angle are given in the two plots on the right. In all of these comparisons, the present theoretical results are in excellent agreement with both established theoretical methods and experiment.

Figure 6 exhibits a comparison of results predicted by the implicit method for a solar wind calculation. The upper plot of the figure displays the locations of the bow wave and sonic line for flow past the equatorial trace of the magnetopause for  $M_\infty = 8$  and  $\gamma = 5/3$ . The density distribution along the magnetosphere boundary and along the shock wave for this flow are given in the lower plot. Included in both of these figures is the solution calculated by Spreiter et al. (ref. 3) using the inverse method of Inouye and Lomax (ref. 30). Excellent agreement is obtained between the present implicit technique and the inverse method. Figure 7 provides analogous results for the equatorial trace of the magnetopause for a variety of Mach numbers typical of solar wind flows, and illustrates the Mach number capability of the present IMP code.

With regard to solar wind flows past nonmagnetic planets, figure 8 displays results for the bow shock location for  $M_\infty = 8$  and  $\gamma = 5/3$  flow past various ionopause shapes with  $H/R_0 = 0.01, 0.1, 0.2, 0.25, 0.50, 0.75$  and 1.0. Not included in that figure for clarity of presentation are the results of Spreiter et al. (ref. 5) obtained by using the inverse method. Those results and the predictions of the present implicit method given in figure 8 are essentially indistinguishable.



As an illustration of the geometric flexibility of the present implicit method and also as a critical test of its ability to capture embedded shock waves besides the bow shock, a feature which the inverse method cannot duplicate, figures 9 and 10 have been prepared. This calculation corresponds to the  $M_\infty = 5$  and  $\gamma = 5/3$  flow around the axisymmetric shape generated by rotating the principal meridian of the magnetopause about its axis and compares with an experimental test by Spreiter et al. (ref. 3). This particular profile shape contains a pronounced dent with a concave corner in the vicinity of the neutral point. Spreiter et al. (ref. 3) have argued that the presence of a concave corner in the magnetopause is unrealistic and would not occur in nature, but should be replaced by a free surface created by drawing a tangent line across the corner. In figure 9, we present results for both the concave and the free surfaces, denoted by solid and dashed lines, respectively. For the concave surface, a pocket of embedded subsonic flow is seen to form behind the embedded shock wave which was caused by the indented profile. If the surface is modified to the free surface shape, the embedded wave disappears completely as expected. The corresponding pressure coefficients on the magnetosphere boundary are presented in figure 10. For the concave surface, the shock wave is located on the body at approximately  $\beta = 80^\circ$ , while for the free surface, the pressure coefficient displays a constant value as anticipated. Finally, we note that the calculation of a supersonic flow with an embedded shock and subsequent subsonic pocket provides a severe test for any blunt body procedure. The ability of the present code to provide convergent results for such a flow demonstrates the capability for further extension and application to more generalized profiles than was heretofore possible.

As a final indication of the range of solar wind flows over which the implicit code has been tested, we have prepared figure 11 which displays the variation of shock stand-off distance with oncoming Mach number and ratio of specific heats for three different magneto/ionopause shapes. These include the rotated equatorial trace of the magnetopause, and the ionopause shapes for  $H/R_\odot = 0.01$  and  $0.5$ . Those shapes and the corresponding ranges of  $M_\infty$  and  $\gamma$  essentially span the entire range of interest of geometry and solar wind conditions for which the computer programs developed herein would be normally applied.

In order to demonstrate the ability of the marching code to continue the blunt-body IMP solution downstream to some arbitrarily-specified

downstream location, and also to verify its stability and convergence for application to these classes of flows, we have calculated marching solutions for a variety of cases typical of solar wind interactions. Figure 12 exhibits the location of the bow wave for flows with  $\gamma = 5/3$  and  $M_\infty = 3, 8, \text{ and } 25$  past the rotated equatorial trace of the magnetopause as the flow proceeds downstream from the nose region to  $x/D = -11$ . For this calculation, starting conditions for the marching code (SCT) have been provided by the blunt-body (IMP) code on the line  $x/D = 0.0$ , which is the usual location at which the two solutions are joined by the computer program. The marching code then determines the remainder of the flow field back to the specified downstream location. Since for the particular shapes considered herein the downstream flows are quite smooth, the marching calculation is very efficient (less than 30 sec., CDC 7600, OPT=2 compiler). Similar results are presented in figure 13 for  $M_\infty = 8$  and  $\gamma = 5/3$  flow past an ionopause shape with  $H/R_0 = 0.1$ . Those results have been carried downstream to  $x/R_0 = -20$  since this distance is more typical of the region of interest for nonmagnetic planets. This is so because of the different scalings ( $D, R_0$ ) used for the magnetic and nonmagnetic applications. For Venus and Mars, the location of the ionopause nose is at a distance only slightly greater than the planetary radius, as compared with the location of the magnetopause nose for the Earth which is of the order of 10 planetary radii.

In order to illustrate the capability of the present procedures to determine streamlines, contour maps of various flow properties, and magnetic field lines and contours, as well as to demonstrate the automated plotting capability for displaying these results, figures 14 and 15 have been prepared. Figure 14 illustrates the computer generated streamline locations and contour maps of density  $\rho/\rho_\infty$  and velocity ratio  $V/V_\infty$  for the complete near and far field flow about the equatorial trace of the magnetosphere for  $M = 8$  and  $\gamma = 5/3$ . Based on this gasdynamic solution, figure 15 exhibits the corresponding results for the magnetic field components  $(B/B_\infty)_\perp$  and  $(B/B_\infty)_\parallel$  in the plane of symmetry. Both magnetic field line locations and contours are provided. In addition to demonstrating the overall smoothness of the computed results, these two figures illustrate the ability of the present techniques to provide the completely automated production of report quality plots of both gasdynamic and magnetic field properties for solar wind flows past axisymmetric magneto/ionopause shapes

## CONCLUDING REMARKS

Theoretical analysis and associated development of computer programs were carried out for the purpose of developing computational techniques for predicting the interaction of solar wind flows with both magnetic and nonmagnetic terrestrial planets. Based on the identical theoretical model employed in previous work, i.e. the steady, dissipationless, magnetohydrodynamic model for axisymmetric, supersonic, super-Alfvénic solar wind flow a new and more powerful solution procedure has been developed. The procedure is built upon an assemblage of computer codes, including:

- Blunt-body code - to determine gasdynamic solution near obstacle nose
- Marching code - to determine gasdynamic solution downstream of obstacle nose
- Streamline code - to determine flow field streamlines
- Contour code - to determine contour maps of flow and magnetic field properties
- Magnetic field code - to determine frozen-in magnetic field
- Plotting code - to plot selected flow and magnetic field results

Comparisons are reported which demonstrate the accuracy of the present techniques by comparison with previously-established theoretical methods as well as limited experimental data. Furthermore, new results are presented for a variety of solar wind flows which illustrate the flexibility and generality of the component methods. The computational procedures are fully automated and provide detailed flow field and magnetic field properties in convenient output format, including an automatic plot capability. The programs are documented and are presented in a general user's manual included as part of this report.

With regard to improvements of the present techniques to provide a more accurate mathematical representation of solar wind flow, a number of items for further study are recommended. The first of these involves extension of the present capability from axisymmetric to three-dimensional nonaxisymmetric obstacle shapes representative of planetary magnetopauses. The second involves the merging of the present procedures for determining the magnetic field exterior to the magnetosphere boundary with a method, such as the Olsen-Pfitzer model, for calculating the confined magnetic field so as to provide a complete magnetic field representation. Lastly, the capability for determining numerical solutions of the complete magnetohydrodynamic equations, rather than the frozen magnetic field approximation,

should be actively pursued. Although this extension represents a major advance in magnetospheric physics and computational fluid dynamics, in view of the success of the currently employed methods, its successful achievement appears highly promising. The component methods on which the present procedure is based are directly capable of extension in these as well as other directions. Moreover, the efficiency of the present calculations indicates that the improved representation achieved by these improvements will not result in prohibitive computational costs.

## APPENDIX A

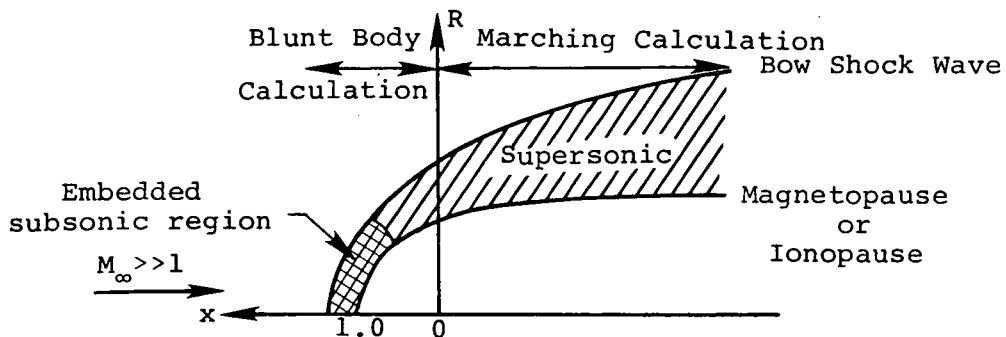
### A.1 Introduction

The purpose of this appendix is to describe the operation of the assemblage of computer codes which were developed in conjunction with the theoretical work presented in this report and organized into one program, and to provide sufficient detail to permit understanding and use of the program. The program computes the flow field of the solar wind about a terrestrial planet, using a procedure for the calculation of supersonic/hypersonic flow about an axisymmetric blunt body. The corresponding frozen-in magnetic field is then calculated from the previously determined velocity and density fields. Streamlines and contour lines of various flow field properties and magnetic field components are also determined.

A description of the general operating procedure of the program is given, with descriptions of input and output. The program is written in FORTRAN IV and has been developed on a CDC 7600 computer. University Computing Company (UCC) Standard Plotting Software and Functional Software packages are used to produce automated plots. Files used, besides TAPE5 for INPUT and TAPE6 for OUTPUT, are TAPE1 for the plot file (system default), TAPE4 for input file for rerun option, and TAPE9 for storing data for rerun. Typical run times for cases using the default parameters are 40 to 50 seconds, using the OPT=2 compiler. For a case using the rerun option, which employs a previously calculated flow field, the run time is approximately 5 seconds.

### A.2 Program Description

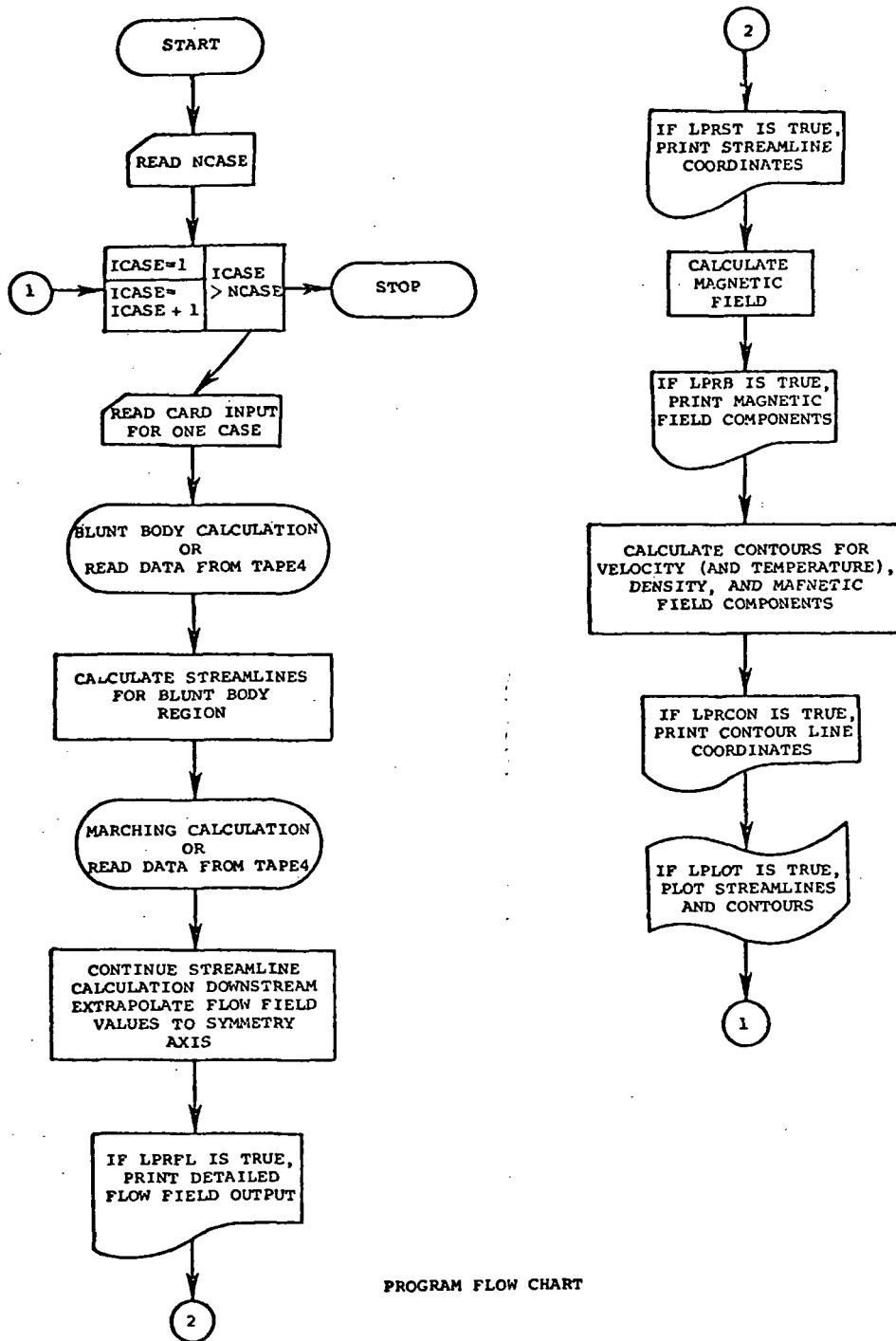
For computational purposes, the flow is subdivided into two regions, as indicated in the sketch below, with the center of the planet as origin.



The region near the nose of the magnetopause/ionopause includes all of the imbedded subsonic flow and part of the supersonic flow. An axisymmetric

implicit unsteady Euler equation solver is used to calculate this part of the flow field. Using the solution plane at  $x = 0.0$  to provide starting conditions, the flow field in the purely supersonic downstream region is determined by integrating the steady Euler equations using a spatial marching procedure. Streamlines, the magnetic field, and contours are calculated using the entire flow field, distinguishing between the two regions as required by the different forms of the computational grids. A rerun capability is provided, where flow field data is read from a file written on a previous run, rather than repeating the blunt body and marching calculations. The computations proceed as shown in the sketch below, which provides an overall flow chart of the complete program. The program provides for several cases to be run consecutively.

APPENDIX A

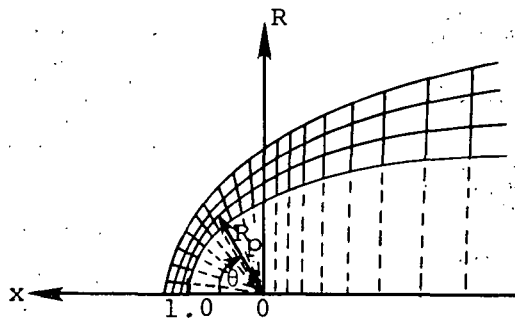


PROGRAM FLOW CHART

## A.2.1 Calculation Procedure

After reading in the number of cases in the run, each case is calculated independently. Subroutine INPUT reads in all card input required for one case, viz. a title, flow conditions, obstacle geometry, calculation and print control parameters, and desired contour values. The user may supply the obstacle geometry in the form of a shape table for an axisymmetric body, or use one of the default shapes which are calculated internally by the program. These default shapes are the magnetopause equatorial trace and a constant scale-height ionopause for which  $H/R_0$  is specified by the user. The input is printed as the first item of output.

A computational mesh in polar  $(R_p, \theta)$  coordinates is established for the blunt body calculation; then, for the marching calculation, this is extended into a cylindrical  $(x, R)$  system, as indicated below:



All lengths,  $x$ ,  $R$ ,  $R_p$ , are scaled so that the nose of the obstacle is at  $x = 1.0$ . For the default shapes, rays at equal angular increments of  $\Delta\theta$  are used, starting at  $-\Delta\theta/2$ , up to  $90^\circ + \Delta\theta$ , where  $\Delta\theta = 90^\circ / (\text{NBLUNT} - 1.5)$  and NBLUNT is an input parameter describing the number of angular mesh points to be used in the blunt-body calculation. Program default value is NBLUNT = 24, so that for the default mesh,  $\Delta\theta = 4^\circ$ . The obstacle shape is determined by integrating the appropriate differential equation by a trapezoidal predictor-corrector method. For a user-supplied shape, the  $\theta$  grid is determined by rays from the origin through the first NBLUNT points, and the reflection of the first ray in the  $x$ -axis. Values for  $R_p$  are determined by dividing the line segments between the body and bow shock wave into  $NR - 1$  equal intervals. Thus, including the obstacle and bow shock wave, the grid forms  $NR$  arcs around the obstacle. A starting solution for the blunt-body calculation is obtained by guessing a bow shock shape and by prescribing a Newtonian pressure distribution on the body.



## APPENDIX A

Noting that the maximum entropy streamline wets the body, other flow properties on the body surface can then be calculated. An initial flow field is then established by linear interpolation between the obstacle and the guessed bow shock, where the Rankine-Hugoniot relations hold. The integration proceeds in time for ITER steps. The initial bow shock shape used for the magnetopause equatorial trace and for an ionopause with  $H/R_0 \geq 0.1$  is a correlation shape depending on  $(M_\infty, \gamma, H/R_0)$  and given by the parabola  $R_p = \delta_1 \sqrt{\delta_0 - x} / \sqrt{\delta_0}$  where

$$\delta_0 = 1.0 + 1.1 \left[ \frac{((\gamma-1)M_\infty^2 + 2)}{(\gamma+1)M_\infty^2} \right] \times (0.9 + 0.5 H/R_0)$$

$$\delta_1 = \Delta_0 \{ (1.273 + 0.009 M_\infty^2) (0.904 + 0.655 H/R_0)$$

$$\times (3.95 - 5.3 H/R_0 + 3.85 (H/R_0)^2) \} + (R_{\text{body}})_x = 0.0$$

$$\Delta_0 = \left[ \frac{(\gamma-1)M_\infty^2 + 2}{(\gamma+1)M_\infty^2} \right] \times 0.78$$

For a user-supplied obstacle shape and for an ionopause with  $H/R_0 < 0.1$ , the initial shock shape used is the curve  $R_p = \sqrt{(1 + \Delta_0 (1 + 0.680^2 + 0.160^4))}$ . Information on convergence, the final sonic line locations, and the body and final bow shock shape are printed from this calculation.

The results at  $\theta = 90^\circ$ , i.e. at  $x = 0.0$ , are used as starting conditions for the marching calculation, after proper normalization. For default geometries, the integration of the appropriate differential equation is continued downstream at equal  $\theta$  increments to form a body shape table. The stepsize along the x-axis is recalculated at every ICØNST(49) with ICØNST(49) being set to 10. At each x-location,  $R_{\text{body}}$  is determined by linear interpolation. The computational mesh is extended by adding the line perpendicular to the x-axis at each step, divided in the same manner as for the blunt nose. The calculation marches downstream with a maximum stepsize of 1.0 until the terminal location specified by the user has been passed. However, the number of steps is limited to 75, after which the calculation will end regardless of the x-location. The coordinates of the obstacle and bow shock are printed at each step.

The grid coordinates and flow field values are written to a file, TAPE9, which may be saved to use as input for a later run. This rerun option, which replaces constructing the computational mesh and performing

the blunt body and marching calculations with reading the rerun input file, TAPE4, is described in section A.2.2.

The streamlines are calculated in two sections, following each of the flow field calculations. Using the results of the blunt body calculation, i.e. the  $(x, R)$  grid coordinates,  $(R_p, \theta)$  grid coordinates, density  $\rho/\rho_\infty$ , and velocity components  $v_X/v_\infty$  and  $v_R/v_\infty$ , the velocity magnitude  $|v|/v_\infty$  and flow angle are calculated. Density  $\rho/\rho_\infty$  and velocity  $|v|/v_\infty$  are smoothed along the rays of constant- $\theta$ , using a third degree least squares fit with respect to  $R_p$ . Streamlines are then calculated downstream to  $x = 0.0$ , using the trajectory method, integrating through the velocity field by means of a third-order modified Euler integration procedure, using the grid locations on the bow shock as starting positions. The flow angle  $\phi = \tan^{-1}(v_R/v_X)$  at each point is determined using bivariate linear interpolation in  $\theta$ , then  $R_p$ . Points for which  $\theta < 0^\circ$  or  $\theta > 90^\circ$  are discarded in the interpolation.

The marching calculation provides  $(x, R)$  grid coordinates, and values of density  $\rho/\rho_t$ , and velocity components  $v_X/v_t$  and  $v_R/v_t$ , where  $t$  denotes free-stream stagnation conditions. For compatibility with the blunt body solution, the flow field values are converted to  $\rho/\rho_\infty$ ,  $v_X/v_\infty$ ,  $v_R/v_\infty$  before calculating the resultant velocity magnitude  $|v|/v_\infty$  and flow angle  $\phi$ . The streamline calculation is continued downstream, employing the same method as in the nose region. Starting positions on the shock wave for the streamline calculation in the marching zone are set at equal  $R$ -increments, with a maximum of 50 streamlines calculated. The flow angle is determined using bivariate linear interpolation first in  $x$ , then in  $R$ .

Along the symmetry axis, values of  $x$ ,  $\rho/\rho_\infty$ , and  $|v|/v_\infty$  are determined by extrapolation, using a third-order Lagrangian polynomial in  $\theta$  on each arc of the computational grid. Exact values for the stagnation streamline are used where possible, viz.

at the bow shock

$$\rho/\rho_\infty = (\gamma+1)M_\infty^2 / \left[ (\gamma-1)M_\infty^2 + 2 \right]$$

$$|v|/v_\infty = 1/(\rho/\rho_\infty)$$

APPENDIX A

at the body surface

$$\rho/\rho_\infty = (\rho/\rho_\infty)_{\text{shock}} \left\{ \left[ \frac{(\gamma+1)M_\infty^2}{4\gamma M_\infty^2 - 2(\gamma-1)} \right]^{1/(\gamma-1)} \right\}$$

$$|\tilde{v}|/v_\infty = 0.0$$

$$x = 1.0$$

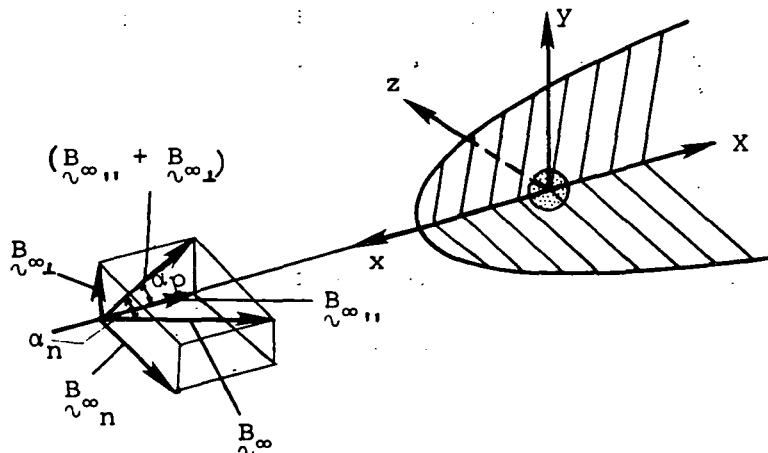
Detailed flow field output may now be printed by subroutine FLØUT, with LPRFL as print control variable. In addition to grid coordinates, density, velocities and flow angle, values of temperature  $T/T_\infty$  and pressure  $P/P_\infty$  are output, where

$$T/T_\infty = 1 + \left[ (\gamma-1)/2 \right] M_\infty^2 \left[ 1 - (|\tilde{v}|/v_\infty)^2 \right]$$

$$P/P_\infty = (\rho/\rho_\infty) (T/T_\infty)$$

Streamline coordinates may also be printed by subroutine STØUT, with LPRST as print control variable.

The magnetic field is determined by separately calculating the components whose field lines are parallel, perpendicular, and normal to the flow, in the undisturbed solar wind. These components are then added vectorially, the resultant being expressed in orthogonal  $(x,y,z)$  components. The angles in the free stream  $\alpha_p$  and  $\alpha_n$  between the magnetic field and the flow, as shown in the sketch below, are input variables. The components are calculated using the following formulae, in which  $\tilde{e}$  signifies a vector of magnitude  $e$ , in the direction of the component field line, and  $\hat{n}$  the unit normal vector.



$$\left(\frac{B}{B_\infty}\right)_{\parallel} = \left(\frac{V}{V_\infty}\right) \left(\frac{\rho}{\rho_\infty}\right); \quad \left(\frac{B}{B_\infty}\right)_{\perp} = \left(\frac{\Delta\ell}{\Delta\ell_\infty}\right) \left(\frac{\rho}{\rho_\infty}\right); \quad \left(\frac{B}{B_\infty}\right)_n = \left(\frac{R}{R_\infty}\right) \left(\frac{\rho}{\rho_\infty}\right)$$

$$\left(\frac{B}{B_\infty}\right) = \left(\frac{B}{B_\infty}\right)_{\parallel} \left(\frac{B_{\infty\parallel}}{B_\infty}\right) + \left(\frac{B}{B_\infty}\right)_{\perp} \left(\frac{B_{\infty\perp}}{B_\infty}\right) + \hat{n} \left(\frac{B}{B_\infty}\right)_n \left(\frac{B_{\infty n}}{B_\infty}\right)$$

The magnetic field line vector component  $B_{\parallel}$ , which results from the interplanetary component  $B_{\infty\parallel}$ , that is parallel to the undisturbed solar flow has local magnitude given by  $(|V|/V_\infty)(\rho/\rho_\infty)$ , and the same local direction  $\phi$  as the fluid flow. Determination of the normal magnetic field component  $B_n$  requires calculation of  $R/R_\infty$ , where  $R_\infty$  is the free stream cylindrical R-ordinate of the streamline through the point under consideration. This is calculated by linearly interpolating in the local radial cylindrical coordinate  $R$  between the streamlines, with  $R/R_\infty = 1.0$  along the x-axis. The magnetic field vector component  $B_{\perp}$  resulting from the interplanetary component  $B_{\infty\perp}$  which is perpendicular to the undisturbed solar wind flow requires the distance vector  $\Delta\ell/\Delta\ell_\infty$ , whose magnitude is  $\Delta\ell/\Delta\ell_\infty$  and direction is  $\psi$ , where  $\Delta\ell/\Delta\ell_\infty$  is the stretching factor of the perpendicular field at the point, and  $\psi$  is the direction of the field line through the point. The perpendicular field lines are determined by integrating  $\int v dt$  along each streamline, using trapezoidal integration to locate points along the streamline at regular increments in time,  $\Delta t$ , starting at a perpendicular field line ahead of the bow shock. Values for  $\Delta\ell/\Delta\ell_\infty$  and  $\psi$  are calculated at the points where the perpendicular field lines and streamlines intersect, interpolating only along the field lines. A generalized quadrilateral interpolation scheme is then employed to determine  $\Delta\ell/\Delta\ell_\infty$  and  $\psi$  at the computational grid points, using the quadrilateral containing the point formed by the intersection of pairs of adjacent streamlines and perpendicular field lines. At the bow shock, an exact formula is used, viz.

$$(\Delta\ell/\Delta\ell_\infty)^2 = 1 + \cot^2\theta(1+D^2) - 2D \times \csc\theta \times \cot\theta \times \cos(\theta-\delta)$$

$$\psi = \theta + \sin^{-1}\{D \times \cot\theta \times \sin(\theta-\delta)/(\Delta\ell/\Delta\ell_\infty)\}$$

## APPENDIX A

where

$$D^2 = 1 - 4(M_\infty^2 \sin^2 \theta - 1)(\gamma M_\infty^2 \sin^2 \theta + 1) / \left\{ (\gamma + 1)^2 M_\infty^4 \sin^2 \theta \right\}$$

$$\cot \delta = \tan \theta \times \left\{ (\gamma + 1) M_\infty^2 / \left[ 2(M_\infty^2 \sin^2 \theta - 1) \right] - 1 \right\}$$

$$\theta = \tan^{-1} \left\{ \frac{dR_{\text{shock}}}{dx} \right\}$$

The values of  $\Delta l / \Delta l_\infty$  at the grid points are smoothed using fifth-order least squares fit with respect to arc length along the arcs of the grid. The resultant magnetic field is expressed in orthogonal (x,y,z) components, where

$$B_x / B_\infty = \cos \alpha_n \times \left[ \cos \phi \times \cos \alpha_p \times (|B| / B_\infty)_n + \cos \psi \times \sin \alpha_p \times (|B| / B_\infty)_\perp \right]$$

$$B_y / B_\infty = \cos \alpha_n \times \left[ \sin \phi \times \cos \alpha_p \times (|B| / B_\infty)_n + \sin \psi \times \sin \alpha_p \times (|B| / B_\infty)_\perp \right]$$

$$B_z / B_\infty = \sin \alpha_n \times (B / B_\infty)_n$$

Magnetic field components may now be printed by subroutine BOUT, with LPRB as print control parameter. The magnetic field is not calculated when LPRB = .FALSE. and KBCON=0.

Contours are calculated for velocity  $|v|/v_\infty$ , density  $\rho/\rho_\infty$ , and magnetic field components  $(B/B_\infty)_n$  and  $(B/B_\infty)_\perp$ . The method used is a modified version of a procedure developed by R. Sorenson of NASA/Ames Research Center. The boundary is searched for intervals which bracket a contour point. Having found one point, the remainder of the contour is determined by 'walking' around the contour, searching at each step for the interval through which the contour line next passes, until a boundary point is reached. Then closed contours are found in a similar manner. Linear interpolation is used throughout the process. Note that since  $T/T_\infty$  is a function of  $|v|/v_\infty$  only, velocity contours may also be considered as temperature contours. The coordinates of the contour lines can be printed by subroutine CONOUT, with LPRCON as print control parameter. The section of the program which creates the plots is accessed only when the control parameter LPLOT = .TRUE.

### A.2.2 Rerun Option

The rerun option is used when LRERUN = .TRUE. The blunt body and marching calculations are replaced with reading the grid coordinates and flow field values from the rerun file, TAPE4, which contains data written to TAPE9, then saved, on a previous run. Different values for any parameter not used in the flow field calculations may be specified, viz. contour values, plot length, magnetic field angles, and output options. Values of AMACH, GAMMA, and  $HR\emptyset$  are required input, to ensure that the input rerun file does contain the case desired for rerun. If the geometry is user-supplied, the body shape table will be read from TAPE4, and should not be input from cards.

After reading the card input, AMACH, GAMMA, and  $HR\emptyset$  are tested against values from TAPE4. The grid coordinates and flow field values from the blunt body calculation are read in, then smoothed, and streamlines calculated for this region, as previously described. The results of the marching calculation are then read, and the streamline calculation continued downstream. The calculations then proceed as described in section A.2.1.

A run must not contain more than one case which uses the rerun option.

### A.2.3 Program Limitations and Precautions

The program makes some assumptions about the geometry of the obstacle shape around which flow is to be calculated, and about the flow field. The obstacle shape is assumed to be monotonically increasing in R, going downstream. The nose of the obstacle is at  $x = 1.0$ . The origin of the (x, R) coordinate system is the center of the planet. Obstacle shapes with sharp corners should be avoided. The flow at  $x = 0.0$ , which is used as the starting plane for the marching calculation, must be such that the axial (x-direction) Mach number is purely supersonic. This is a basic requirement of the marching code and is associated with the manner in which the code advances the solution. That condition is violated for ionopause shapes with  $H/R\emptyset > 0.5$ , so that with the present joining procedure employed (i.e. at  $x = 0.0$ ) those shapes cannot be treated. In the magnetic field calculation, the first streamline is assumed to be inside the arc described by the grid points immediately off the body, downstream of  $x = 0.0$ . To reduce computational costs, a grid using  $NR = 10$  may be used, in which case a lower value of CN may be required. This would

## APPENDIX A

reduce the running line by approximately 40 percent. A free stream Mach number less than 3.0 is not advised.

### A.2.4 Convergence Criteria for Blunt Body Calculation

The output provides two measures of the convergence of the blunt body calculation. The RMS of shock speed and maximum shock speed are printed at each iteration. These quantities should both tend to zero. A value for  $q_{\text{RMS}}$ , RMS of shock speed, of

$$q_{\text{RMS}} < \sqrt{\gamma} \times M_{\infty} \times 10^{-3}$$

where  $\gamma$  is the specific heat ratio, and  $M_{\infty}$  is the free stream Mach number, usually indicates a converged solution. The RMS of error in enthalpy, HT, should be less than 1 percent, with the maximum enthalpy error also of that order.

The Courant number, CN, determines the time step size used by the calculation. A value not greater than the default of 3.0 should be used. For low Mach numbers or a coarser mesh than the default, a lower value may be preferable. If the default value does not generate a converged solution, or if the error message from subroutine SHOCK is printed, try lowering CN in increments of 0.5 to find a better value of CN. User-supplied bodies may also require a lower Courant number.

### A.3 Description of Input

This section describes the card input for the program. An alphabetized dictionary of input variables is provided, defining the variables, listing default values and limitations. A discussion of the preparation of the card input is then presented, followed by a description of the input card format.

#### A.3.1 Dictionary of Input Variables

AMACH	free-stream Mach number; $3.0 \leq \text{AMACH} \leq 25.0$ is recommended
ANGN	the angle, in degrees, measuring the deviation of the free-stream magnetic field from the plane in which $B_{\infty 0}$ and $B_{\infty 1}$ lie; equal to $\tan^{-1}(B_{\infty 0} / \sqrt{ B_{\infty 0} ^2 +  B_{\infty 1} ^2})$
ANGP	the angle, in degrees, measuring the deviation of the in-plane magnetic component ( $B_{\infty 0}$ , + $B_{\infty 1}$ ) from the direction of flow; equal to $\tan^{-1}(B_{\infty 1} / B_{\infty 0})$

BCØN(I) KBCØN-dimensional array specifying values to be used for mag-  
 netic field strength contours

CN Courant number used for blunt body calculation; program default  
 value is 3.0

GAMMA free-stream ratio of specific heats

HRØ obstacle geometry indicator:
 

- HRØ > 0 - ionopause with  $H/R_0 = HRØ$
- HRØ = 0 - magnetopause equatorial trace
- HRØ < 0 - geometry is user-supplied

ITER integer, number of iterations for blunt body calculation;  
 program default value is 300

KBCØN integer, number of values specified for magnetic field contours;  
 $0 \leq KBCØN \leq 20$

KRCØN integer, number of values specified for density contours;  
 $0 \leq KRCØN \leq 20$

KVCØN integer, number of values specified for velocity contours;  
 $0 \leq KVCØN \leq 20$

LPLOT logical variable indicating whether to create plots or plot file
 

- FALSE - no
- TRUE - yes

LPRB logical variable indicating whether to print magnetic field  
 output
 

- FALSE - no
- TRUE - yes

LPRCØN logical variable indicating whether to print coordinates of  
 contour lines
 

- FALSE - no
- TRUE - yes

LPRFL logical variable indicating whether to print detailed flow field  
 output
 

- FALSE - no
- TRUE - yes

LPRST logical variable indicating whether to print coordinates of  
 streamlines
 

- FALSE - no
- TRUE - yes



## APPENDIX A

LRERUN	logical variable indicating whether this case uses rerun option FALSE - perform blunt body and marching calculations TRUE - read results of a previous calculation from TAPE4
NBLUNT	integer, number of angular mesh points for blunt body calculation; for user-supplied geometry, $XX(NBLUNT-1)=0.0$ ; program default value, and maximum, is 24
NBØD	integer, number of points in body shape table when geometry is user-supplied; $1 \leq NBØD \leq 100$
NCASE	integer, number of cases to be run consecutively; $NCASE \geq 1$
NR	integer, number of radial mesh points; program default value, and maximum, is 19
RCØN(I)	KRCØN - dimensional array specifying values to be used for density contours
RR(I)	NBØD - dimensional array representing the R-locations, in cylindrical (x,R) coordinates, of the user-supplied body shape
TITLE	descriptive heading of the case, to be printed on the first page of output; may contain up to 80 characters, including blanks
VCØN(I)	KVCØN - dimensional array specifying values to be used for velocity contours
XCALC	terminal downstream x-location for marching calculation of flow field; $XCALC < 0.0$ ; program default value is -1.0
XPLØT	terminal downstream x-location for calculation of streamlines, magnetic field, and contours; $XCALC \leq XPLØT < 0.0$ ; program default value is -1.0
XX(I)	NBØD - dimensional array representing the x-locations, in cylindrical (x,R) coordinates, of the user-supplied body shape

### A.3.2 Preparation of Input Data

The card input for a run consists of one card containing the number of cases to be run consecutively, Item 0, followed by a set of input for each case, Item 1 through Item 7, and Item 8 if required. Where a default value is to be used, the input field should be left blank. For each case, all required variables which do not assume their default values should be specified. The input format for all cards is described in section A.3.3.

Item 0 - This item consists of one card, containing the number of cases in this run, NCASE.

Item 1 - This card provides identification of the case, TITLE, which is printed on the first page of the output for this case.

Item 2 - This card contains information on the flow conditions and body geometry, and parameters required for the blunt body and marching calculations. AMACH, GAMMA, and HRØ must be specified for each case. For the rerun option, the values are tested against the values from the rerun file. The parameters XCALC, NR, NBLUNT, CN, ITER are used only when the flow field is to be calculated. These variables each assume a default value if the input field is blank.

Item 3 - This item consists of one card containing the rerun indicator, LRERUN, and the output control variables LPRFL, LPRST, LPRCØN, LPRB, and LPLØT.

Item 4 - This card contains the variables XPLØT, ANGP, and ANGN. The value for XPLØT is changed by the program to be the x-location of the marching calculation immediately upstream of the input value for XPLØT. The angles describing the deviation of the magnetic field from the flow, ANGP and ANGN, are not required when LPRB=.FALSE. and KBCØN=0, since the magnetic field is not calculated under these conditions. ANGP is the angle between the vectors  $(B_{\infty\perp} + B_{\infty\parallel})$  and  $v_{\infty}$ , while ANGN is the angle between  $B_{\infty}$  and  $(B_{\infty\perp} + B_{\infty\parallel})$ , where  $B_{\infty\parallel}$ ,  $B_{\infty\perp}$ ,  $B_{\infty n}$  are the components of the free-stream magnetic field,  $B_{\infty}$ , which are parallel, perpendicular, and normal to  $v_{\infty}$ , and are as indicated in figure 4 of the text. The two angles ANGP and ANGN fully determine the half plane for which the magnetic field is to be calculated. The magnetic field for the other half of the plane may be calculated by rerunning with the sign of ANGP reversed. When  $(B_{\infty\perp} + B_{\infty\parallel}) = 0$ ,  $ANGN = \pm 90^\circ$ ,  $ANGP = 0^\circ$ ; and, when  $B_{\infty n} = 0$ ,  $ANGN = 0^\circ$ .

Item 5 - This item contains the values for the velocity contours. The first card contains KVCØN, the number of values specified for VCØN. If KVCØN=0, only this card is required, and no velocity contours are calculated. If KVCØN > 0, the contour values are then read. Up to three cards may be required to accommodate the values, eight per card, maximum of 20. The contour values should be monotonically increasing, with at least one value within the range of the magnitude of the velocity in the region for which contours are to be calculated.

Item 6 - This item contains the values for the density contours. The description is similar to that for item 5, with KRCØN being the number of values specified, and RCØN the array of values.

Item 7 - This item contains the values for the magnetic field contours. The description is similar to that for item 5, with KBCØN

## APPENDIX A

being the number of values specified, and BCØN the array of values. Note that the same contour values are used for the parallel and perpendicular components.

Item 8 - This optional item is required when  $HRØ < 0.0$  and  $LRERUN = .FALSE.$ , and contains the body shape table for the user-supplied geometry. The first card contains NBØD, the number of points in the shape table. The next NBØD cards contain the cylindrical (x,R) coordinates of these points, (XX(I), RR(I)), one point per card. The points supplied by the user determine the  $\theta$ -spacing of the mesh used for the blunt body calculation. The first point should be near, but not on, the x-axis. A suggested location is such that the  $\theta$ -spacing between the first point and the x-axis is half the  $\theta$ -spacing between the first two points. The blunt body calculation adds a point which is the reflection about the x-axis of the first point in the body shape table. The (NBLUNT-1)<sup>th</sup> point should be at  $x=0.0$ . The BLUNT<sup>th</sup> point is also used to create the grid for the blunt body calculation. The coordinates must be normalized so that the planet center is at (0.,0.) and the nose of the body at (1.,0.).

### A.3.3 Format of Input Data

Four format types are used for the input data. For real numbers (F-format), a decimal point is required. Integers (I-format) should be right-adjusted in the field. For logical variables (L-format), the first non-blank character in the field, which should be 'T' or 'F', determines the value. Note that a blank input field is interpreted as 'FALSE'. The title, which is in A-format, may contain any valid character.

A description of the card format of the input data follows, with item numbers corresponding to those in section A.3.2:

Item No. 0: 1 card

Variable	NCASE
Card Column	10
Format Type	I

Item No. 1: 1 card

Variable	TITLE			
Card Column	1			
Format Type	A			

Item No. 2: 1 card

Variable	AMACH	GAMMA	HRØ	XCALC	NR	NBLUNT	CN	ITER
Card Column	10	20	30	40	50	60	70	80
Format Type	F	F	F	F	I	I	F	I

Item No. 3: 1 card

Variable	LRERUN	LPRL	LPRST	LPRCØN	LPRB	LPLØT
Card Column	10	20	30	40	50	60
Format Type	L	L	L	L	L	L

Item No. 4: 1 card

Variable	XPLØT	ANGP	ANGN
Card Column	10	20	30
Format Type	F	F	F

Item No. 5:

Variable	KVCØN
Card Column	10
Format Type	I

(1) 1 card

(2) 0 to 3 cards as needed for up to 20 values, 8 per card

Variable	VCØN(1)	VCØN(2)	VCØN(KVCØN)
Card Column	10	20	30
Format Type	F	F	F

	40	50	60	70	80
	F	F	F	F	F

Input Data Card Format

Item No. 6:

(1) 1 card

Variable	KRCØN
Card Column	10
Format Type	I

Variable  
Card Column  
Format Type

(2) 0 to 3 cards as needed for up to 20 values, 8 per card

Variable	RCØN(1)	RCØN(2)	RCØN(KRCØN)		
Card Column	10	20	30	40	50
Format Type	F	F	F	F	F
					70
					80
					F
					F

Item No. 7:

(1) 1 card

Variable	KRCØN
Card Column	10
Format Type	I

Variable  
Card Column  
Format Type

(2) 0 to 3 cards as needed for up to 20 values, 8 per card

Variable	BCØN(1)	BCØN(2)	BCØN(KBCØN)		
Card Column	10	20	30	40	50
Format Type	F	F	F	F	F
					70
					80
					F
					F

Item No. 8: (required only when HRØ < 0.0 and LRERUN=.FALSE.)  
(1) 1 card

Variable	NBØD
Card Column	10
Format Type	I

Variable  
Card Column  
Format Type

(2) I = 1 to NBØD; NBØD cards

Variable	XX(I)	RR(I)
Card Column	10	20
Format Type	F	F

Variable  
Card Column  
Format Type

#### A.4 Description of Output

This section describes the output of the computer program. The contents of each output item are specified and discussed. The printed output consists of six items, four of which are optional, with input control parameters. Plotted output is also optional.

The first output item consists of the input data. The title for the case is printed first, followed by all input variables, with identification of each variable. Default values are printed as if they were input. Parameters CN, NR, NBLUNT, ITER for the blunt body calculation and XCALC, the terminal location for the marching calculation, are printed only when the flow field is to be calculated. When the geometry is user-supplied, the input body shape table is printed. For a default geometry, the body shape is indicated by the description "default magnetopause coordinates - equatorial trace" or "default ionopause coordinates -  $H/R\emptyset =$  ".

The second output item is not printed when LRERUN=.TRUE. From the blunt body calculation, the shock speed at each iteration, the final enthalpy error, final sonic line location, and body and final bow shock shape are printed. For convergence criteria of this calculation, the downstream location and body and shock ordinates are output. There is no control variable allowing the user to suppress this item of output when the flow field is calculated.

Detailed flow field output is the third item, and is printed only when LPRFL=.TRUE. Coordinates are labeled as X/D, R/D, RP/D, or X/RO, R/RO, RP/RO, to emphasize that distances are normalized by the distance from the center of the planet to the nose of the body, D for the magnetopause, RO for an ionopause. Along the symmetry axis, the values printed are velocity magnitude  $V/V_{\text{INF}}$ , density  $RH\emptyset/RH\emptyset_{\text{INF}}$ , temperature  $T/T_{\text{INF}}$ , and pressure  $P/P_{\text{INF}}$ . Over the rest of the flow field values are also given for velocity components  $VX/V_{\text{INF}}$ ,  $VR/V_{\text{INF}}$ , and flow angle  $\phi$ . Note that the flow angle is the deviation of the flow about the obstacle, and so  $0^\circ \leq \phi < 90^\circ$ .

The next output item is the (x,R) coordinates of the streamlines. For the blunt body region, the  $(R_p, \theta)$  coordinates of the starting position on the bow shock wave are also given. This item is printed only when LPRST=.TRUE.

## APPENDIX A

The magnetic field components are then printed, if LPRB=.TRUE. . The location of each point is defined in  $(R_p, \theta)$  coordinates for the blunt body region, and  $(x, R)$  coordinates for the downstream marching region. The components along field lines parallel, perpendicular, and normal to the flow in the free stream are printed as B/BINF(PARALLEL), B/BINF(PERP), B/BINF(NORMAL). The orthogonal  $(x, y, z)$  components of the resultant are printed as BX/BINF(RESULTANT), BY/BINF(RESULTANT), BZ/BINF(RESULTANT). The magnetic field in the symmetry  $(x, y)$  plane, defined by the vector sum  $\{(B/B_\infty)_x + (B/B_\infty)_y\}$ , is also printed, and is given by the magnitude B/BINF(IN-PLANE) and direction B-ANGLE(IN-PLANE) of the vector. The B-ANGLE  $\psi$  is the angle between the magnetic field and the flow, and generally has the same sign as ANGP.

The last item printed is the  $(x, R)$  coordinates of the contours, for which LPRCON is the logical control variable. Noting that temperature and velocity contours coincide, the corresponding value of T/TINF is printed along with V/VINF for the velocity contours. There are three nonfatal error messages which may occur - see section A.5.

The program also has the capability of producing plotted output, using UCC plot routines AXIS, CHAR, DASH, DDTLN, ENPLT, GREEK, MATH, NUMPLT, PLPT, PLTLN, POLAR, SCALF, VECTOR. Plots are not produced when LPLPT=.FALSE. The plots provide pictorial representation of the streamlines and contours, with a maximum of six frames produced. The first frame is a plot of the streamlines. Then contour plots of velocity, temperature, and density are drawn. The last two frames are contour plots of the parallel and perpendicular magnetic field components, with field lines added to indicate direction. Frames are omitted when no contour levels are provided.

### A.5 Program Error Messages

This section lists the messages printed by the program, and indicates what action should be taken by the user.

- (1) \*\*\*\*\* EXECUTION TERMINATED \*\*\*\*\*  
 RERUN DATA ON TAPE4 DOES NOT AGREE  
 WITH CASE SPECIFIED ON CARD INPUT:  
 MACH NØ. GAMMA M/RO

FROM CARDS  
 FROM TAPE4

The first three parameters of item 2 of the input for a case using the rerun option should agree with those used when creating the file. The tolerance used in comparing the values is  $10^{-5}$ . For a user-supplied geometry, it is sufficient for both values of H/R<sub>0</sub> to be negative.

- (2) \*\*\*\*\* EXECUTION TERMINATED \*\*\*\*\*  
 ARRAY OF CONTOUR VALUES IMPROPERLY SPECIFIED

When specified, the contour values should be monotonically increasing, with at least one value in the range of the velocity, density, or magnetic field strength for the region under consideration. This error does not inhibit generation of the rerun file.

- (3) CONTOUR SEARCH ABORTED - TABLE OVERFLOW IN NAD

The program allows for 29 contour lines to be found, storing the starting address of each contour in array NAD. This message indicates that at least one more contour line could be found. If the user requires all the contours of the levels specified, the case should be rerun in two parts. Otherwise, reduce the number of contour levels specified.

- (4) CONTOUR SEARCH ABORTED - TABLE OVERFLOW IN (X,Y)

The contour lines may be described by up to 1000 points, stored in arrays X and Y. This message indicates that more points would be required for the contour lines requested. The last contour line found will be incomplete. As with (3), either reduce the number of contour levels or run as two cases.

- (5) NEGATIVE PRESSURE DETECTED BY SHOCK AT J=  
 PN= PØ= PTAU=

This message is printed when a negative pressure has been calculated at the shock on this iteration, at radial location J. The quantities printed are: PN, the pressure calculated on this step; PØ, the pressure from the previous step; and PTAU, the partial derivative of pressure with



## APPENDIX A

respect to time. This condition indicates that the shock wave motion is too extreme. Lowering the value of CN, and thus reducing the time step, may remove the problem.

The following messages (6)-(10) usually result from using an obstacle geometry which is in some way too severe for the program to handle in its present form. The obstacle slope may be sufficiently high at  $x = 0.0$  that the axial Mach number becomes subsonic in the starting solution for the marching calculation, or there may be a sharp corner in the profile. Check input, particularly free stream Mach number and body geometry.

(6) NEGATIVE PRESSURE  $\emptyset$ N B $\emptyset$ DY DETECTED BY BNDRY, PB= AT J=

This message indicates that a negative pressure on the body, PB, has been calculated at radial location J.

(7) NEGATIVE PRESSURE  $\emptyset$ R DENSITY  $\emptyset$ N B $\emptyset$ DY DETECTED BY BNDRYM AT X=  
PB= RH $\emptyset$ B= VXB= VRB=

The program makes internal corrections when this condition occurs, resulting pressure PB, density RH $\emptyset$ B, and velocity components VXB and VRB.

(8) NEGATIVE SIGMA-BAR-1 IN EIGENM INDICATES SUBS $\emptyset$ NIC FL $\emptyset$ W AT I=

(9) NEGATIVE SIGMA-BAR-2 IN EIGENM INDICATES SUBS $\emptyset$ NIC FL $\emptyset$ W AT I=

These messages are printed when subsonic flow is detected by the marching calculation. The computed stepsize for this region will be quite small.

(10) -----BODY TURN STOPPED AT M2=100-----

This message indicates that the body has a sharp corner, which has been limited to  $100^\circ$  when being transformed.

### A.6 Sample Case

A sample case is presented in this section. Figures A.1, A.2, and A.3 illustrate the input data, portions of the printed output, and the plotted output, respectively.

The sample case is run alone and is set up so as to produce all possible output. Flow is to be calculated about the rotated equatorial

trace of the magnetopause to a downstream location of  $x = -10.0$ , with  $M_\infty = 8$ ,  $\gamma = 5/3$ . Streamlines, magnetic field components, and contours are desired to a downstream location of  $x = -5.0$ . The magnetic field forms angles of  $\alpha_p = -45^\circ$ ,  $\alpha_n = 45^\circ$  with the solar wind flow. Contour values are specified for all quantities.

The input data is tabulated in figure A.1, with item numbers corresponding to those in sections A.3.2 and A.3.3. The first card, item 0, indicates that there is one case to be run. The remaining 13 cards provide the data required for this case. Item 1 contains the identifying title. On the next card, item 2, values are specified for AMACH, GAM, HRØ, and XCALC. The other data fields are left blank to indicate that the default values will be used. The values of the logical variables of item 3 specify that the flow field is to be calculated, and that full printed and plotted output is to be produced. Item 4 defines the plot length to be  $-5.0$ , and the magnetic field angles as ANGP =  $-45.0$  and ANGN =  $45.0$ . Items 5, 6, 7 specify the contour levels to be used - 12 for velocity and temperature, 10 for density, and 12 for magnetic field strength. Item 8 is omitted, since the obstacle geometry is one of the default shapes for which the coordinates are calculated internally by the program.

Figure A.2 presents portions of the printed output from the sample case using the data deck of figure A.1. The full printed output for this case is approximately 5,000 lines. The first item of printed output, figure A.2(a), is the input variables. Then in figure A.2(b), the output from the blunt body calculation is shown, omitting shock speed values for iterations 6 to 295. Note that the convergence criteria described in section A.2.4 are satisfied. Figure A.2(c) provides the output from the marching calculation. Figures A.2(d), (e), (f) show the detailed flow field output in four areas: near the symmetry axis; near  $x = 0.0$ , when the two calculation schemes are joined; around  $x = -5.0$ , the value of XPLØT; and the last two locations calculated. An example of the streamline output is shown in figures A.2(g), (h). Figures A.2(h), (i), (j) provide the magnetic field components at the same locations chosen to illustrate the flow field output. Examples of the printed output of the contour lines are shown in figures A.2(k), (l), (m), choosing two contour lines for each quantity. Note that for  $(|B|/B_\infty)_\perp$ , the different contour lines for the same contour level are considered to be two separate and distinct lines.

Figure A.3 shows the six plots which are produced by the program for this case.

APPENDIX A

Item No.	Column No.	10	20	30	40	50	60	70	80
0		1							
1		SAMPLE CASE		DEFAULT MAGNETØPAUSE EQUATØRIAL TRACE					
2	8.0	1.666666667	0.0	-10.0					
3	FALSE	TRUE	TRUE	TRUE	TRUE	TRUE			
4	-5.0	-45.0	45.0						
5		12							
	0.1	0.2	0.3	0.4	0.5	0.6	0.7	0.75	
	0.8	0.85	0.88	0.9					
6		-10							
	0.8	1.2	1.6	2.0	2.5	3.0	3.5	3.8	
	4.0	4.2							
7		12							
	0.5	0.75	1.0	1.25	1.5	2.0	2.5	3.0	
	3.5	4.0	5.0	6.0					

Figure A-1. - Card input for sample case.

FIGURE A.2

## ABBREVIATED OUTPUT FOR SAMPLE CASE

SAMPLE CASE      DEFAULT MAGNETOPAUSE EQUATORIAL TRACE

INPUT VARIABLES  
\*\*\*\*\*

FREESTREAM MACH NO. = 8.00  
 SPECIFIC HEAT RATIO = 1.667  
 OBSTACLE GEOMETRY: DEFAULT MAGNETOPAUSE COORDINATES - EQUATORIAL TRACE  
 PARAMETERS FOR BLUNT BODY CALCULATION  
     NO. OF RADIAL MESH POINTS = 17  
     NO. OF ANGULAR MESH POINTS = 24  
     COURANT NUMBER            = 3.00  
     NO. OF ITERATIONS         = 300  
 TERMINAL DOWNSTREAM LOCATION FOR MARCHING CALCULATION = -10.00  
 TERMINAL DOWNSTREAM LOCATION FOR PLOTTING = -5.00  
 IN-PLANE DEVIATION OF MAGNETIC FIELD FROM FLOW = -45.00 DEGREES  
 DEVIATION OF MAGNETIC FIELD FROM PLANE OF FLOW = 45.00 DEGREES  
 LRRUN = F  
 LPRFL = T  
 LPRST = T  
 LPRCON = T  
 LPRB = T  
 LPLUT = T

VALUES SPECIFIED FOR CONTOUR CALCULATION  
\*\*\*\*\*

## 12 CONTOUR LEVELS FOR VELOCITY:

.200	.250	.300	.400	.500	.600
.700	.750	.800	.850	.900	.950

## 12 CONTOUR LEVELS FOR DENSITY:

.800	1.200	1.600	2.000	2.500	3.000
3.500	3.600	4.100	4.200		

## 12 CONTOUR LEVELS FOR MAGNETIC FIELD STRENGTH:

.500	.750	1.000	1.250	1.500	2.000
2.500	3.000	3.500	4.000	5.000	6.000

Figure A.2(a)

BLUNT BODY CALCULATION  
\*\*\*\*\*

ITERATION 1	RMS OF SHOCK SPEED= 1.2458E-02	MAXIMUM SHOCK SPEED= 3.6519E-02 AT J=25
ITERATION 2	RMS OF SHOCK SPEED= 1.2445E-02	MAXIMUM SHOCK SPEED= 3.1748E-02 AT J=25
ITERATION 3	RMS OF SHOCK SPEED= 2.1994E-02	MAXIMUM SHOCK SPEED= 3.2075E-02 AT J=25
ITERATION 4	RMS OF SHOCK SPEED= 3.4842E-02	MAXIMUM SHOCK SPEED= 5.0377E-02 AT J=16
ITERATION 5	RMS OF SHOCK SPEED= 4.9444E-02	MAXIMUM SHOCK SPEED= 7.2239E-02 AT J=16
ITERATION 296	RMS OF SHOCK SPEED= 3.7908E-03	MAXIMUM SHOCK SPEED= 9.6232E-03 AT J=10
ITERATION 297	RMS OF SHOCK SPEED= 3.7524E-03	MAXIMUM SHOCK SPEED= 9.1111E-03 AT J=15
ITERATION 298	RMS OF SHOCK SPEED= 3.7140E-03	MAXIMUM SHOCK SPEED= 9.1274E-03 AT J=17
ITERATION 299	RMS OF SHOCK SPEED= 3.6752E-03	MAXIMUM SHOCK SPEED= 8.9772E-03 AT J=17
ITERATION 300	RMS OF SHOCK SPEED= 3.6352E-03	MAXIMUM SHOCK SPEED= 8.6374E-03 AT J=14

FINAL SONIC LINE LOCATION

XSL= .5982	RSL= .9649
XSL= .6171	RSL= .9571
XSL= .6347	RSL= .9702
XSL= .6541	RSL= .9812
XSL= .6742	RSL= .9909
XSL= .6959	RSL= .9988
XSL= .7187	RSL= 1.0043
XSL= .7425	RSL= 1.0081
XSL= .7665	RSL= 1.0117
XSL= .7914	RSL= 1.0154
XSL= .8172	RSL= 1.0191
XSL= .8437	RSL= 1.0228
XSL= .8694	RSL= 1.0264
XSL= .8967	RSL= .9951
XSL= .9246	RSL= .9871
XSL= .9518	RSL= .9774
XSL= .9795	RSL= .9661
XSL= 1.0077	RSL= .9529
XSL= 1.0370	RSL= .9372

<<<< X ERROR IN HT = .3822E+01 RMS OF X ERROR IN HT = .6475E-01 >>>>

BODY AND FINAL SHOCK SHAPE

J	X(BODY)	R(BODY)	X(SHOCK)	R(SHOCK)
2	-.9995	.0349	-1.2775	.0444
3	-.9597	.1046	-1.2662	.1331
4	-.9879	.1742	-1.2592	.2218
5	-.9754	.2434	-1.2456	.3136
6	-.9611	.3122	-1.2292	.3994
7	-.9447	.3815	-1.2032	.4882
8	-.9185	.4485	-1.1634	.5772
9	-.8925	.5147	-1.1137	.6661
10	-.8667	.5805	-1.0571	.7554
11	-.8250	.6453	-1.0014	.8449
12	-.7874	.7105	-1.0383	.9349
13	-.7448	.7713	-.9898	1.0250
14	-.6994	.8323	-.9357	1.1153
15	-.6480	.8939	-.8777	1.2082
16	-.5935	.9459	-.8130	1.3013
17	-.5359	1.0002	-.7418	1.3951
18	-.4723	1.0609	-.6643	1.4914
19	-.4054	1.1137	-.5793	1.5886
20	-.3340	1.1648	-.4844	1.6892
21	-.2531	1.2138	-.3819	1.7922
22	-.1772	1.2611	-.2668	1.8987
23	-.0973	1.3067	-.1425	2.0088
24	.0000	1.3491	-.0000	2.1245

Figure A.2(b) - continued

MARCHING CALCULATION  
 \*\*\*\*\*

STEP NO.	DOWNSTREAM LOCATION	BODY ORDINATE	SHOCK ORDINATE
1	-0.302	1.3622	2.1483
2	-0.604	1.3751	2.1719
3	-0.906	1.3874	2.1951
4	-1.206	1.3993	2.2181
5	-1.510	1.4108	2.2408
6	-1.812	1.4219	2.2633
7	-2.114	1.4326	2.2855
8	-2.416	1.4430	2.3074
9	-2.718	1.4531	2.3292
10	-3.023	1.4639	2.3511
11	-3.328	1.4743	2.3729
12	-3.632	1.4848	2.3949
13	-3.937	1.4949	2.4169
14	-4.242	1.5052	2.4383
15	-4.546	1.5148	2.4592
16	-4.851	1.5246	2.4815
17	-5.156	1.5338	2.5033
18	-5.460	1.5433	2.5247
19	-5.765	1.5524	2.5466
20	-6.069	1.5618	2.5679
21	-6.373	1.5713	2.5891
22	-6.677	1.5807	2.6102
23	-6.981	1.5904	2.6312
24	-7.285	1.5999	2.6523
25	-7.589	1.6097	2.6734
26	-7.893	1.6187	2.6944
27	-8.197	1.6277	2.7154
28	-8.501	1.6369	2.7364
29	-8.805	1.6459	2.7574
30	-9.109	1.6552	2.7784
31	-9.413	1.6643	2.7994
32	-9.717	1.6736	2.8204
33	-10.021	1.6828	2.8414
34	-10.325	1.6921	2.8624
35	-10.629	1.7013	2.8834
36	-10.933	1.7107	2.9044
37	-11.237	1.7199	2.9254
38	-11.541	1.7293	2.9464
39	-11.845	1.7387	2.9674
40	-12.149	1.7481	2.9884
41	-12.453	1.7573	3.0094
42	-12.757	1.7667	3.0304
43	-13.061	1.7759	3.0514
44	-13.365	1.7853	3.0724
45	-13.669	1.7947	3.0934
46	-13.973	1.8041	3.1144
47	-14.277	1.8135	3.1354
48	-14.581	1.8229	3.1564
49	-14.885	1.8323	3.1774
50	-15.189	1.8417	3.1984
51	-15.493	1.8511	3.2194
52	-15.797	1.8605	3.2404
53	-16.101	1.8699	3.2614
54	-16.405	1.8793	3.2824
55	-16.709	1.8887	3.3034
56	-17.013	1.8981	3.3244
57	-17.317	1.9075	3.3454
58	-17.621	1.9169	3.3664
59	-17.925	1.9263	3.3874
60	-18.229	1.9357	3.4084

Figure A.2(c) - continued

DETAILED FLOW FIELD OUTPUT  
\*\*\*\*\*

FLOW FIELD VALUES EXTRAPOLATED TO SYMMETRY AXIS, THETA = 2.00 DEGREES

I	X/D	V/VINF	RHO/RHOINF	T/TINF	P/PINF
1	1.0000	1.0000	4.2291	22.3333	94.4497
2	1.0150	.01e4	4.2200	22.3276	94.2214
3	1.0301	.03e7	4.2156	22.3133	94.0645
4	1.0451	.0451	4.2089	22.2899	93.8164
5	1.0602	.0597	4.1998	22.2572	93.4765
6	1.0752	.0745	4.1883	22.2149	93.0430
7	1.0903	.0894	4.1744	22.1629	92.5177
8	1.1053	.1043	4.1582	22.1012	91.9079
9	1.1204	.1192	4.1395	22.0300	91.1941
10	1.1354	.1341	4.1185	21.9494	90.3992
11	1.1505	.1490	4.0951	21.8599	89.5189
12	1.1655	.1637	4.0693	21.7618	88.5562
13	1.1805	.1782	4.0412	21.6558	87.5148
14	1.1956	.1925	4.0106	21.5424	86.3989
15	1.2106	.2066	3.9777	21.4225	85.2129
16	1.2257	.2204	3.9424	21.2969	83.9618
17	1.2407	.2339	3.9048	21.1666	82.6538
18	1.2558	.2469	3.8647	21.0326	81.2854
19	1.2708	.2617	3.8209	20.8721	79.7595

FLOW FIELD VALUES FROM BLUNT BODY CALCULATION

ANGULAR LOCATION NO. 2, AT THETA = 2.0000 DEGREES

I	RP/D	R/D	X/D	VR/VINF	VX/VINF	FLOW ANGLE	V/VINF	RHO/RHOINF	T/TINF	P/PINF
1	1.0000	.0349	.9995	.0117	.0003	88.4170	.0103	4.2264	22.3311	94.3802
2	1.0152	.0354	1.0146	.0179	.0159	48.3361	.0245	4.2230	22.3206	94.2596
3	1.0302	.0360	1.0296	.0198	.0315	32.0664	.0386	4.2175	22.3016	94.0567
4	1.0453	.0365	1.0446	.0194	.0486	21.7493	.0526	4.2099	22.2742	93.7714
5	1.0603	.0370	1.0597	.0184	.0638	16.1277	.0667	4.2001	22.2384	93.4034
6	1.0754	.0375	1.0747	.0181	.0788	12.9421	.0808	4.1982	22.1941	92.9527
7	1.0904	.0381	1.0898	.0179	.0934	10.8570	.0948	4.1740	22.1415	92.4194
8	1.1055	.0386	1.1048	.0177	.1079	9.3428	.1088	4.1577	22.0806	91.8036
9	1.1205	.0391	1.1199	.0176	.1221	8.1878	.1228	4.1390	22.0114	91.1056
10	1.1356	.0396	1.1349	.0174	.1361	7.2935	.1368	4.1181	21.9339	90.3258
11	1.1507	.0402	1.1499	.0173	.1501	6.5784	.1508	4.0948	21.8482	89.4648
12	1.1657	.0407	1.1650	.0172	.1639	5.9916	.1648	4.0692	21.7542	88.5233
13	1.1808	.0412	1.1800	.0171	.1778	5.4997	.1787	4.0413	21.6521	87.5019
14	1.1958	.0417	1.1951	.0170	.1916	5.0828	.1926	4.0109	21.5419	86.4017
15	1.2109	.0423	1.2101	.0170	.2054	4.7228	.2065	3.9780	21.4235	85.2237
16	1.2259	.0428	1.2252	.0169	.2193	4.4117	.2204	3.9428	21.2970	83.9689
17	1.2410	.0433	1.2402	.0169	.2334	4.1354	.2343	3.9050	21.1625	82.6387
18	1.2560	.0436	1.2553	.0169	.2474	3.9001	.2481	3.8646	21.0200	81.2346
19	1.2711	.0444	1.2703	.0169	.2621	3.6835	.2620	3.8218	20.8695	79.7581

ANGULAR LOCATION NO. 3, AT THETA = 6.0000 DEGREES

I	RP/D	R/D	X/D	VR/VINF	VX/VINF	FLOW ANGLE	V/VINF	RHO/RHOINF	T/TINF	P/PINF
1	1.0001	.1046	.9957	.0350	.0029	85.2522	.0409	4.2139	22.2977	93.9609
2	1.0153	.1042	1.0117	.0543	.0185	71.1386	.0525	4.2102	22.2745	93.7792
3	1.0304	.1038	1.0257	.0585	.0369	58.4397	.0642	4.2045	22.2454	93.5316
4	1.0455	.1034	1.0408	.0573	.0516	48.0188	.0760	4.1970	22.2102	93.2169
5	1.0606	.1030	1.0558	.0559	.0670	39.4164	.0878	4.1875	22.1689	92.8335
6	1.0757	.1025	1.0708	.0541	.0817	33.5384	.0997	4.1761	22.1212	92.3799
7	1.0908	.1021	1.0859	.0536	.0953	29.0690	.1117	4.1625	22.0670	91.8546
8	1.1059	.1017	1.1009	.0531	.1107	25.6199	.1239	4.1469	22.0058	91.2559
9	1.1221	.1013	1.1159	.0526	.1249	22.8317	.1362	4.1291	21.9376	90.5823
10	1.1372	.1009	1.1309	.0522	.1389	20.5983	.1487	4.1091	21.8619	89.8321
11	1.1522	.1004	1.1458	.0519	.1529	18.7485	.1613	4.0868	21.7784	89.0035
12	1.1674	.1000	1.1610	.0516	.1667	17.2044	.1741	4.0622	21.6886	88.0951
13	1.1825	.1000	1.1760	.0514	.1806	15.8878	.1871	4.0352	21.5863	87.1050
14	1.1976	.1000	1.1911	.0512	.1944	14.7565	.2004	4.0058	21.4768	86.0317
15	1.2128	.1000	1.2061	.0510	.2083	13.7666	.2139	3.9739	21.3576	84.8737
16	1.2279	.1000	1.2211	.0509	.2222	12.8966	.2276	3.9395	21.2282	83.6293
17	1.2430	.1000	1.2362	.0507	.2364	12.1097	.2416	3.9025	21.0881	82.2972
18	1.2581	.1000	1.2512	.0506	.2504	11.4144	.2559	3.8629	20.9364	80.8760
19	1.2732	.1000	1.2662	.0503	.2652	10.7386	.2705	3.8206	20.7726	79.3645

Figure A.2(d) - continued





APPENDIX A

ADDITIONAL AXIAL LOCATION NO.45, AT X/D = -4.6689

I	R/D	VR/VINF	VX/VINF	FLOW ANGLE	V/VINF	RHO/RHOINF	T/TINF	P/PINF
1	1.7691	.0073	.6043	.607	.9044	.4326	4.8848	2.1132
2	1.9171	.0155	.9173	.3494	.9077	.4504	4.7561	2.1421
3	2.0649	.0210	.9112	2.2599	.9114	.4728	4.6136	2.1813
4	2.2128	.0276	.9144	1.7062	.9148	.4989	4.4819	2.2358
5	2.3616	.0354	.9175	2.2076	.9182	.5317	4.3473	2.3116
6	2.5095	.0447	.9203	2.7800	.9214	.5726	4.2267	2.4167
7	2.6584	.0553	.9228	3.4322	.9244	.6236	4.1024	2.5584
8	2.8043	.0672	.9248	4.2552	.9272	.6871	3.9912	2.7422
9	2.9522	.0800	.9255	4.9335	.9299	.7652	3.8848	2.9725
10	3.1000	.0934	.9279	5.7464	.9325	.8603	3.7812	3.2531
11	3.2479	.1071	.9289	6.5772	.9351	.9753	3.6795	3.5887
12	3.3958	.1209	.9297	7.4113	.9376	1.1128	3.5822	3.9850
13	3.5437	.1347	.9302	8.2382	.9399	1.2753	3.4885	4.4490
14	3.6916	.1482	.9312	9.0545	.9419	1.4658	3.4052	4.9915
15	3.8394	.1614	.9299	9.8443	.9438	1.6855	3.3316	5.6155
16	3.9873	.1743	.9290	10.6241	.9452	1.9374	3.2740	6.3429
17	4.1352	.1872	.9275	11.3488	.9464	2.2159	3.2265	7.1496
18	4.2831	.1995	.9258	12.0355	.9468	2.5309	3.2082	8.1195
19	4.4310	.2119	.9240	12.7372	.9473	2.8557	3.1897	9.1089

ADDITIONAL AXIAL LOCATION NO.46, AT X/D = -4.9175

I	R/D	VR/VINF	VX/VINF	FLOW ANGLE	V/VINF	RHO/RHOINF	T/TINF	P/PINF
1	1.7710	.0113	.9155	.4016	.9055	.4269	4.8417	2.0669
2	1.9237	.0124	.9089	.7818	.9099	.4444	4.7070	2.1917
3	2.0765	.0168	.9125	1.1776	.9128	.4663	4.5583	2.2525
4	2.2293	.0220	.9161	1.6632	.9154	.4918	4.4183	2.1731
5	2.3820	.0334	.9194	2.0776	.9200	.5238	4.2764	2.2398
6	2.5348	.0422	.9225	2.5194	.9234	.5635	4.1412	2.3334
7	2.6875	.0514	.9252	3.2396	.9256	.6131	4.0151	2.4018
8	2.8403	.0630	.9274	3.9352	.9276	.6752	3.8974	2.0314
9	2.9931	.0713	.9293	4.6915	.9324	.7519	3.7863	2.8468
10	3.1456	.0854	.9309	5.4892	.9351	.8458	3.6798	3.1124
11	3.2981	.1030	.9320	6.3093	.9377	.9596	3.5770	3.4325
12	3.4512	.1116	.9328	7.1363	.9401	1.0960	3.4790	3.8131
13	3.6040	.1315	.9333	7.9591	.9424	1.2576	3.3879	4.2606
14	3.7568	.1441	.9333	9.7735	.9444	1.4472	3.3073	4.7862
15	3.9095	.1572	.9330	9.5633	.9461	1.6659	3.2371	5.3925
16	4.0623	.1701	.9320	10.3447	.9474	1.9168	3.1836	6.0123
17	4.2151	.1821	.9309	11.0702	.9485	2.1937	3.1406	6.8896
18	4.3679	.1945	.9287	11.8280	.9488	2.5068	3.1272	7.8393
19	4.5206	.2119	.9268	12.4641	.9492	2.8289	3.1137	8.8381

ADDITIONAL AXIAL LOCATION NO.59, AT X/D = -9.8284

I	R/D	VR/VINF	VX/VINF	FLOW ANGLE	V/VINF	RHO/RHOINF	T/TINF	P/PINF
1	1.7848	.0109	.9296	.3577	.9196	.3564	4.2931	1.5302
2	2.0220	.0113	.9249	.3892	.9245	.3738	4.0994	1.9322
3	2.2591	.0111	.9296	.5816	.9297	.3953	3.8951	1.5398
4	2.4963	.0117	.9348	.9635	.9349	.4208	3.6854	1.5508
5	2.7335	.0203	.9402	1.2367	.9404	.4519	3.4675	1.5071
6	2.9706	.0250	.9454	1.5168	.9458	.4890	3.2515	1.5922
7	3.2078	.0310	.9515	1.8183	.9519	.5334	3.0425	1.6229
8	3.4450	.0381	.9581	2.1318	.9557	.5867	2.8474	1.6705
9	3.6821	.0421	.9590	2.3163	.9600	.6516	2.6742	1.7426
10	3.9193	.0512	.9622	2.9890	.9635	.7321	2.5288	1.8514
11	4.1565	.0548	.9645	3.5531	.9663	.8218	2.4029	2.0069
12	4.3936	.0717	.9659	4.1939	.9685	.9536	2.3246	2.2466
13	4.6308	.0823	.9655	4.3767	.9700	1.0988	2.2598	2.4831
14	4.8680	.0945	.9654	4.5002	.9710	1.2693	2.2180	2.8154
15	5.1051	.1044	.9658	4.3153	.9726	1.4622	2.1942	3.2084
16	5.3423	.1186	.9643	7.2594	.9726	1.6837	2.1949	3.6890
17	5.5795	.1302	.9625	7.7513	.9713	1.9134	2.2068	4.2225
18	5.8166	.1424	.9598	8.4982	.9703	2.1720	2.2468	4.8800
19	6.0538	.1527	.9573	9.1393	.9694	2.4334	2.2863	5.5565

ADDITIONAL AXIAL LOCATION NO.60, AT X/D = -10.3000

I	R/D	VR/VINF	VX/VINF	FLOW ANGLE	V/VINF	RHO/RHOINF	T/TINF	P/PINF
1	1.7854	.0008	.9209	.0476	.9209	.3501	4.2424	1.4854
2	2.0329	.0101	.9259	.3733	.9259	.3676	4.0439	1.4866
3	2.2803	.0117	.9311	.6598	.9312	.3894	3.8350	1.4935
4	2.5278	.0152	.9365	.9330	.9356	.4154	3.6203	1.5039
5	2.7752	.0217	.9419	1.2185	.9421	.4472	3.3972	1.5191
6	3.0227	.0242	.9473	1.4646	.9476	.4951	3.1763	1.5447
7	3.2702	.0289	.9524	1.7406	.9529	.5302	2.9028	1.5710
8	3.5175	.0341	.9572	2.0415	.9578	.5841	2.7637	1.6143
9	3.7650	.0402	.9613	2.3948	.9621	.6491	2.5869	1.6799
10	4.0124	.0477	.9645	2.8314	.9637	.7288	2.4391	1.7777
11	4.2599	.0566	.9668	3.3631	.9635	.8273	2.3227	1.9215
12	4.5073	.0672	.9683	3.9775	.9706	.9475	2.2300	2.1186
13	4.7548	.0785	.9689	4.6429	.9721	1.0908	2.1742	2.3716
14	5.0022	.0914	.9688	5.3477	.9730	1.2587	2.1365	2.6891
15	5.2496	.1022	.9691	6.0493	.9735	1.4478	2.1171	3.0653
16	5.4971	.1144	.9690	6.7819	.9733	1.6615	2.1223	3.5262
17	5.7445	.1257	.9648	7.4643	.9735	1.8881	2.1385	4.0377
18	5.9920	.1377	.9621	8.2005	.9729	2.1395	2.1818	4.6679
19	6.2394	.1481	.9595	8.9371	.9709	2.3901	2.2247	5.3173

Figure A.2(f) - continued

STREAMLINE TRAJECTORY CALCULATION  
 \*\*\*\*\*

43 STREAMLINES CALCULATED

STREAMLINE NO. 1, STARTING AT X/D = 1.2723, R/D = .0444  
 (CORRESPONDS TO THETA = 2.00 DEGREES, RP/D = 1.2711)

X/D	R/D
1.2703	.0444
1.2403	.0465
1.2153	.0483
1.1903	.0515
1.1653	.0552
1.1403	.0600
1.1153	.0670
1.0903	.0730
1.0653	.0988
1.0403	.1233
1.0153	.1688
.9903	.2680
.9653	.3498
.9353	.4353
.9103	.4954
.8853	.5509
.8603	.6002
.8353	.6454
.8103	.6859
.7853	.7257
.7603	.7621
.7353	.7961
.7103	.8284
.6853	.8539
.6603	.8879
.6303	.9209
.6053	.9471
.5803	.9721
.5553	.9961
.5303	1.0191
.5053	1.0412
.4803	1.0624
.4553	1.0829
.4303	1.1026
.4053	1.1216
.3803	1.1400
.3553	1.1577
.3253	1.1782
.3003	1.1947
.2753	1.2106
.2503	1.2260
.2253	1.2409
.2003	1.2554
.1753	1.2694
.1503	1.2831
.1253	1.2962
.1003	1.3090
.0753	1.3214
.0503	1.3334
.0253	1.3451
-.0047	1.3530
-.0216	1.3542
-.0426	1.3577
-.0684	1.3538
-.0920	1.3509
-.1131	1.3503
-.12129	1.3543
-.14243	1.3673
-.15755	1.3936
-.18170	1.4093
-.20284	1.4223
-.22096	1.4316
-.24210	1.4407
-.26325	1.4484
-.28137	1.4541
-.30251	1.4597
-.32064	1.4639
-.34278	1.4681
-.36292	1.4713
-.38104	1.4746
-.40219	1.4774
-.42333	1.4799
-.44145	1.4819
-.46259	1.4839
-.48372	1.4859
-.49175	1.4865

Figure A.2(g) - continued

APPENDIX A

STREAMLINE NO.42, STARTING AT X/D = -4.3769, R/D = 4.3233

X/D	R/D
-4.3769	4.3233
-4.5683	4.3717
-4.7998	4.4187
-4.9175	4.4442

STREAMLINE NO.43, STARTING AT X/D = -4.6915, R/D = 4.4391

X/D	R/D
-4.6915	4.4391
-4.9029	4.4861
-4.9175	4.4893

MAGNETIC FIELD COMPONENTS  
\*\*\*\*\*

ANGULAR LOCATION NO. 1, AT THETA = 0.000 DEGREES

I	RP/D	B/BINF (PARALLEL)	B/BINF (PERP)	B/BINF (IN-PLANE)	B-ANGLE (IN-PLANE)	B/BINF (NORMAL)	BX/BINF (RESULTANT)	BY/BINF (RESULTANT)	BZ/BINF (RESULTANT)
1	1.0000	0.0000	0.0000	0.0000	0.0000	0.0000	0.0000	0.0000	0.0000
2	1.0156	0.0693	19.5068	13.7949	-89.7964	4.2200	0.0347	-9.7544	2.9846
3	1.0321	0.2292	15.3355	11.5321	-89.5076	4.2156	0.0646	-7.5177	2.9809
4	1.0485	0.4866	11.7067	8.2804	-89.0712	4.2089	0.0949	-5.8544	2.9761
5	1.0642	0.7419	8.6738	6.9841	-88.5445	4.1998	0.1254	-4.9369	2.9697
6	1.0792	0.9921	6.5664	6.0615	-87.9137	4.1885	0.1561	-4.0283	2.9616
7	1.0943	1.2371	4.8505	5.3667	-87.1821	4.1744	0.1865	-3.7903	2.9518
8	1.1093	1.4767	3.6434	4.8521	-86.3759	4.1582	0.2169	-3.4241	2.9403
9	1.1244	1.7106	2.8933	4.4951	-85.5100	4.1395	0.2468	-3.1476	2.9271
10	1.1394	1.9387	2.4912	4.2847	-84.6424	4.1185	0.2762	-2.9456	2.9122
11	1.1544	2.1611	2.3159	3.9241	-83.6888	4.0951	0.3052	-2.7580	2.8957
12	1.1693	2.3778	2.2139	3.7157	-82.7222	4.0693	0.3330	-2.6369	2.8775
13	1.1841	2.5889	2.1602	3.5301	-81.7056	4.0412	0.3601	-2.4721	2.8575
14	1.1988	2.7944	2.1254	3.3875	-80.7244	4.0106	0.3861	-2.3042	2.8360
15	1.2134	2.9944	2.1244	3.2454	-79.6958	3.9777	0.4111	-2.2096	2.8127
16	1.2277	3.1889	2.1401	3.1101	-78.6277	3.9424	0.4341	-2.1602	2.7877
17	1.2419	3.3782	2.1699	3.0185	-77.6478	3.9048	0.4566	-2.0850	2.7611
18	1.2558	3.5624	2.1799	2.9202	-76.6392	3.8647	0.4772	-2.0293	2.7328
19	1.2706	3.7411	3.0249	2.7928	-75.3336	3.8209	0.5000	-1.9104	2.7018

ANGULAR LOCATION NO. 2, AT THETA = 2.000 DEGREES

I	RP/D	B/BINF (PARALLEL)	B/BINF (PERP)	B/BINF (IN-PLANE)	B-ANGLE (IN-PLANE)	B/BINF (NORMAL)	BX/BINF (RESULTANT)	BY/BINF (RESULTANT)	BZ/BINF (RESULTANT)
1	1.0000	0.0000	0.0000	0.0000	0.0000	0.0000	0.0000	0.0000	0.0000
2	1.0152	0.0457	19.6130	13.3129	-91.2200	6.8133	-0.2680	-9.7650	4.8177
3	1.0302	0.1606	14.9735	11.5251	-93.7384	6.6524	-0.0959	-7.4417	4.7039
4	1.0453	0.2216	11.6901	8.2968	-97.0175	6.4249	-0.0118	-5.8231	4.5431
5	1.0603	0.2802	8.6697	6.9237	-99.2630	6.2297	0.0630	-4.8954	4.4051
6	1.0754	0.3363	6.5682	6.0071	-88.4334	6.0636	0.1172	-4.2450	4.2452
7	1.0904	0.3908	4.8690	5.3183	-87.0814	5.7595	0.1587	-3.7571	4.0514
8	1.1054	0.4422	3.8536	4.8053	-86.0891	5.5336	0.1962	-3.3922	3.9129
9	1.1204	0.5084	3.3059	4.4193	-85.7462	5.3252	0.2318	-3.1167	3.7655
10	1.1354	0.5653	3.0903	4.1350	-84.8951	5.1444	0.2602	-2.9123	3.6378
11	1.1504	0.6175	3.5201	3.8743	-84.0020	4.9735	0.2863	-2.7246	3.5168
12	1.1654	0.6714	3.2160	3.5645	-83.1898	4.8030	0.3073	-2.5729	3.3962
13	1.1804	0.7241	2.9449	3.4755	-82.3421	4.6355	0.3276	-2.4337	3.2916
14	1.1954	0.7725	2.7240	3.3267	-81.4203	4.5090	0.3512	-2.3275	3.1841
15	1.2104	0.8219	2.5131	3.1872	-80.4476	4.3604	0.3740	-2.2225	3.0830
16	1.2254	0.8650	2.3112	3.0529	-79.4317	4.2117	0.3971	-2.1219	2.9822
17	1.2404	0.9148	2.1574	2.9234	-78.3632	4.0825	0.4212	-2.0454	2.8888
18	1.2554	0.9589	2.0049	2.8555	-77.2813	3.9556	0.4446	-1.9696	2.7971
19	1.2711	1.0011	3.0248	2.7358	-75.0273	3.8218	0.4673	-1.8786	2.7024

Figure A.2(h) - continued

ANGULAR LOCATION NO. 3, AT THETA = 6.0000 DEGREES

I	RP/D	B/BINF (PARALLEL)	B/BINF (PERP)	B/BINF (IN-PLANE)	B-ANGLE (IN-PLANE)	B/BINF (NORMAL)	BX/BINF (RESULTANT)	BY/BINF (RESULTANT)	BZ/BINF (RESULTANT)
1	1.0011	.1723							
2	1.0163	.2211	19.7354	13.8038	-94.0993	12.0951	-.6977	-0.7358	8.5525
3	1.0314	.2700	14.8020	10.2979	-93.4057	11.6519	-.4326	-7.2588	8.2391
4	1.0465	.3188	11.6097	8.8349	-92.1443	10.9525	-.2126	-5.6776	7.7466
5	1.0616	.3676	9.8224	6.7739	-91.0505	10.3597	-.0878	-4.7891	7.3254
6	1.0767	.4164	8.5379	5.8698	-89.9227	8.6352	.0096	-4.1506	6.1060
7	1.0918	.4651	7.5758	5.1945	-88.9634	7.5921	.0664	-3.6725	5.3048
8	1.1069	.5138	6.8514	4.6877	-87.9932	6.8321	.1161	-3.3127	4.8310
9	1.1221	.5624	6.3034	4.3063	-87.0325	6.3063	.1576	-3.0459	4.4592
10	1.1372	.6108	5.8859	4.0167	-86.1842	5.9080	.1890	-2.8339	4.1776
11	1.1523	.6592	5.5298	3.7568	-85.2620	5.5322	.2194	-2.6474	3.9119
12	1.1674	.7073	5.2036	3.5460	-84.4222	5.1748	.2437	-2.4955	3.6591
13	1.1825	.7551	4.9275	3.3572	-83.4894	4.9048	.2692	-2.3586	3.4682
14	1.1976	.8027	4.7026	3.2041	-82.6489	4.6555	.2899	-2.2470	3.2919
15	1.2128	.8499	4.4867	3.0578	-81.7628	4.4481	.3098	-2.1399	3.1453
16	1.2279	.8966	4.2843	2.9220	-80.7752	4.2662	.3312	-2.0395	3.0166
17	1.2430	.9429	4.1259	2.8199	-79.6869	4.0980	.3583	-1.9615	2.8977
18	1.2581	.9885	3.9738	2.7231	-78.4669	3.9595	.3850	-1.8866	2.7998
19	1.2732	1.0334	3.8123	2.6216	-77.1723	3.8206	.4116	-1.8075	2.7016

ANGULAR LOCATION NO. 23, AT THETA = 86.0000 DEGREES

I	RP/D	B/BINF (PARALLEL)	B/BINF (PERP)	B/BINF (IN-PLANE)	B-ANGLE (IN-PLANE)	B/BINF (NORMAL)	BX/BINF (RESULTANT)	BY/BINF (RESULTANT)	BZ/BINF (RESULTANT)
1	1.3092	1.1539							
2	1.3484	1.2145	8.5172	5.1726	-149.3591	11.8723	-3.1469	-1.8541	8.3950
3	1.3875	1.2577	5.7915	5.2113	-146.2984	7.1832	-1.8891	-1.2599	5.0793
4	1.4266	1.3240	4.5546	2.3029	-142.7691	5.6294	-1.2965	-.9952	3.9806
5	1.4658	1.3738	3.6240	1.7525	-138.9333	4.8498	-.9343	-.8141	3.4293
6	1.5049	1.4376	3.3967	1.4204	-133.7244	4.3286	-.6942	-.7258	3.0698
7	1.5441	1.5057	3.1593	1.1903	-127.5731	4.0145	-.5132	-.6671	2.8387
8	1.5832	1.5787	2.9117	1.0309	-120.5963	3.7970	-.3707	-.6269	2.6849
9	1.6223	1.6509	2.7665	.9111	-112.9630	3.6526	-.2513	-.5931	2.5828
10	1.6615	1.7407	2.6534	.8274	-104.3051	3.5498	-.1446	-.5669	2.5101
11	1.7006	1.8307	2.5789	.7682	-95.5531	3.4850	-.0526	-.5437	2.4643
12	1.7397	1.9272	2.5202	.7392	-85.8703	3.4386	.0376	-.5213	2.4314
13	1.7789	2.0307	2.4826	.7373	-76.2889	3.4192	.1236	-.5065	2.4177
14	1.8180	2.1415	2.4593	.7494	-67.5293	3.4158	.2025	-.4897	2.4154
15	1.8571	2.2601	2.4524	.7576	-59.3933	3.4262	.2836	-.4793	2.4227
16	1.8963	2.3869	2.4456	.8376	-51.7332	3.4525	.3668	-.4650	2.4413
17	1.9354	2.5223	2.4446	.8986	-44.9234	3.4900	.4499	-.4487	2.4678
18	1.9745	2.6666	2.4489	.9694	-38.9013	3.5389	.5335	-.4305	2.5024
19	2.0137	2.8201	2.4452	1.0402	-33.6877	3.5964	.6162	-.4015	2.5430

ANGULAR LOCATION NO. 24, AT THETA = 90.0000 DEGREES

I	RP/D	B/BINF (PARALLEL)	B/BINF (PERP)	B/BINF (IN-PLANE)	B-ANGLE (IN-PLANE)	B/BINF (NORMAL)	BX/BINF (RESULTANT)	BY/BINF (RESULTANT)	BZ/BINF (RESULTANT)
1	1.3491	1.1925							
2	1.3922	1.2443	7.7661	4.6839	-151.7632	10.8083	-2.9163	-1.5700	7.6424
3	1.4352	1.1989	5.3267	2.9243	-148.1538	6.5661	-1.7565	-1.0912	4.6430
4	1.4783	1.2567	4.1933	2.0885	-144.2240	5.1963	-1.1981	-.8634	3.6744
5	1.5214	1.3184	3.5221	1.5802	-139.7697	4.4745	-.8530	-.7216	3.1639
6	1.5645	1.3844	3.1343	1.2765	-133.7249	4.0266	-.6239	-.6523	2.8472
7	1.6076	1.4552	2.8746	1.0666	-127.0528	3.7522	-.4544	-.6019	2.6932
8	1.6506	1.5314	2.7021	.9232	-119.2654	3.5687	-.3191	-.5695	2.5234
9	1.6937	1.6133	2.5728	.8176	-110.9357	3.4484	-.2066	-.5400	2.4384
10	1.7368	1.7016	2.4808	.7494	-101.2592	3.3707	-.1034	-.5197	2.3834
11	1.7799	1.7968	2.4151	.7039	-91.6648	3.3186	-.0145	-.4975	2.3466
12	1.8230	1.8992	2.3690	.6984	-80.6905	3.2934	.0799	-.4873	2.3302
13	1.8660	2.0195	2.3428	.6981	-71.5558	3.2924	.1562	-.4862	2.3281
14	1.9091	2.1281	2.3295	.7355	-62.1816	3.3035	.2427	-.4800	2.3359
15	1.9522	2.2554	2.3311	.7869	-54.2423	3.3327	.3251	-.4513	2.3565
16	1.9953	2.3920	2.3315	.8436	-46.9440	3.3742	.4073	-.4359	2.3859
17	2.0384	2.5383	2.3372	.9186	-40.4107	3.4282	.4946	-.4211	2.4241
18	2.0814	2.6946	2.3469	.9964	-34.6920	3.4919	.5793	-.4010	2.4691
19	2.1245	2.8613	2.3530	1.0732	-29.3214	3.5676	.6617	-.3716	2.5226

Figure A.2(1) - continued



VELOCITY AND TEMPERATURE CONTOURS  
\*\*\*\*\*

12 VELOCITY (TEMPERATURE) CONTOUR LINES FOUND

11 POINTS IN CONTOUR LINE OF V/VINF = .100, T/TINF = 22.120

X/D	R/D
.9853	.1901
1.0019	.1832
1.0109	.1783
1.0186	.1740
1.0353	.1664
1.0527	.1465
1.0707	.1133
1.0712	.1126
1.0856	.0614
1.0933	.0353
1.1010	0.0000

20 POINTS IN CONTOUR LINE OF V/VINF = .200, T/TINF = 21.480

X/D	R/D
.9447	.3497
.9614	.3489
.9785	.3462
.9961	.3417
1.0142	.3352
1.0328	.3266
1.0453	.3196
1.0516	.3155
1.0704	.3215
1.0897	.3144
1.1095	.2542
1.1151	.2780
1.1294	.2577
1.1498	.2253
1.1614	.2148
1.1705	.1811
1.1806	.1251
1.1913	.1212
1.2031	.0420
1.2136	0.0000

DENSITY CONTOURS  
\*\*\*\*\*

10 DENSITY CONTOUR LINES FOUND

9 POINTS IN CONTOUR LINE OF RHO/RHOINF = 4.200

X/D	R/D
.9930	.1282
1.0036	.1251
1.0247	.1171
1.0346	.1086
1.0417	.0925
1.0597	.0376
1.0598	.0376
1.0599	.0242
1.0599	0.0000

Figure A.2(k) - continued

APPENDIX A

27 POINTS IN CONTOUR LINE OF  $\rho/\rho_{\infty} = 4.000$

X/D	R/D
.9483	.3572
.9617	.3678
.9754	.3776
.9895	.3861
1.0039	.3933
1.0189	.3986
1.0344	.4016
1.0508	.4026
1.0681	.3977
1.0867	.3886
1.1071	.3722
1.1286	.3426
1.1508	.3406
1.1558	.2882
1.1559	.2881
1.1795	.2182
1.1874	.1641
1.1933	.1255
1.2101	.0419
1.2005	0.0000

MAGNETIC FIELD CONTOURS  
\*\*\*\*\*

11 MAGNETIC FIELD CONTOUR LINES FOUND  
(FOR COMPONENT ALONG FIELD LINES PARALLEL TO FLOW IN FREESTREAM)

13 POINTS IN CONTOUR LINE OF  $B/B_{\infty}$  (PARALLEL) = .900

X/D	R/D
.9789	.2283
.9954	.2226
1.0123	.2144
1.0296	.2033
1.0473	.1892
1.0654	.1754
1.0849	.1609
1.0831	.1405
1.0966	.1153
1.1018	.0983
1.1176	.0791
1.1202	.0668
1.1220	0.0000

19 POINTS IN CONTOUR LINE OF  $B/B_{\infty}$  (PARALLEL) = .750

X/D	R/D
.9513	.3464
.9684	.3437
.9860	.3391
1.0041	.3326
1.0122	.3289
1.0222	.3242
1.0403	.3126
1.0589	.3004
1.0780	.2845
1.0911	.2721
1.0973	.2651
1.1166	.2406
1.1364	.2116
1.1427	.2015
1.1564	.1691
1.1744	.1234
1.1767	.1108
1.1883	.0415
1.1892	0.0000

Figure A.2(1) - continued

12 MAGNETIC FIELD CONTOUR LINES FOUND  
 (FOR COMPONENT ALONG FIELD LINES PERPENDICULAR TO FLOW IN FREESTREAM)

45 POINTS IN CONTOUR LINE OF  $\delta/BIN$  (PERPENDICULAR) = 2.200

X/D	R/D
-1.8975	2.7899
-1.8527	1.7957
-1.7055	1.8142
-1.6156	1.8226
-1.5257	1.8283
-1.5027	1.8253
-1.4359	1.8246
-1.3459	1.8394
-1.2964	1.8414
-1.2667	1.8407
-1.1279	1.8396
-1.0762	1.8425
-0.9863	1.8446
-0.8404	1.8430
-0.8542	1.8409
-0.8165	1.8453
-0.7530	1.8480
-0.6996	1.8499
-0.6814	1.8500
-0.6461	1.8559
-0.5926	1.8625
-0.5428	1.8651
-0.5392	1.8728
-0.4857	1.8677
-0.4838	1.8882
-0.4322	1.9140
-0.4277	1.9165
-0.3885	1.9497
-0.3786	1.9667
-0.3651	1.9890
-0.3355	2.0345
-0.3628	2.0697
-0.3788	2.1363
-0.3845	2.1924
-0.4257	2.2261
-0.4322	2.2404
-0.4766	2.3274
-0.4857	2.3311
-0.5307	2.3978
-0.5392	2.4695
-0.5926	2.4803
-0.6496	2.5617
-0.6461	2.5431
-0.6996	2.6170
-0.7337	2.6567

6 POINTS IN CONTOUR LINE OF  $\delta/BIN$  (PERPENDICULAR) = 2.000

X/D	R/D
-3.6973	1.8865
-3.4232	1.9133
-4.1718	1.9388
-4.4214	1.9599
-4.6655	1.9766
-4.9175	1.9883

Figure A.2(m) - concluded



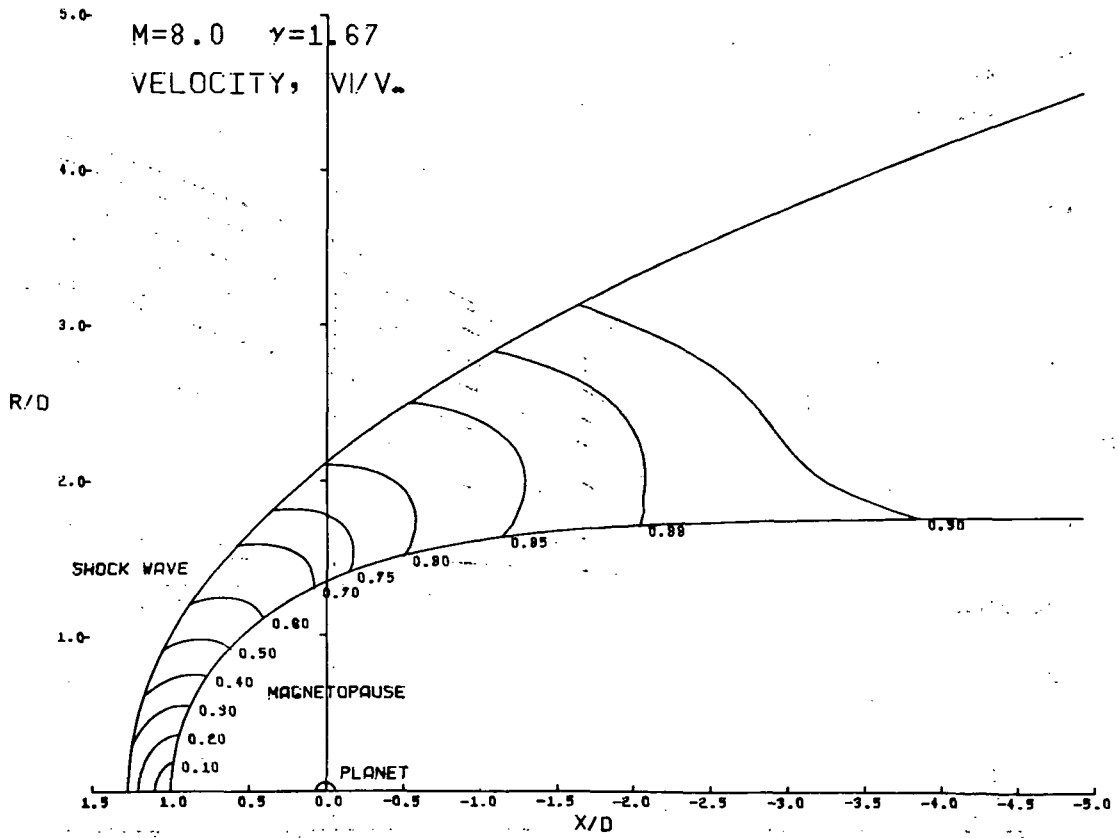
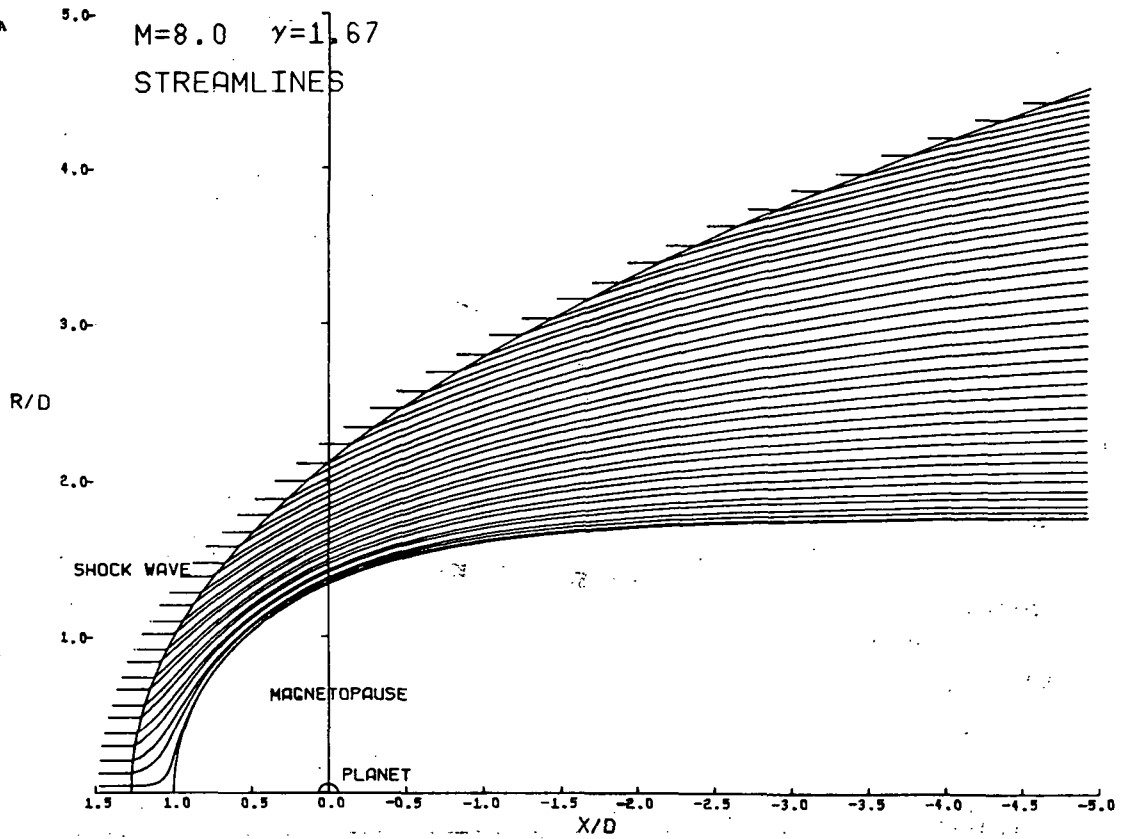


Figure A.3. - Plot output for sample case.

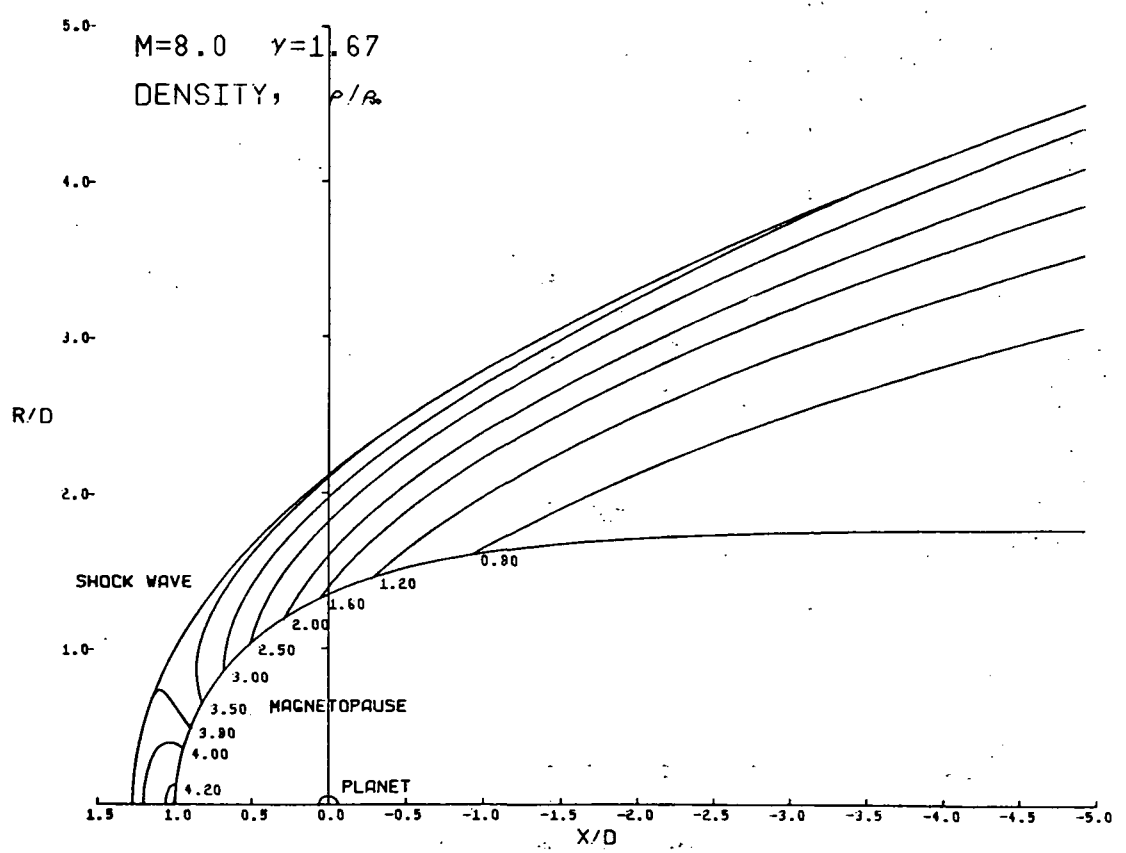
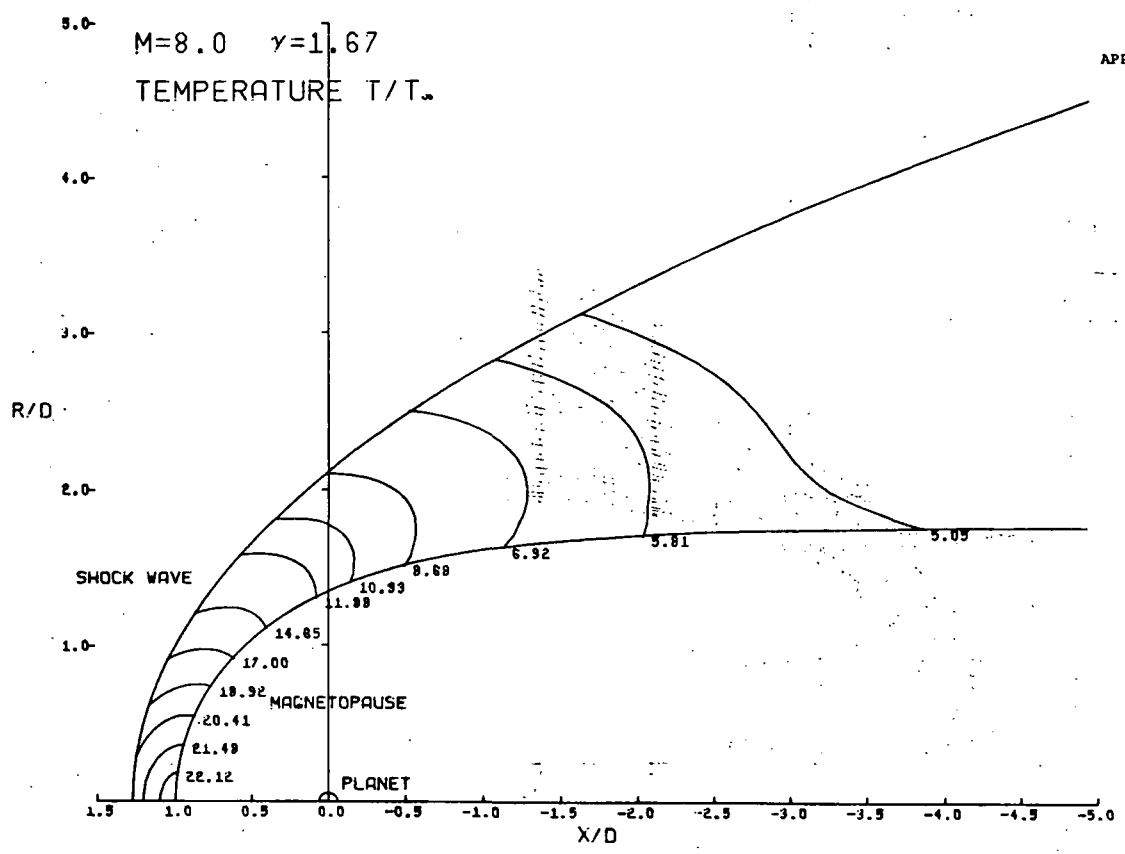


Figure A.3. - Continued.

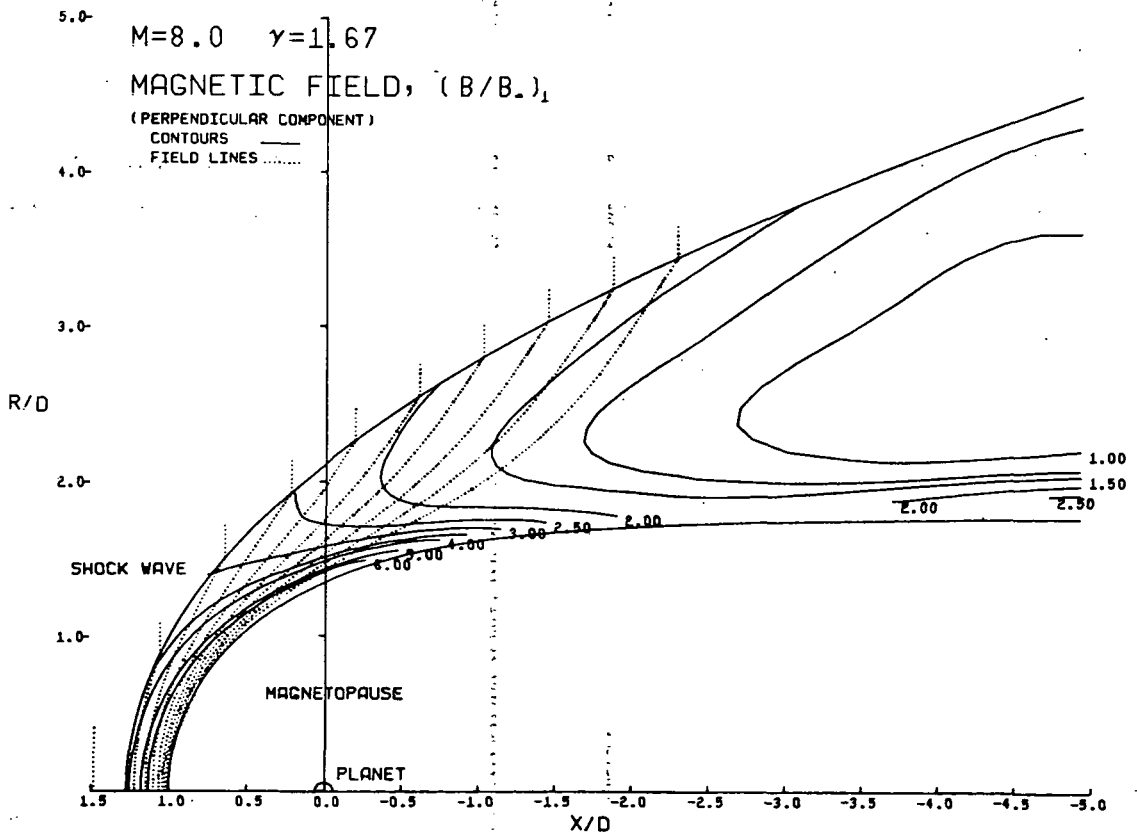
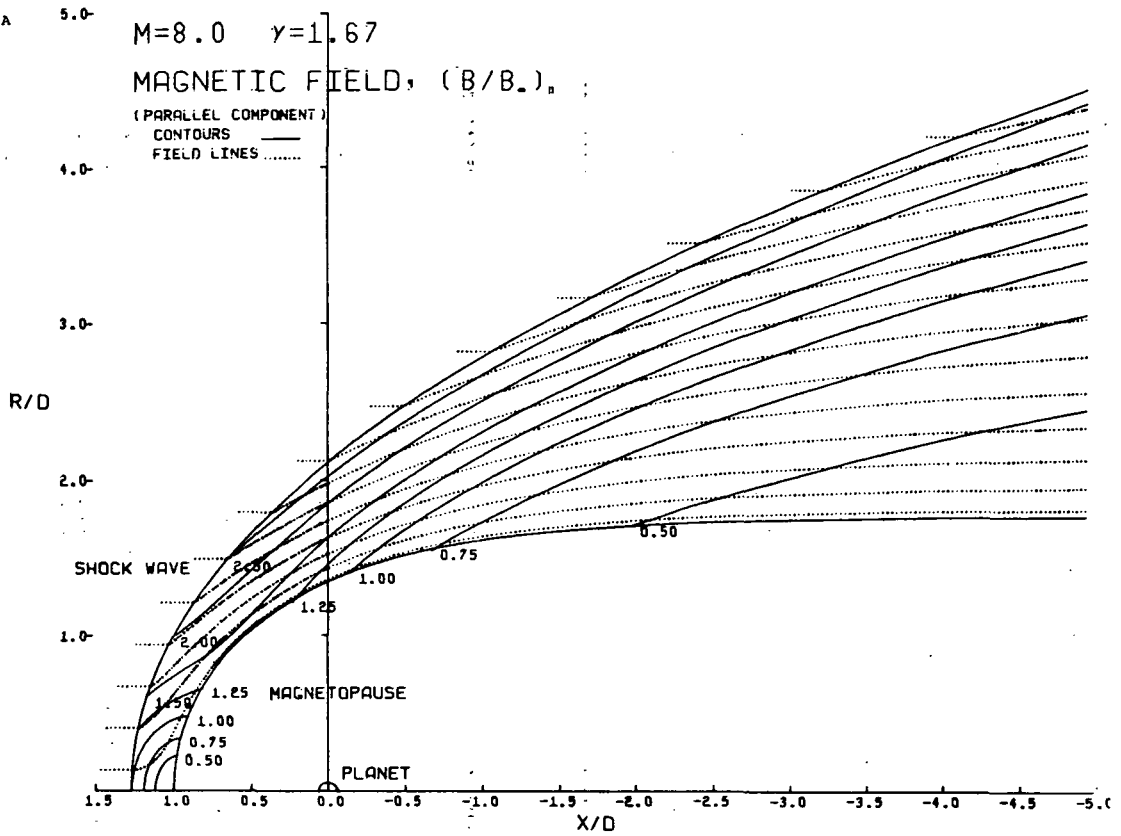


Figure A.3. - Concluded.

```

PROGRAM MAIN (INPUT,OUTPUT,TAPE5=INPUT,TAPE6=OUTPUT,
      TAPE7=TAPE5,TAPE8=TAPE6)
LOGICAL LBEUN,LPRFL,LPRST,LPRCON,LPRB,LPLDT
COMMON /COMMON/LBEUN,LPRFL,LPRST,LPRCON,LPRB,LPLDT
READ(5,100) NCASE
DO 25 J=1,NCASE
CALL TAPU
CALL LBEUN6 GO TO 10
CALL LBEUN16
CALL LPRB
CALL LPRC
CALL LPRD
GO TO 15
10 CALL LBEUN
15 CALL LPRB
IF (LPRC) CALL FLOWT
IF (LPRD) CALL STOUT
CALL BCMP
IF (LPRB) CALL BOUT
CALL CCNTUR
25 CONTINUE
STOP
100 FORMAT(IIC)
END
SUBROUTINE BCMP
THIS SUBROUTINE CALCULATES THE COMPONENTS OF THE MAGNETIC FIELD
PARALLEL, PERPENDICULAR AND NORMAL TO THE FLOW.
COMMON/CONT/ XVCOM,XCOM(20),YVCOM,YCOM(20),XC(20),YC(20),I0,J0
VF(EG,100),RADF(20,150)
COMMON/BLUNT/ IMETA(20),RPI(2,2)
LEVEL 2, XST,RST,NUM,NST
COMMON/ROUND/ XBD(1,7),YBD(1,7),XASX(1,3),YASX(1,3),NMXX,NZMAX,
1 APACH,GAMMA,RK2,MHIND
LEVEL 2, BPARA,RPR,RDRM,BMA,BMANG
COMMON/RGCOMP/ BPAK(20,100),BP(2,2),ICOM,BNDRM(20,100)
BPAK(20,100),ANG(20,100)
LOGICAL LBEUN,LPRFL,LPRST,LPRCON,LPRB,LPLDT
COMMON /PACT/ LP,RFL,LPRFL,LPRST,LPRCON,LPRB,LPLDT
COMMON /BINA/ ANGP,ANKL,KRCOM,BCOM(20)
DIMENSION X(100),Y(100),A(100),V(50),C(100)
DATA W/100,160/
CALCULATE PERPENDICULAR FIELD LINES
IF (RBCOM.EQ. C .AND. .NOT.LPRB) RETURN
CALL BCMP
CALL BFGM
CALCULATE X/Y LINE AND X/Y LINE AT EACH GRID POINT, THEN SMOOTH
ALONG CONSTANT-X LINES, USING FIFTH-ORDER LEAST SQUARES FIT
NPM=NRPAK-1
NZM=NZMAX-1
DO 10 J=1,NZMAX
ENGLP(MPAR,J)=RNYFIN(MPAR,J)
PFLP(MNPAP,J)=VELLINE(ENGLPAP,J)
LANG(MNMAA,J)=SLOPE(LNMAA,J)
DO 10 I=2,NPM
ENRPP(I,J)=ENRINE(I,J)
BPPRPI(I,J)=LLINF(I,J)
BANG(I,J)=SLP(L(I,J))
10 CONTINUE
ALSC(3)=E1
DO 25 J=2,PKM
DO 25 I=1,NZM
DO 25 J=1,NZM
VLSO(4)=1+VLSO(3)+2*V((YC(I,J)-VC(I,J))**2)
*ALC(I,J)+4C(I,J)**2)
25 CONTINUE
DO 45 J=1,NZMAX
VLSO(4)=BPPRPI(I,J)
45 CONTINUE
CALL FLSOY(NZMAX,2,ALC,VLSO,W,ALU,S,5,2,1,5)
DO 50 J=1,NZMAX
2*VLSO(3)
BPPRPI(I,J)=((1+(C)*RAX+(C))**2+4*(4))**2)*VAX(J)+4*ALC(I,J)**2+4*AL(1)
50 CONTINUE
50 CONTINUE

```

- 52 BCMP
- 53 BCMP
- 54 BCMP
- 55 BCMP
- 56 BCMP
- 57 BCMP
- 58 BCMP
- 59 BCMP
- 60 BCMP
- 61 BCMP
- 62 BCMP
- 63 BCMP
- 64 BCMP

- 2 BELGAM
- 3 BVAL
- 4 BVAL
- 5 DMSTRM
- 6 STREAM
- 7 STREAM
- 8 SHOCKS
- 9 BELGAM
- 10 BELGAM
- 11 BELGAM
- 12 BELGAM
- 13 BELGAM
- 14 BELGAM
- 15 BELGAM
- 16 BELGAM
- 17 BELGAM
- 18 BELGAM
- 19 BELGAM
- 20 BELGAM
- 21 BELGAM
- 22 BELGAM
- 23 BELGAM
- 24 BELGAM
- 25 BELGAM
- 26 BELGAM
- 27 BELGAM
- 28 BELGAM
- 29 BELGAM
- 30 BELGAM
- 31 BELGAM
- 32 BELGAM
- 33 BELGAM
- 34 BELGAM
- 35 BELGAM
- 36 BELGAM
- 37 BELGAM
- 38 BELGAM
- 39 BELGAM
- 40 BELGAM
- 41 BELGAM
- 42 BELGAM
- 43 BELGAM
- 44 BELGAM
- 45 BELGAM
- 46 BELGAM
- 47 BELGAM
- 48 BELGAM
- 49 BELGAM
- 50 BELGAM
- 51 BELGAM
- 52 BELGAM
- 53 BELGAM
- 54 BELGAM
- 55 BELGAM
- 56 BELGAM
- 57 BELGAM
- 58 BELGAM
- 59 BELGAM
- 60 BELGAM
- 61 BELGAM
- 62 BELGAM
- 63 BELGAM
- 64 BELGAM
- 65 BELGAM
- 66 BELGAM
- 67 BELGAM
- 68 BELGAM

```

SUBROUTINE BCMP
LEVEL 2, NB, NBF, XBF, RBF, ELBF, GAMBF
COMMON /BVAL/ NB, NBF(1,1), XBF(51,100), RBF(51,100), ELBF(51,100),
* GAMBF(51,100)
COMMON/DNST/ KM7, ZPLOT, NBLUNT, NZEND, NZADD
LEVEL 2, XST, RST, NUM, NST
COMMON /STREAM/ XST(50,150), RST(150,150), NUM(50), NST
COMMON /SHOCKS/ DRSD(100), DST(150)
DATA PLONZ /1657079613277/
THIS SUBROUTINE CALCULATES THE MAGNITUDE AND DIRECTION OF
FL/LINE AT THE POINTS WHERE THE STREAMLINES INTERSECT THE
MAGNETIC FIELD LINES WHICH ARE PERPENDICULAR TO THE FLOW
IN FREESTREAM
DST(1)=.55/DST(1,1)
DO 10 I=2,PKST
DST(I)=1.0/D(I)*DST(I,1)-NST(I-1,1)
10 CONTINUE
SET AFFAYS TO FREE STREAM VALUES
NSTP=NST+1
JBFMAX=NBF(1,1)
DO 30 I=1,PKSTPI
IF (NBF(I,1) .LT. JBFMAX) GO TO 30
JBFMAX=NBF(I,1)
30 CONTINUE
DC Z= J=1, JBFMAX
DO 20 I=1,PKSTPI
:ELBF(I,J)=Z+U
:ELBF(I,J)=PJONZ
20 CONTINUE
VALU=5 ALONG FIELD LINES WHICH CROSS SHOCK
DO 100 J=2,NB
IF (J.EQ. NB+1) GO TO 100
PJ=SORT(XBF(2,J)-XBF(1,J))**2+RBF(2,J)**2)*2.0
PLP(I,J)=LLINF(I,J)
GAP=PIONZ
DZ=XBF(3,J)-XBF(2,J)
PZ=XBF(3,J)-XBF(2,J)
LZ=SCAT(IONZ+XZ+DRZ+GRZ)
SAP=ALFIN(IONZ+OXZ)
LPLP(I,J)=L-LLP(I,J)
:GAMBF(I,J)=(GAMI+DZ+CANZ*O(1)/I0)+DZ
GO TO 74E
100 CONTINUE
DI=SORT(XBF(2,J)-XBF(2,J)-XBF(2,J))**2+RBF(2,J)**2)*2.0
DZ=XBF(3,J)-XBF(2,J)
DZ=XBF(3,J)-XBF(2,J)
PZ=XBF(3,J)-XBF(2,J)
LZ=SCAT(IONZ+XZ+DRZ+GRZ)
GAP=ALFIN(IONZ+OXZ)
LPLP(I,J)=L-LLP(I,J)
:GAMBF(I,J)=(GAMI+DZ+CANZ*O(1)/I0)+DZ
GO TO 74E
100 CONTINUE
DO 110 I=1,PKST
DI=0
GAP=0
IF (EN(1+I,J) .LT. XST(I,1)) GO TO 120
EY=XBF(1+I,J)-XBF(1,1)
EY=XBF(1+I,J)-XBF(1,1)
EY=XBF(1+I,J)-XBF(1,1)
PZ=SCAT(IONZ+XZ+DRZ+GRZ)
LPLP(I,J)=L-LLP(I,J)
:GAMBF(I,J)=(GAMI+DZ+CANZ*O(1)/I0)+DZ
CALL FLSOY(NZMAX,2,ALC,VLSO,W,ALU,S,5,2,1,5)
50 CONTINUE
50 CONTINUE

```

- 52 BCMP
- 53 BCMP
- 54 BCMP
- 55 BCMP
- 56 BCMP
- 57 BCMP
- 58 BCMP
- 59 BCMP
- 60 BCMP
- 61 BCMP
- 62 BCMP
- 63 BCMP
- 64 BCMP
- 65 BCMP
- 66 BCMP
- 67 BCMP
- 68 BCMP



Line #	Code	Description / Command	Variable / Comment
31	ROUT	DU IO J=2,NRMAX	
32	ROUT	B1=SCANP*90*PP(I,J)	
33	ROUT	B2=CANGP*BPARA(I,J)	
34	ROUT	F1=CGS(ANG(I,J))+42+CGS(ANG(I,J))*91	
35	ROUT	F2=SIN(ANG(I,J))+62+SIN(ANG(I,J))*91	
36	ROUT	BHAG(I,J)=SORT(F1+F2*F2)	
37	ROUT	BANG(I,J)=ATAN2(F2,F1)*90	
38	ROUT	PA=F1+CANGN	
39	ROUT	9Y=F2+CANGN	
40	ROUT	B1=BNORM(I,J)*SANGN	
41	ROUT	W1=C(6+126) 1,RP(I,J),BPARA(I,J),BPERR(I,J),BHAG(I,J),BANG(I,J)	
42	ROUT	*BNORM(I,J),BX,BY,BZ	
43	ROUT	10 CONTINUE	
44	ROUT	C	
45	ROUT	C	
46	ROUT	C	
47	ROUT	DD 2C JZ=1,NZADD	
48	ROUT	J=J2+NBUNLNT	
49	ROUT	Z=Z-FC(I,J)	
50	ROUT	IF (NHINDX.EO. 1) GO TO 13	
51	ROUT	WRITE(6,136) JZ,Z	
52	ROUT	GO TO 15	
53	ROUT	13 WRITE(6,135) JZ,Z	
54	ROUT	15 I=1	
55	ROUT	WRITE(6,120) 1,FC(I,J),BPARA(I,J)	
56	ROUT	DD 2C J=2,NRMAX	
57	ROUT	B1=SCANP*90*PP(I,J)	
58	ROUT	B2=CANGP*BPARA(I,J)	
59	ROUT	F1=CGS(ANG(I,J))+42+CGS(ANG(I,J))*91	
60	ROUT	F2=SIN(ANG(I,J))+62+SIN(ANG(I,J))*91	
61	ROUT	BHAG(I,J)=SORT(F1+F2*F2)	
62	ROUT	BANG(I,J)=ATAN2(F2,F1)*90	
63	ROUT	BX=F1+CANGN	
64	ROUT	BY=F2+CANGN	
65	ROUT	B1=BNORM(I,J)*SANGN	
66	ROUT	WRITE(6,126) 1,FC(I,J),BPARA(I,J),BPERR(I,J),BHAG(I,J),BANG(I,J)	
67	ROUT	*BNORM(I,J),BX,BY,BZ	
68	ROUT	20 CONTINUE	
69	ROUT	RETURN	
70	ROUT	C	
71	ROUT	116 FORMAT(1H//52X,25MAGNETIC FIELD COMPONENTS/52X,2D(1H*))	
72	ROUT	117 FORMAT(12H ANGLAR LOCATION NO.,12I2E6, AT THEIA ,F6.4)	
73	ROUT	* ON 050ELS//	
74	ROUT	* 4Y 3H1.64 *HRP(B1,216)B1/BIKE,6H4/B1/BIKE,54,7H6-ANGLE,5X,	
75	ROUT	* 7H 8/B1/BIKE,4Y 7H6-ANGLE,5X,20Y 7/B1/BIKE,7H6-ANGLE,5X,	
76	ROUT	* 21X 1CH(4PARALLELS),4Y 7H6-ANGLE,5X,20Y 7H6-ANGLE,5X,	
77	ROUT	* 6H1(NORMAL),1Y 311X,11H(REZULTANTI)	
78	ROUT	* 6H DIRESL//22H ANGLAR LOCATION NO.,12I2E6, AT THEIA ,F6.4,	
79	ROUT	* 6Y 3H1.64 *HRP(B1,216)B1/BIKE,6H4/B1/BIKE,54,7H6-ANGLE,5X,	
80	ROUT	* 7H 8/B1/BIKE,4Y 7H6-ANGLE,5X,20Y 7/B1/BIKE,7H6-ANGLE,5X,	
81	ROUT	* 21X 1CH(4PARALLELS),4Y 7H6-ANGLE,5X,20Y 7H6-ANGLE,5X,	
82	ROUT	* 6H1(NORMAL),1Y 311X,11H(REZULTANTI)	
83	ROUT	120 FORMAT(12H ANGLAR LOCATION NO.,12I2E6, AT X/D ,F6.4//	
84	ROUT	* ON 050ELS//	
85	ROUT	* 4Y 3H1.64 *HRP(B1,216)B1/BIKE,6H4/B1/BIKE,54,7H6-ANGLE,5X,	
86	ROUT	* 7H 8/B1/BIKE,4Y 7H6-ANGLE,5X,20Y 7/B1/BIKE,7H6-ANGLE,5X,	
87	ROUT	* 21X 1CH(4PARALLELS),4Y 7H6-ANGLE,5X,20Y 7H6-ANGLE,5X,	
88	ROUT	* 6H1(NORMAL),1Y 311X,11H(REZULTANTI)	
89	ROUT	* 6Y 3H1.64 *HRP(B1,216)B1/BIKE,6H4/B1/BIKE,54,7H6-ANGLE,5X,	
90	ROUT	* 7H 8/B1/BIKE,4Y 7H6-ANGLE,5X,20Y 7/B1/BIKE,7H6-ANGLE,5X,	
91	ROUT	* 21X 1CH(4PARALLELS),4Y 7H6-ANGLE,5X,20Y 7H6-ANGLE,5X,	
92	ROUT	* 6H1(NORMAL),1Y 311X,11H(REZULTANTI)	
93	ROUT	* 6Y 3H1.64 *HRP(B1,216)B1/BIKE,6H4/B1/BIKE,54,7H6-ANGLE,5X,	
94	ROUT	* 7H 8/B1/BIKE,4Y 7H6-ANGLE,5X,20Y 7/B1/BIKE,7H6-ANGLE,5X,	
95	ROUT	* 21X 1CH(4PARALLELS),4Y 7H6-ANGLE,5X,20Y 7H6-ANGLE,5X,	
96	ROUT	* 6H1(NORMAL),1Y 311X,11H(REZULTANTI)	
97	ROUT	END	
2	BSHKL	SUBROUTINE BSHKL (X,R,ANG,VEL)	
3	BSHKL	THIS SUBROUTINE CALCULATES THE MAGNITUDE AND DIRECTION OF	
4	BSHKL	VEL/ELIN AT THE SHOCK, AND THE R-LOCATION, GIVEN THE	
5	BSHKL	X-LOCATION OF THE POINT	
6	BSHKL	C	
7	BSHKL	COMMON /BOUND/ X8OD(10),Y8OD(10),X8K(100),Y8K(100),NRMAX,	
8	BSHKL	NZMAX,AMACH,GAM,HRD,NHINDX	
9	BSHKL	DD IO J=1,NZMAX	
10	BSHKL	IF (X.LT. XSHK(J)) GO TO 20	
11	BSHKL	J=NRMAX	
12	BSHKL	R=YSHK(J-1)+(X-XSHK(J-1))*YSHK(J)-YSHK(J-1)/(ASHK(J)-XSHK(J-1))	
13	BSHKL	THEI=ATAN(ORSO(X(J-1))	
14	BSHKL	THE2=ATAN(ORSO(X(J)	
15	BSHKL	THE1=THEI+(X-XSHK(J-1))*(THE2-THEI)/(ASHK(J)-XSHK(J-1))	
16	BSHKL	17	
17	BSHKL		
18	BSHKL		
19	BSHKL		
20	BSHKL		
21	BSHKL		
22	BSHKL		
23	BSHKL		
24	BSHKL		
25	BSHKL		
26	BSHKL		
27	BSHKL		
28	BSHKL		
29	BSHKL		
30	BSHKL		
31	BSHKL		
32	BSHKL		
33	BSHKL		
34	BSHKL		
35	BSHKL		
36	BSHKL		
37	BSHKL		
38	BSHKL		
39	BSHKL		
40	BSHKL		
41	BSHKL		
42	BSHKL		
43	BSHKL		
44	BSHKL		
45	BSHKL		
46	BSHKL		
47	BSHKL		
48	BSHKL		
49	BSHKL		
50	BSHKL		
51	BSHKL		
52	BSHKL		
53	BSHKL		
54	BSHKL		
55	BSHKL		
56	BSHKL		
57	BSHKL		
58	BSHKL		
59	BSHKL		
60	BSHKL		
61	BSHKL		
62	BSHKL		
63	BSHKL		
64	BSHKL		
65	BSHKL		
66	BSHKL		
67	BSHKL		
68	BSHKL		
69	BSHKL		
70	BSHKL		
71	BSHKL		
72	BSHKL		
73	BSHKL		
74	BSHKL		
75	BSHKL		
76	BSHKL		
77	BSHKL		
78	BSHKL		
79	BSHKL		
80	BSHKL		
81	BSHKL		
82	BSHKL		
83	BSHKL		
84	BSHKL		
85	BSHKL		
86	BSHKL		
87	BSHKL		
88	BSHKL		
89	BSHKL		
90	BSHKL		
91	BSHKL		
92	BSHKL		
93	BSHKL		
94	BSHKL		
95	BSHKL		
96	BSHKL		
97	BSHKL		
98	BSHKL		
99	BSHKL		
100	BSHKL		
101	BSHKL		
102	BSHKL		
103	BSHKL		
104	BSHKL		
105	BSHKL		
106	BSHKL		
107	BSHKL		
108	BSHKL		
109	BSHKL		
110	BSHKL		
111	BSHKL		
112	BSHKL		
113	BSHKL		
114	BSHKL		
115	BSHKL		
116	BSHKL		
117	BSHKL		
118	BSHKL		
119	BSHKL		
120	BSHKL		
121	BSHKL		
122	BSHKL		
123	BSHKL		
124	BSHKL		
125	BSHKL		
126	BSHKL		
127	BSHKL		
128	BSHKL		
129	BSHKL		
130	BSHKL		
131	BSHKL		
132	BSHKL		
133	BSHKL		
134	BSHKL		
135	BSHKL		
136	BSHKL		
137	BSHKL		
138	BSHKL		
139	BSHKL		
140	BSHKL		
141	BSHKL		
142	BSHKL		
143	BSHKL		
144	BSHKL		
145	BSHKL		
146	BSHKL		
147	BSHKL		
148	BSHKL		
149	BSHKL		
150	BSHKL		



```

31 4000001
32 4000002
33 4000003
34 4000004
35 4000005
36 4000006
37 4000007
38 4000008
39 4000009
40 4000010
41 4000011
42 4000012
43 4000013
44 4000014
45 4000015
46 4000016
47 4000017
48 4000018
49 4000019
50 4000020
51 4000021
52 4000022
53 4000023
54 4000024
55 4000025
56 4000026
57 4000027
58 4000028
59 4000029
60 4000030
61 4000031
62 4000032
63 4000033
64 4000034
65 4000035
66 4000036
67 4000037
68 4000038
69 4000039
70 4000040
71 4000041
72 4000042
73 4000043
74 4000044
75 4000045
76 4000046
77 4000047
78 4000048
79 4000049
80 4000050
81 4000051
82 4000052
83 4000053
84 4000054
85 4000055
86 4000056
87 4000057
88 4000058
89 4000059
90 4000060
91 4000061
92 4000062
93 4000063
94 4000064
95 4000065
96 4000066
97 4000067
98 4000068
99 4000069
100 4000070
101 4000071
102 4000072
103 4000073
104 4000074
105 4000075
106 4000076
107 4000077
108 4000078
109 4000079
110 4000080
111 4000081
112 4000082
113 4000083
114 4000084
115 4000085
116 4000086
117 4000087
118 4000088
119 4000089
120 4000090
121 4000091
122 4000092
123 4000093
124 4000094
125 4000095
126 4000096
127 4000097
128 4000098
129 4000099
130 4000100
131 4000101
132 4000102
133 4000103
134 4000104
135 4000105
136 4000106
137 4000107
138 4000108
139 4000109
140 4000110
141 4000111
142 4000112
143 4000113
144 4000114
145 4000115
146 4000116
147 4000117
148 4000118
149 4000119
150 4000120

```













```

74 FLOWM 75 FLSQFY 55
76 FLOWM 76 FLSQFY 56
77 FLOWM 77 FLSQFY 57
78 FLOWM 78 FLSQFY 58
79 FLOWM 79 FLSQFY 59
80 FLOWM 80 FLSQFY 60
81 FLOWM 81 FLSQFY 61
82 FLOWM 82 FLSQFY 62
83 FLOWM 83 FLSQFY 63
84 FLOWM 84 FLSQFY 64
85 FLOWM 85 FLSQFY 65
86 FLOWM 86 FLSQFY 66
87 FLOWM 87 FLSQFY 67
88 FLOWM 88 FLSQFY 68
89 FLOWM 89 FLSQFY 69
90 FLOWM 90 FLSQFY 70
91 FLOWM 91 FLSQFY 71
92 FLOWM 92 FLSQFY 72
93 FLOWM 93 FLSQFY 73
94 FLOWM 94 FLSQFY 74
95 FLOWM 95 FLSQFY 75
96 FLOWM 96 FLSQFY 76
97 FLOWM 97 FLSQFY 77
98 FLOWM 98 FLSQFY 78
99 FLOWM 99 FLSQFY 79
100 FLOWM 100 FLSQFY 80
101 FLOWM 101 FLSQFY 81
102 FLOWM 102 FLSQFY 82
103 FLOWM 103 FLSQFY 83

```

```

C *** THIRD ORDER MODIFIED EULER INTEGRATION PROCEDURE
C
C DO 10 A=1,NLIM
  ORX=ORX(MIXS)
  IF (IAS*DX .GT. XF) GO TO 11
  RS=RS+URA*DX
  XS=XS+DX
  SLOPE=S*(URK+ORAMIXS+XSLI)
  RS=RS+SLOPE*DX
  IF (XSLT*WRT) GO TO 10
  MN=MN+1
  XXX(I,MN)=XS
  RPL(I,MN)=RS
  WRT=AMPT*ORX
  10 CONTINUE
  11 CONTINUE
  12 CONTINUE
  END

```

```

C ***** SUBROUTINE FLSQFY (N1,N2,X,Y,M,N1,S1,A,IER)
C
C PURPOSE
C - CALCULATE LEAST SQUARES POLYNOMIAL APPROXIMATION
C - TO A GIVEN SET OF DATA POINTS WITH
C - GIVEN WEIGHTS USING ORTHOGONAL POLYNOMIALS.
C
C USAGE
C CALL FLSQFY (N1,N2,X,Y,M,N1,S1,A,IER)
C
C INPUT PARAMETERS
C N1 - NUMBER OF DATA POINTS
C N2 - DEGREE OF POLYNOMIAL DESIRED, N1.LT.M
C X - ARRAY OF INDEPENDENT VARIABLE
C Y - ARRAY OF DEPENDENT VARIABLE
C M - ARRAY OF POSITIVE WEIGHTS
C N1 - ROW DIMENSION OF SCRATCH ARRAY S1, N1.GE.M
C S1 - SCRATCH ARRAY
C
C IN THE COLUMN DEFINITIONS BELOW,
C 1 - REFERS TO POLYNOMIAL ORDER
C COL 1 - POLYNOMIAL P(I-1), VALUE AT EACH X(I) I=RU 24
C COL 2 - COEFFICIENT OF EACH X**(J-1) TERM AFTER 240
C COL 3 - POLYNOMIAL P(I), SAME FORM AS COL 1.
C COL 4 - ALPHA(I+1), WHERE I=J-1
C COL 5 - S(I), WHERE I=J-1
C COL 6 - SIGMA*Z, WHERE I=J-1
C
C OUTPUT PARAMETERS
C A - ARRAY OF COMPUTED COEFFICIENTS
C ALL THRU A(N+1) CONTAIN COMPUTED POLYNOMIAL
C COEFFICIENTS IN ORDER OF INCREASING DEGREE.
C IER - ERROR INDICATOR
C .EQ.0 SUCCESS
C .EQ.1 (N.GE.M).OR.(N.LE.0)
C .EQ.2 M.LT.M
C .EQ.3 M.LE.1
C .EQ.4 M.LT.LC.0
C
C REFERENCE
C FORSTNER, G. E., GENERATION AND USE OF ORTHOGONAL
C POLYNOMIALS FOR DATA-FITTING WITH A DIGITAL COMPUTER,
C J. SIAM, VOL. 5, NO. 2, (JUNE 1957) PP. 74-88.
C
C NOTE - MOST NOTATION AND MOST LOCAL VARIABLE NAMES ARE
C BASED ON THE REFERENCES, IE WPP IS W(I), I=1(I), P(I),
C BUT W, WT AND W(I) REFER TO THE WEIGHTS ARRAY.
C ***** DIMENSION X(I),Y(I),M(I),S1(MN),I,A(I)
C
C *** INITIAL SET-UP ***
C IER = 0
C IF (N1.GE.M).OR.(N1.LE.0) IER=1
C IF (M.LT.N) IER=2
C IF (M.LE.1) IER=3

```

```

74 FLOWM 75 FLSQFY 55
76 FLOWM 76 FLSQFY 56
77 FLOWM 77 FLSQFY 57
78 FLOWM 78 FLSQFY 58
79 FLOWM 79 FLSQFY 59
80 FLOWM 80 FLSQFY 60
81 FLOWM 81 FLSQFY 61
82 FLOWM 82 FLSQFY 62
83 FLOWM 83 FLSQFY 63
84 FLOWM 84 FLSQFY 64
85 FLOWM 85 FLSQFY 65
86 FLOWM 86 FLSQFY 66
87 FLOWM 87 FLSQFY 67
88 FLOWM 88 FLSQFY 68
89 FLOWM 89 FLSQFY 69
90 FLOWM 90 FLSQFY 70
91 FLOWM 91 FLSQFY 71
92 FLOWM 92 FLSQFY 72
93 FLOWM 93 FLSQFY 73
94 FLOWM 94 FLSQFY 74
95 FLOWM 95 FLSQFY 75
96 FLOWM 96 FLSQFY 76
97 FLOWM 97 FLSQFY 77
98 FLOWM 98 FLSQFY 78
99 FLOWM 99 FLSQFY 79
100 FLOWM 100 FLSQFY 80
101 FLOWM 101 FLSQFY 81
102 FLOWM 102 FLSQFY 82
103 FLOWM 103 FLSQFY 83

```

```

C IF ((I+NL+4) GO TO 490
  BETA(I)=D; P(I)=A; P(I-1)=J; W(I)=S(SUM(W(I)))
  C
  C NA = N+1
  S(I+4)=0.
  CSQ=0.
  DO 110 M=1,M
  WPP=M.
  S(I+2)=M.
  S(I+1)=0.
  WT=M(I).
  IF (M1.L.C.) GO TO 490
  WPP = WPP*WT
  11) DSQ = DSQ+WT*(Y(I)-W(I))
  C *** GENERATE ORTHOGONAL POLYNOMIALS - THRU 240 ***
  DO 240 I=1,NL
  WPP=0.
  COMPUTE (W(I),X(I)), AND UMLGA(I)=(F,P(I))
  DO 240 J=1,M
  TEMP=W(I)*S(J+2)
  IF (I.LT.N) WPP=WPP+TEMP*(J)*S(J+2)
  240 WPP=WPP+TEMP*(J)*S(J+2)
  S(I+2)=WPP/WPP
  S(I+1)=M(I)/M(I)
  DELTA**2(I)=S(I)-S(I)**2*(I)
  SIGMA**2(I)=DELTA**2(I)/(DEGREES OF FREEDOM)
  BK = M-1
  IF (BK.NE.C.) BK = DSQ/BK
  S(I+4) = BK
  ALPHA(I)=WPP(X(I))/X(I)
  IF (I.GE.N) GO TO 240
  WPP=0
  230 S(I+1)=S(I)+2
  S(I+2)=M(I)
  S(I+3)=WPP/WPP
  240 CONTINUE
  C *** COMPUTE COEFFICIENTS OF LEAST SQUARES POLYNOMIAL
  C A = S(I)P(I) ** S(N)P(N) ***
  C P(I)=D; P(I-1)=J; W(I)=S(SUM(W(I)))
  DO 300 I=1,NL
  WPP=0.
  S(I+2)=M(I)
  S(I+1)=0.
  WT=M(I).
  IF (M1.L.C.) GO TO 490
  WPP = WPP*WT
  300 S(I+2)=M(I)
  S(I+1)=0.
  WT=M(I).
  IF (M1.L.C.) GO TO 490
  WPP = WPP*WT
  SUP LOOP THRU 310, I = ORDER OF POLYNOMIAL FORMED
  DO 310 I=1,NL
  AL=S(I+3)
  BT=S(I+4)
  12=0.
  I1 = I+1
  FOPM (F(I)=W(I)-ALPHA(I)*P(I)-BETA(I)*P(I-1))
  AND ADD TO POLYNOMIAL SUM IN A
  DO 310 I=1,NL
  J1=AL*S(I+1)+BT*S(I+2)-BT*S(I+1)
  12=S(I+2)+J1
  S(I+2)=S(I+1)+J1
  310 S(I+1)=S(I)+J1
  IER = 0
  990 RETURN
  END
  SUBROUTINE INPUT
  THIS ROUTINE READS ALL DATA REQUIRED FOR ONE CASE,
  EXCEPT FLOW FIELD DATA FOR RERUN
  COMMON /BIN/ ANGP,ANGN,KBCOM,BCOM(20)

```









```

C SURROUTINE SETUP ESTABLISHES PERMANENT PLOT ORIGIN
C DRAWS AXES, LABELS, AND TITLE
C SUPROUTINE ROUND DRAWS AND LABELS STOCK WAY, PLANET,
C AND MAGNETOSPHERE (1800Y=J) UP LONGSPHERE
C (1800Y=1) BOUNDARY
C
C IF (IPLT.NE.3) GO TO 14
C CALL DASH(1,2,3,4,5,6,7,8,9,10,11)
C CALL PLOT(1,2,3,4,5,6,7,8,9,10,11)
C CALL SETUP(1,2,3,4,5,6,7,8,9,10,11)
C CALL ROUND(1,2,3,4,5,6,7,8,9,10,11)
C CALL CONT(1,2,3,4,5,6,7,8,9,10,11)
C CALL SPLI(1,2,3,4,5,6,7,8,9,10,11)
C RETURN
C
C DRAW COUNTOUR PLOTS
C
C CONTINUE
C CALL SETUP(1,2,3,4,5,6,7,8,9,10,11)
C CALL ROUND(1,2,3,4,5,6,7,8,9,10,11)
C CALL CONT(1,2,3,4,5,6,7,8,9,10,11)
C CALL SPLI(1,2,3,4,5,6,7,8,9,10,11)
C RETURN
C
C CHANGE VELOCITY COUNTOUR VALUES TO TEMPERATURE
C
C 20 I=1,4
C FACT=2*(100-1000)*PAC+AMACH
C VPL=VPL(I)
C DO 21 I=1,NV
C CONTINUE
C GO TO 10
C
C 21 CONTINUE
C
C FUNCTION QUAD (X,Y,P,XP,YP)
C
C THIS FUNCTION PERFORMS A GENERALIZED QUADRILATERAL INTERPOLATION
C GIVEN THE COORDINATES OF THE VERTICES, THE VALUES OF THE FUNCTION
C AT THOSE POINTS, AND THE COORDINATES OF THE POINT AT WHICH A
C VALUE OF THE FUNCTION IS DESIRED, (XP,YP)
C X AND Y ARE THE DOMINANT ARRAYS AND F IS THE FUNCTION ARRAY
C
C DIMENSION X(4),Y(4),F(4)
C S1=4-J*XP-(X(1)+X(2)+X(3)+X(4))
C S2=X(1)+X(2)-X(3)-X(4)
C S3=X(1)-X(2)+X(3)-X(4)
C S4=X(1)+X(2)+X(3)-X(4)
C T1=4-J*YP-(Y(1)+Y(2)+Y(3)+Y(4))
C T2=Y(1)+Y(2)-Y(3)-Y(4)
C T3=Y(1)-Y(2)+Y(3)-Y(4)
C T4=Y(1)+Y(2)+Y(3)-Y(4)
C A=S2*T3-S3*T2
C B=S1*T3+S3*T4-S3*T1-S4*T2
C C=S1*T4-S4*T1
C D=SORT(ABS(A+C))
C ETA=(B+D)/(A+2*C)
C IF (ABS(ETA).GT.1.0) ETA=ETA/D/A
C XI=(S1+ETA*S2)/T1S+ETA*S3
C QUAD=0.25*(XI*(1.0-ETA)+(1.0+XI)*F(4)+(1.0+ETA)*(1.0-XI)
C *F(3)+(1.0-ETA)*(1.0-XI)*F(4)+(1.0+ETA)*(1.0-XI))
C
C RETURN
C
C SUBROUTINE REKUN
C COMMON/CONT/,KVCN,VCON(25),KRCN,PCN(20),XC(20,100),YC(20,100),
C *VF(20,100),RHO(20,100)
C COMMON /BLUNT/ ,THETA(25),RP(20,25)
C LEVEL 2, V, VY
C COMMON /CDMP/ ,VA(20,100),VY(20,100)
C COMMON /BOUND/ ,VX(20,100),VY(20,100),XSHK(100),YSHK(100),NRMAX,
C *NZMAX,AMACH,GAM,HHO,NHNDX
C COMMON /DNSTRM/ ,ZPLOI,NBLUNT,NZEND,NZADD
C COMMON /NRUD0/ ,X(100),Y(100),NUD0
C COMMON /BIN/ ,ANGP,ANGN,KBCN,PCN(20)
C LOGICAL LRERUN,LPREF,LPBST,LPQCN,LPKST,LPKON,LPKPB,LPLOT
C COMMON /PROPT/ ,LRERUN,LPREF,LPBST,LPKON,LPKPB,LPLOT
C COMMON /SHOCKS/ ,DRSDX(100),OST(50)
C
C 22 CONTINUE
C
C 23 CONTINUE
C
C 24 CONTINUE
C
C 25 CONTINUE
C
C 26 CONTINUE
C
C 27 CONTINUE
C
C 28 CONTINUE
C
C 29 CONTINUE
C
C 30 CONTINUE
C
C 31 CONTINUE
C
C 32 CONTINUE
C
C 33 CONTINUE
C
C 34 CONTINUE
C
C 35 CONTINUE
C
C 36 CONTINUE
C
C 37 CONTINUE
C
C 38 CONTINUE
C
C 39 CONTINUE
C
C 40 CONTINUE
C
C 41 CONTINUE
C
C 42 CONTINUE
C
C 43 CONTINUE
C
C 44 CONTINUE
C
C 45 CONTINUE
C
C 46 CONTINUE
C
C 47 CONTINUE
C
C 48 CONTINUE
C
C 49 CONTINUE
C
C 50 CONTINUE
C
C 51 CONTINUE
C
C 52 CONTINUE
C
C 53 CONTINUE
C
C 54 CONTINUE
C
C 55 CONTINUE
C
C 56 CONTINUE
C
C 57 CONTINUE
C
C 58 CONTINUE
C
C 59 CONTINUE
C
C 60 CONTINUE
C
C 61 CONTINUE
C
C 62 CONTINUE
C
C 63 CONTINUE
C
C 64 CONTINUE
C
C 65 CONTINUE
C
C 66 CONTINUE
C
C 67 CONTINUE
C
C 68 CONTINUE
C
C 69 CONTINUE
C
C 70 CONTINUE
C
C 71 CONTINUE
C
C 72 CONTINUE
C
C 73 CONTINUE
C
C 74 CONTINUE
C
C 75 CONTINUE
C
C 76 CONTINUE
C
C 77 CONTINUE
C
C 78 CONTINUE
C
C 79 CONTINUE
C
C 80 CONTINUE
C
C 81 CONTINUE
C
C 82 CONTINUE
C
C 83 CONTINUE
C
C 84 CONTINUE
C
C 85 CONTINUE
C
C 86 CONTINUE
C
C 87 CONTINUE
C
C 88 CONTINUE
C
C 89 CONTINUE
C
C 90 CONTINUE
C
C 91 CONTINUE
C
C 92 CONTINUE
C
C 93 CONTINUE
C
C 94 CONTINUE
C
C 95 CONTINUE
C
C 96 CONTINUE
C

```

```

30 CONTINUE
  NZ=ND-NZADD
  CALL FLGRP
  RETURN

C PRINT ERROR MESSAGE IF TAPC4 IS NOT THE SAME CASE AS
C SPECIFIED IN CARD INPUT - PROGRAM IS STOPPED
C
100 WK11:=(6+350) AMAC+GAM*HR0+AMACH+GAM*HR06
1100 FORMAT(10I10,19X,5(11),2X,ZOME EXECUTION TERMINATED 2X,5(11),1726X,
* 34HR1RIN DATA UN TAPC4 DOES NOT AGREE(21X)GK(1TH CASE
* 24X)SPECIFIED UN CARD INPUT(12X)FHMACH NO.24X)5GAMMA,5X,
* 5HR1R0(12X)1GHRUM CAPD,5(14X,F10.4)12X)10HRUM TAPC4,
* 2(4X)F10.4)
STOP
END

FUNCTION RINF(I,J)
C THIS ROUTINE CALCULATES R/INFL AT THE (I,J) GRID POINT
C
COMMON/COMMON/ XBD0(100),ASHK(100),YSHK(100),YSHK(100),NMKMAX,
1 COMMON/COUNT/ NZMX,AMAC,GAM,HRU,MINDX
* VF1ZC,100),K4UF(20,100)
LEVEL Z, XSI,FKST,NUM,NST
COMMON /STREAM/ RST(50,150),RST(50,150),NUM(50),NST
C IF POINT IS ON SHOCK BOUNDARY R/INF=1.0
C
IF (I.EQ.1).AND. (J.GT. 1) GO TO 10
RINF=1.0
RETURN

C
C
10 CONTINUE
X=XC(I,J)
Y=YC(I,J)
Z=Z0
GO TO JST,NST
NM=NUM(JST)
OU SC R4ZPMN
IF (KST(JST,K).GT. X) GO TO 40
30 CONTINUE
40 CONTINUE
J2=JST-1
IF (K.EQ. 1) R2=NST(J2,1)
IF (K.EQ. 2) R2=NST(J2,K-1)+KXSI(J2,K)-RST(J2,K-1)
IF (K.EQ. 3) R2=NST(J2,K)-RST(J2,K-1)
IF (K.EQ. 4) R2=NST(J2,K)-RST(J2,K-1)
IF (K.EQ. 5) R2=NST(J2,K)-RST(J2,K-1)
IF (K.EQ. 6) R2=NST(J2,K)-RST(J2,K-1)
IF (K.EQ. 7) R2=NST(J2,K)-RST(J2,K-1)
IF (K.EQ. 8) R2=NST(J2,K)-RST(J2,K-1)
IF (K.EQ. 9) R2=NST(J2,K)-RST(J2,K-1)
IF (K.EQ. 10) R2=NST(J2,K)-RST(J2,K-1)
IF (K.EQ. 11) R2=NST(J2,K)-RST(J2,K-1)
IF (K.EQ. 12) R2=NST(J2,K)-RST(J2,K-1)
IF (K.EQ. 13) R2=NST(J2,K)-RST(J2,K-1)
IF (K.EQ. 14) R2=NST(J2,K)-RST(J2,K-1)
IF (K.EQ. 15) R2=NST(J2,K)-RST(J2,K-1)
IF (K.EQ. 16) R2=NST(J2,K)-RST(J2,K-1)
IF (K.EQ. 17) R2=NST(J2,K)-RST(J2,K-1)
IF (K.EQ. 18) R2=NST(J2,K)-RST(J2,K-1)
IF (K.EQ. 19) R2=NST(J2,K)-RST(J2,K-1)
IF (K.EQ. 20) R2=NST(J2,K)-RST(J2,K-1)
IF (K.EQ. 21) R2=NST(J2,K)-RST(J2,K-1)
IF (K.EQ. 22) R2=NST(J2,K)-RST(J2,K-1)
IF (K.EQ. 23) R2=NST(J2,K)-RST(J2,K-1)
IF (K.EQ. 24) R2=NST(J2,K)-RST(J2,K-1)
IF (K.EQ. 25) R2=NST(J2,K)-RST(J2,K-1)
IF (K.EQ. 26) R2=NST(J2,K)-RST(J2,K-1)
IF (K.EQ. 27) R2=NST(J2,K)-RST(J2,K-1)
IF (K.EQ. 28) R2=NST(J2,K)-RST(J2,K-1)
IF (K.EQ. 29) R2=NST(J2,K)-RST(J2,K-1)
IF (K.EQ. 30) R2=NST(J2,K)-RST(J2,K-1)
IF (K.EQ. 31) R2=NST(J2,K)-RST(J2,K-1)
IF (K.EQ. 32) R2=NST(J2,K)-RST(J2,K-1)
IF (K.EQ. 33) R2=NST(J2,K)-RST(J2,K-1)
IF (K.EQ. 34) R2=NST(J2,K)-RST(J2,K-1)
IF (K.EQ. 35) R2=NST(J2,K)-RST(J2,K-1)
IF (K.EQ. 36) R2=NST(J2,K)-RST(J2,K-1)
IF (K.EQ. 37) R2=NST(J2,K)-RST(J2,K-1)
IF (K.EQ. 38) R2=NST(J2,K)-RST(J2,K-1)
IF (K.EQ. 39) R2=NST(J2,K)-RST(J2,K-1)
IF (K.EQ. 40) R2=NST(J2,K)-RST(J2,K-1)
IF (K.EQ. 41) R2=NST(J2,K)-RST(J2,K-1)
IF (K.EQ. 42) R2=NST(J2,K)-RST(J2,K-1)
IF (K.EQ. 43) R2=NST(J2,K)-RST(J2,K-1)
IF (K.EQ. 44) R2=NST(J2,K)-RST(J2,K-1)
IF (K.EQ. 45) R2=NST(J2,K)-RST(J2,K-1)
IF (K.EQ. 46) R2=NST(J2,K)-RST(J2,K-1)
IF (K.EQ. 47) R2=NST(J2,K)-RST(J2,K-1)
IF (K.EQ. 48) R2=NST(J2,K)-RST(J2,K-1)
IF (K.EQ. 49) R2=NST(J2,K)-RST(J2,K-1)
IF (K.EQ. 50) R2=NST(J2,K)-RST(J2,K-1)
IF (K.EQ. 51) R2=NST(J2,K)-RST(J2,K-1)
IF (K.EQ. 52) R2=NST(J2,K)-RST(J2,K-1)
IF (K.EQ. 53) R2=NST(J2,K)-RST(J2,K-1)
IF (K.EQ. 54) R2=NST(J2,K)-RST(J2,K-1)
IF (K.EQ. 55) R2=NST(J2,K)-RST(J2,K-1)
IF (K.EQ. 56) R2=NST(J2,K)-RST(J2,K-1)
IF (K.EQ. 57) R2=NST(J2,K)-RST(J2,K-1)
IF (K.EQ. 58) R2=NST(J2,K)-RST(J2,K-1)
IF (K.EQ. 59) R2=NST(J2,K)-RST(J2,K-1)
IF (K.EQ. 60) R2=NST(J2,K)-RST(J2,K-1)
IF (K.EQ. 61) R2=NST(J2,K)-RST(J2,K-1)
IF (K.EQ. 62) R2=NST(J2,K)-RST(J2,K-1)
IF (K.EQ. 63) R2=NST(J2,K)-RST(J2,K-1)
IF (K.EQ. 64) R2=NST(J2,K)-RST(J2,K-1)
IF (K.EQ. 65) R2=NST(J2,K)-RST(J2,K-1)
IF (K.EQ. 66) R2=NST(J2,K)-RST(J2,K-1)
IF (K.EQ. 67) R2=NST(J2,K)-RST(J2,K-1)
IF (K.EQ. 68) R2=NST(J2,K)-RST(J2,K-1)
IF (K.EQ. 69) R2=NST(J2,K)-RST(J2,K-1)
IF (K.EQ. 70) R2=NST(J2,K)-RST(J2,K-1)
IF (K.EQ. 71) R2=NST(J2,K)-RST(J2,K-1)
IF (K.EQ. 72) R2=NST(J2,K)-RST(J2,K-1)
IF (K.EQ. 73) R2=NST(J2,K)-RST(J2,K-1)
IF (K.EQ. 74) R2=NST(J2,K)-RST(J2,K-1)
IF (K.EQ. 75) R2=NST(J2,K)-RST(J2,K-1)
IF (K.EQ. 76) R2=NST(J2,K)-RST(J2,K-1)
IF (K.EQ. 77) R2=NST(J2,K)-RST(J2,K-1)
IF (K.EQ. 78) R2=NST(J2,K)-RST(J2,K-1)
IF (K.EQ. 79) R2=NST(J2,K)-RST(J2,K-1)
IF (K.EQ. 80) R2=NST(J2,K)-RST(J2,K-1)
IF (K.EQ. 81) R2=NST(J2,K)-RST(J2,K-1)
IF (K.EQ. 82) R2=NST(J2,K)-RST(J2,K-1)
IF (K.EQ. 83) R2=NST(J2,K)-RST(J2,K-1)
IF (K.EQ. 84) R2=NST(J2,K)-RST(J2,K-1)
IF (K.EQ. 85) R2=NST(J2,K)-RST(J2,K-1)
IF (K.EQ. 86) R2=NST(J2,K)-RST(J2,K-1)
IF (K.EQ. 87) R2=NST(J2,K)-RST(J2,K-1)
IF (K.EQ. 88) R2=NST(J2,K)-RST(J2,K-1)
IF (K.EQ. 89) R2=NST(J2,K)-RST(J2,K-1)
IF (K.EQ. 90) R2=NST(J2,K)-RST(J2,K-1)
IF (K.EQ. 91) R2=NST(J2,K)-RST(J2,K-1)
IF (K.EQ. 92) R2=NST(J2,K)-RST(J2,K-1)
IF (K.EQ. 93) R2=NST(J2,K)-RST(J2,K-1)
IF (K.EQ. 94) R2=NST(J2,K)-RST(J2,K-1)
IF (K.EQ. 95) R2=NST(J2,K)-RST(J2,K-1)
IF (K.EQ. 96) R2=NST(J2,K)-RST(J2,K-1)
IF (K.EQ. 97) R2=NST(J2,K)-RST(J2,K-1)
IF (K.EQ. 98) R2=NST(J2,K)-RST(J2,K-1)
IF (K.EQ. 99) R2=NST(J2,K)-RST(J2,K-1)
IF (K.EQ. 100) R2=NST(J2,K)-RST(J2,K-1)

```

```

89 RUN BY REED, JOHNSON, NASA-AMRS RES. CIR., AUG., 1974.
(PDLP100 VERSION)
C THIS SUBROUTINE CHECKS WHETHER A CONTOUR LINE AT LEVEL NVAL
PASSES THROUGH AN INTERVAL HAVING INDICES JPK AT ITS
LEFT END (J,K) OR RIGHT END (J+1, K).
C
DIMENSION A(1),ACONT(1),ICM(4,1)
1 I=I0+(J,K)+1*(K-1)*JDIM
GO TO (2,3),K02
2 I=I0+(J,K+1)
3 I=I0+(J+1,K)
4 I=I0+(J,K)
5 I=I0+(J,K+1)
6 I=I0+(J+1,K)
7 I=I0+(J,K)
8 I=I0+(J,K+1)
9 I=I0+(J+1,K)
10 I=I0+(J,K)
11 I=I0+(J,K+1)
12 I=I0+(J+1,K)
13 I=I0+(J,K)
14 I=I0+(J,K+1)
15 I=I0+(J+1,K)
16 I=I0+(J,K)
17 I=I0+(J,K+1)
18 I=I0+(J+1,K)
19 I=I0+(J,K)
20 I=I0+(J,K+1)
21 I=I0+(J+1,K)
22 I=I0+(J,K)
23 I=I0+(J,K+1)
24 I=I0+(J+1,K)
25 I=I0+(J,K)
26 I=I0+(J,K+1)
27 I=I0+(J+1,K)
28 I=I0+(J,K)
29 I=I0+(J,K+1)
30 I=I0+(J+1,K)
31 I=I0+(J,K)
32 I=I0+(J,K+1)
33 I=I0+(J+1,K)
34 I=I0+(J,K)
35 I=I0+(J,K+1)
36 I=I0+(J+1,K)
37 I=I0+(J,K)
38 I=I0+(J,K+1)
39 I=I0+(J+1,K)
40 I=I0+(J,K)
41 I=I0+(J,K+1)
42 I=I0+(J+1,K)
43 I=I0+(J,K)
44 I=I0+(J,K+1)
45 I=I0+(J+1,K)
46 I=I0+(J,K)
47 I=I0+(J,K+1)
48 I=I0+(J+1,K)
49 I=I0+(J,K)
50 I=I0+(J,K+1)
51 I=I0+(J+1,K)
52 I=I0+(J,K)
53 I=I0+(J,K+1)
54 I=I0+(J+1,K)
55 I=I0+(J,K)
56 I=I0+(J,K+1)
57 I=I0+(J+1,K)
58 I=I0+(J,K)
59 I=I0+(J,K+1)
60 I=I0+(J+1,K)
61 I=I0+(J,K)
62 I=I0+(J,K+1)
63 I=I0+(J+1,K)
64 I=I0+(J,K)
65 I=I0+(J,K+1)
66 I=I0+(J+1,K)
67 I=I0+(J,K)
68 I=I0+(J,K+1)
69 I=I0+(J+1,K)
70 I=I0+(J,K)
71 I=I0+(J,K+1)
72 I=I0+(J+1,K)
73 I=I0+(J,K)
74 I=I0+(J,K+1)
75 I=I0+(J+1,K)
76 I=I0+(J,K)
77 I=I0+(J,K+1)
78 I=I0+(J+1,K)
79 I=I0+(J,K)
80 I=I0+(J,K+1)
81 I=I0+(J+1,K)
82 I=I0+(J,K)
83 I=I0+(J,K+1)
84 I=I0+(J+1,K)
85 I=I0+(J,K)
86 I=I0+(J,K+1)
87 I=I0+(J+1,K)
88 I=I0+(J,K)
89 I=I0+(J,K+1)
90 I=I0+(J+1,K)
91 I=I0+(J,K)
92 I=I0+(J,K+1)
93 I=I0+(J+1,K)
94 I=I0+(J,K)
95 I=I0+(J,K+1)
96 I=I0+(J+1,K)
97 I=I0+(J,K)
98 I=I0+(J,K+1)
99 I=I0+(J+1,K)
100 I=I0+(J,K)

```







```

99 8NDRY
70 8NDRY
71 8NDRY
72 8NDRY
73 8NDRY
74 8NDRY
75 8NDRY
76 8NDRY
77 8NDRY
78 8NDRY
79 8NDRY
80 8NDRY
81 8NDRY
82 8NDRY
83 8NDRY
84 8NDRY
85 8NDRY
86 8NDRY
87 8NDRY
88 8NDRY
89 8NDRY
90 8NDRY
91 8NDRY

```

```

6 ITHETA=1.570796327
7 GO TO 1
7 THETA=PI*(I-1)/(J-1)
8 CONTINUE
9 UI=0.1*CDOS(THETA)
10 VI=0.1*SIN(THETA)
11 THETA=5.0*PI*(I-1)/(J-1)+.24*78
12 O(J,I,1)=1+UI*DI
13 O(J,I,2)=1+VI*DI
14 O(J,I,3)=1+UI*DI
15 O(J,I,4)=1+VI*DI
16 CONTINUE
17 RETURN
18 PRINT MESSAGE FOR NEGATIVE PRESSURE
19 P1=ABS(P1)
20 G TO 10
21 FOPMATH(X)=44*NEGATIVE PRESSURE ON BODY DETECTED BY 8NDRY,24,
22 * 3PRP=PI*EIGU*3*OH AT J=12)
23 FNC
24 SUBROUTINE BODY(X,RNOSE,YANG,H)
25 F(A)=EXP(-ABS(A-RNOSE)/H)
26 F(B)=EXP(-ABS(B-SIN(Z*90)))+(-1)**K*2*SQRT(E(A)-E(A)**2))
27 F(C)=EXP(-ABS(C-SIN(B**2)))
28 F(D)=EXP(-ABS(D-SIN(B**2)))
29 G(A,B)=ABS(A*(A**6)+SIN(B)*COS(B)+SQRT(A**6-1.0))/(A**6+COS(B)**2-1
30 * 0.1)
31 H=NE. 1.0 ; IONORAUSE FOR A NONMAGNETIC PLANET
32 H=EG. 0.0 ; EQUATORIAL PLANE FOR A MAGNETIC PLANET
33 IF(H.EG. 0.0) GO TO 10
34 ***** THIS DETERMINES THE BODY SHAPE OF A NONMAGNETIC PLANET
35 *****
36 IMA=300
37 IMA(XI=IMA)-1
38 IF(ANG.EG. 0.0) IMA(XI=1)
39 PI=3.141592653589793
40 RAD=180/PI
41 ANG=ANG*PI/RAD
42 DELTAT=ANG/FLUAT(IMAXMI)
43 THETA=0
44 R1=RNOSE
45 ISTART=1
46 IF (H.EG. 0.1) G O TO 20
47 ***** PERFORM INTEGRATION FROM 0 TO SANGS DEGREES
48 CONTINUE
49 DD = ISTART, IMA(XI)
50 ***** PREDICTOR
51 K=C
52 X=THETA/RAD
53 N=1
54 R=PI*DELTA/RAD*F(R1,X,N)
55 THETA=THETA+DELTA
56 X=X+THETA/RAD
57 ***** CORRECTOR
58 CONTINUE
59 R=PI*DELTA/RAD*F(R1,X,N)+F(R1,X,N)
60 IF(LK.LT. 5) GO TO 1
61 X=X+R*DELTA/RAD
62 Y=Y+R*SIN(THETA/RAD)
63 R1=R
64 CONTINUE
65 RETURN
66 CONTINUE
67 IF (H.ALT. 0.01) GO TO 30
68 DO 35 J=1, IMA(XI)
69 R=RNOSE+H*SIN(THETA/RAD)**2
70 X=1.0+R*COS(THETA/RAD)
71 Y=H*SIN(THETA/RAD)
72 R1=R
73 CONTINUE
74 IF(THETA.EG. 5.0) GO TO 2

```

```

2 8NDRY
3 8NDRY
4 8NDRY
5 8NDRY
6 8NDRY
7 8NDRY
8 8NDRY
9 8NDRY
10 8NDRY
11 8NDRY
12 8NDRY
13 8NDRY
14 8NDRY
15 8NDRY
16 8NDRY
17 8NDRY
18 8NDRY
19 8NDRY
20 8NDRY
21 8NDRY
22 8NDRY
23 8NDRY
24 8NDRY
25 8NDRY
26 8NDRY
27 8NDRY
28 8NDRY
29 8NDRY
30 8NDRY
31 8NDRY
32 8NDRY
33 8NDRY
34 8NDRY
35 8NDRY
36 8NDRY
37 8NDRY
38 8NDRY
39 8NDRY
40 8NDRY
41 8NDRY
42 8NDRY
43 8NDRY
44 8NDRY
45 8NDRY
46 8NDRY
47 8NDRY
48 8NDRY
49 8NDRY
50 8NDRY
51 8NDRY
52 8NDRY
53 8NDRY
54 8NDRY
55 8NDRY
56 8NDRY
57 8NDRY
58 8NDRY
59 8NDRY
60 8NDRY
61 8NDRY
62 8NDRY
63 8NDRY
64 8NDRY
65 8NDRY
66 8NDRY
67 8NDRY
68 8NDRY

```

```

21 ABMATH 22
22 ABMATH 23
23 ABMATH 24
24 ABMATH 25
25 ABMATH 26
26 ABMATH 27
27 ABMATH 28
28 ABMATH 29
29 ABMATH 30
30 ABMATH 31
31 ABMATH 32
32 ABMATH 33
33 ABMATH 34
34 8NDRY
35 CORL
36 CORL
37 CUR1
38 CUR1
39 CUR2
40 CUR2
41 CUR3
42 CUR3
43 8NDRY
44 8NDRY
45 8NDRY
46 8NDRY
47 8NDRY
48 8NDRY
49 8NDRY
50 8NDRY
51 8NDRY
52 8NDRY
53 8NDRY
54 8NDRY
55 8NDRY
56 8NDRY
57 8NDRY
58 8NDRY
59 8NDRY
60 8NDRY
61 8NDRY
62 8NDRY
63 8NDRY
64 8NDRY
65 8NDRY
66 8NDRY
67 8NDRY
68 8NDRY

```

```

AB(2,2)=XK-YY*(GAM-2.0)*URT
AR(2,3)=Y*GAMP1+VZZ*U
AB(2,4)=Y*GAMM
AB(3,1)=ZZ*SS-V*Y
AB(3,2)=Y*V+ZZ*GAMM*U
AB(3,3)=XK-ZZ*(GAM-2.0)*V*Y
AB(3,4)=ZZ*GAMM
AF(4,1)=1+12.0*SS-W
AF(4,2)=1+SS*Y*Y-GAMM*U*U
AB(4,3)=1+SS*1+ZZ-GAMM*U*U
BLTURN
END
SUBROUTINE 8NDRY
COMMON/COM1/JMAX,KMAX,KMAX,JM,KM,KMACH,ALPHA,GAM,GAMSL,CN,DT,SHU,IPRT,
> CHORD,NCA,NCB,NCC,AA,ADJ,CG,NL,LI,TAU,ITER,ENT,P,PI,PINF,
<PINF,CIN,CLIN,CCS,TH,CLUS,PI,HORN,RNOSE,PCASE,NPUNC4
COMMON /COM2/ X(25,20),Y(25,20),Z(25,20),XEL(25,2),ZEL(2)
* XEY(25,2),ZEL(2),U(25,20)
COMMON /COM3/ Q(25,20,4),FF(25,4),S(25,20,4),G(4),AB(4,4)
DIMENSION P(25,3),PAI(25),PETA(25),UI(25,3),UX(1,25),UETA(25),
* V(25,3),VAI(25),VITA(25),K(25,3)
***** REFLECTION TO SIMULATE PLANE OF SYMMETRY AT J=2
DO 12 K=1,KMAX
60=0(2,K)/U(1,K)
O(1,K,1)=0(2,K,1)*20
O(1,K,2)=0(2,K,2)*100
O(1,K,3)=0(2,K,3)*100
12 O(1,K,4)=0(2,K,4)*100
***** FIRST ORDER CAPTAPULATION TO SIMULATE SUPERSONIC W/FLON
***** BOUNDARY CONDITION AT JMAX
DO 1 N=1,N
DO 1 K=2,KM
1 O(1,K,K,N)=(2.0*O(1,K,K,N)+O(1,K,K,N)-J(1,N-I,K,N)*O(1,K,K,N))/
> O(1,K,K,N)
***** SATISFY TANGENCY CONDITION USING CHARACTERISTIC EQUATION
DO 3 K=1,K3
DO 3 J=2,JMAX
Z(1,0)=O(1,K,1)
V(1,K)=O(1,K,2)
U(1,K)=O(1,K,3)
V(1,K)=O(1,K,3)*2
Z(2,0)=J(1,2)+O(1,K,1)
3 P(1,K)=(12.0*O(1,K,1)+O(1,K,2)+O(1,K,3)+O(1,K,4))/GAMM
***** COMPUTE P-AI, U-XI, V-XI, P-LTAU, U-ETA, AND V-ETA DERIVATIVES
DO 4 J=2,JM
P(1,J)=O(1,K,1)-P(1,J-1)*11*0.5
U(1,J)=O(1,K,2)-U(1,J-1)*11*0.5
V(1,J)=O(1,K,3)-V(1,J-1)*11*0.5
P(1,J)=P(1,J)
V(1,J)=V(1,J)
V(1,J)=V(1,J)
P(1,J)=P(1,J)
P(1,J)=P(1,J)+4.0*P(1,J-1)*O(1,K,1)+O(1,K,2)
V(1,J)=V(1,J)+4.0*V(1,J-1)*O(1,K,2)+O(1,K,3)
DO 5 J=1,JMAX
P(1,J)=1-5.0*(O(1,J,1)+O(1,J,2)+O(1,J,3))+O(1,J,4)
V(1,J)=1-5.0*(O(1,J,1)+O(1,J,2)+O(1,J,3))+O(1,J,4)
P(1,J)=1-5.0*(O(1,J,1)+O(1,J,2)+O(1,J,3))+O(1,J,4)
P(1,J)=1-5.0*(O(1,J,1)+O(1,J,2)+O(1,J,3))+O(1,J,4)
5 CONTINUE
P(1,2)=12.2
V(1,2)=12.0
P(1,2)=12.0
DO 2 M=2,MJMAX
DO 2 N=2,NJMAX
P(1,2)=O(1,K,1)+O(1,K,2)
V(1,2)=O(1,K,2)+O(1,K,3)
U(1,2)=O(1,K,3)+O(1,K,4)
V(1,2)=O(1,K,3)+O(1,K,4)
V(1,2)=O(1,K,3)+O(1,K,4)
E=UBAR*P(1,2)+UR*U(1,2)+V*V(1,2)+W*W(1,2)+X*X(1,2)+Y*Y(1,2)+Z*Z(1,2)
> XEY(1,2)=X*Y(1,2)+Y*Y(1,2)+Z*Z(1,2)+P*P(1,2)+R(R(1,2)+UBAR*V(1,2))
> V(1,2)=V(1,2)+FLOAT(JCS)
PIAU=CBW/Z*PETA(1,2)+R(1,2)+CBB*E*(X(1,2)+Y(1,2)+Z(1,2)+UETA(1,2)+X*Y(1,2)+
> V(1,2))-E
PI=PI/J(1)+PI*TAU*O(1,2)+U(1,2)*U(1,2)
IF (PI.LT. 0.0) GO TO 9
10 CONTINUE
IF(J.LL.2) P1=PI*(P(3,1)-PI)*0.11111111
R1=(PI/PIENI)**(1.0/W/GAM)
C1=SQRT(2-C*GAM/GAMSL)*ABS(PI*PI-R1)
IF(ABS(XEY(1,2))>.006001) 5,6,7

```





INITIA 20
INITIA 21
INITIA 22
INITIA 23
INITIA 24
INITIA 25
INITIA 26
INITIA 27
INITIA 28
INITIA 29
INITIA 30
INITIA 31
INITIA 32
INITIA 33
INITIA 34
INITIA 35
INITIA 36
INITIA 37
INITIA 38
INITIA 39
INITIA 40
INITIA 41
INITIA 42
INITIA 43
INITIA 44
INITIA 45
INITIA 46
INITIA 47
INITIA 48
INITIA 49
INITIA 50
INITIA 51
INITIA 52
INITIA 53
INITIA 54
INITIA 55
INITIA 56
INITIA 57
INITIA 58
INITIA 59
INITIA 60
INITIA 61
INITIA 62
INITIA 63
INITIA 64
INITIA 65
INITIA 66
INITIA 67
INITIA 68
INITIA 69
INITIA 70
INITIA 71
INITIA 72
INITIA 73
INITIA 74
INITIA 75
INITIA 76
INITIA 77
INITIA 78
INITIA 79
INITIA 80
INITIA 81
INITIA 82
INITIA 83
INITIA 84
INITIA 85
INITIA 86
INITIA 87
INITIA 88
INITIA 89
INITIA 90
INITIA 91
INITIA 92
INITIA 93
INITIA 94
INITIA 95
INITIA 96
INITIA 97
INITIA 98
INITIA 99
INITIA 100
INITIA 101
INITIA 102
INITIA 103
INITIA 104

```

C... (I=2) AT A GIVEN NODE POINT
7 EIGEN
8 W=0(J,K)
9 P1=0.5
10 U=0(J,K,2)*K1
11 V=0(J,K,3)*K1
12 W=0(J,K,4)*K1
13 X=0(J,K,5)*K1
14 Y=0(J,K,6)*K1
15 Z=0(J,K,7)*K1
16 CAPU=X*Y*Z
17 CAPV=X*Y*Z
18 CAPW=X*Y*Z
19 CAPX=X*Y*Z
20 CAPY=X*Y*Z
21 CAPZ=X*Y*Z
22 CAPA=X*Y*Z
23 CAPB=X*Y*Z
24 CAPC=X*Y*Z
25 CAPD=X*Y*Z
26 CAPD=0
27 CAPD=0
28 CAPD=0
29 CAPD=0
30 CAPD=0
31 CAPD=0
32 CAPD=0
33 CAPD=0
34 CAPD=0
35 CAPD=0
36 CAPD=0
37 CAPD=0
38 CAPD=0
39 CAPD=0
40 CAPD=0
41 CAPD=0
42 CAPD=0
43 CAPD=0
44 CAPD=0
45 CAPD=0
46 CAPD=0
47 CAPD=0
48 CAPD=0
49 CAPD=0
50 CAPD=0
51 CAPD=0
52 CAPD=0
53 CAPD=0
54 CAPD=0
55 CAPD=0
56 CAPD=0
57 CAPD=0
58 CAPD=0
59 CAPD=0
60 CAPD=0
61 CAPD=0
62 CAPD=0
63 CAPD=0
64 CAPD=0
65 CAPD=0
66 CAPD=0
67 CAPD=0
68 CAPD=0
69 CAPD=0
70 CAPD=0
71 CAPD=0
72 CAPD=0
73 CAPD=0
74 CAPD=0
75 CAPD=0
76 CAPD=0
77 CAPD=0
78 CAPD=0
79 CAPD=0
80 CAPD=0
81 CAPD=0
82 CAPD=0
83 CAPD=0
84 CAPD=0
85 CAPD=0
86 CAPD=0
87 CAPD=0
88 CAPD=0
89 CAPD=0
90 CAPD=0
91 CAPD=0
92 CAPD=0
93 CAPD=0
94 CAPD=0
95 CAPD=0
96 CAPD=0
97 CAPD=0
98 CAPD=0
99 CAPD=0
100 CAPD=0
101 CAPD=0
102 CAPD=0
103 CAPD=0
104 CAPD=0

```

```

C... (I=2) AT A GIVEN NODE POINT
7 EIGEN
8 W=0(J,K)
9 P1=0.5
10 U=0(J,K,2)*K1
11 V=0(J,K,3)*K1
12 W=0(J,K,4)*K1
13 X=0(J,K,5)*K1
14 Y=0(J,K,6)*K1
15 Z=0(J,K,7)*K1
16 CAPU=X*Y*Z
17 CAPV=X*Y*Z
18 CAPW=X*Y*Z
19 CAPX=X*Y*Z
20 CAPY=X*Y*Z
21 CAPZ=X*Y*Z
22 CAPA=X*Y*Z
23 CAPB=X*Y*Z
24 CAPC=X*Y*Z
25 CAPD=X*Y*Z
26 CAPD=0
27 CAPD=0
28 CAPD=0
29 CAPD=0
30 CAPD=0
31 CAPD=0
32 CAPD=0
33 CAPD=0
34 CAPD=0
35 CAPD=0
36 CAPD=0
37 CAPD=0
38 CAPD=0
39 CAPD=0
40 CAPD=0
41 CAPD=0
42 CAPD=0
43 CAPD=0
44 CAPD=0
45 CAPD=0
46 CAPD=0
47 CAPD=0
48 CAPD=0
49 CAPD=0
50 CAPD=0
51 CAPD=0
52 CAPD=0
53 CAPD=0
54 CAPD=0
55 CAPD=0
56 CAPD=0
57 CAPD=0
58 CAPD=0
59 CAPD=0
60 CAPD=0
61 CAPD=0
62 CAPD=0
63 CAPD=0
64 CAPD=0
65 CAPD=0
66 CAPD=0
67 CAPD=0
68 CAPD=0
69 CAPD=0
70 CAPD=0
71 CAPD=0
72 CAPD=0
73 CAPD=0
74 CAPD=0
75 CAPD=0
76 CAPD=0
77 CAPD=0
78 CAPD=0
79 CAPD=0
80 CAPD=0
81 CAPD=0
82 CAPD=0
83 CAPD=0
84 CAPD=0
85 CAPD=0
86 CAPD=0
87 CAPD=0
88 CAPD=0
89 CAPD=0
90 CAPD=0
91 CAPD=0
92 CAPD=0
93 CAPD=0
94 CAPD=0
95 CAPD=0
96 CAPD=0
97 CAPD=0
98 CAPD=0
99 CAPD=0
100 CAPD=0
101 CAPD=0
102 CAPD=0
103 CAPD=0
104 CAPD=0

```













75 GEOM 76 GEOM 77 GEOM 78 GEOM 79 GEOM 80 GEOM 81 GEOM 82 GEOM 83 GEOM 84 GEOM 85 GEOM 86 GEOM 87 GEOM 88 GEOM 89 GEOM 90 GEOM 91 GEOM 92 GEOM 93 GEOM 94 GEOM 95 GEOM 96 GEOM 97 GEOM 98 GEOM 99 GEOM 100 GEOM 101 GEOM 102 GEOM 103 GEOM 104 GEOM 105 GEOM 106 GEOM 107 GEOM 108 GEOM 109 GEOM 110 GEOM 111 GEOM 112 GEOM 113 GEOM 114 GEOM 115 GEOM 116 GEOM 117 GEOM 118 GEOM 119 GEOM 120 GEOM 121 GEOM 122

THETA=90
R1=PNDSZ
C.....PERFORM AN INTEGRATION FROM 90 TO 260 DEGREES
C
DO 15 I=1,IMAX
XX=THETA/RAOI
R=R1+D1\*LAT/RAOI\*(GIRL,XX)
THETA=THETA+DELTA
XXX=THETA/RAOI
C.....CORRECTK
R=R1+D1\*DELTA/RAOI\*(GIRL,XX)\*(R,XXX)
DROTH=GR\*(XXX)
R1=P
IF(THETA.LT.190)GO TO 15
ZSTA(J)=1+K\*CDOS(1270,--THETA)/RAOI
PZ(J)=R\*SIN(1270--THETA)/RAOI
DPOZ(J)=(-ORDI\*H\*CS(XXX)+R\*SIN(XXX))/(-ORDT+\*SIN(XXX))-R\*CDOS(XXX)
J=J+1
15 CONTINUE
RETURN
C.....BODY SHAPE TABLE SUPPLIED BY USER
20 CONTINUE
J=1
DX2=C
DR2=C
NBOIM=NBOU-1
DO 25 I=1,NBOIM
DX1=DX2
DR1=DR2
DX2=XROD(I)+1-XBOD(I)
DR2=YBOD(I)+1-YBOD(I)
IF(XBOD(I).GT.A)C) GO TO 25
ZSTA(J)=1+(-XBOD(I)
RZ(J)=YBOD(I)
C2=SORT(DR1\*CRK+DX1\*DX1)
L2=SORT(DR2\*CRK+DX2\*DX2)
PZ2(J)=(-CR1\*OZ/DR1+UR2\*O1/DR2)/(O1+O2)
J=J+1
25 CONTINUE
ZSTA(J)=1+XOOS(NBOD)
DRZ(J)=YEGEN(NBOD)
PZURN.
END

EIGENM 86 GEOM 2
EIGENM 87 GEOM 3
EIGENM 88 GEOM 4
EIGENM 89 GEOM 5
EIGENM 90 GEOM 6
EIGENM 91 GEOM 7
EIGENM 92 GEOM 8
EIGENM 93 GEOM 9
EIGENM 94 GEOM 10
EIGENM 95 GEOM 11
GEOM 12
GEOM 13
GEOM 14
GEOM 15
GEOM 16
GEOM 17
GEOM 18
GEOM 19
GEOM 20
GEOM 21
GEOM 22
GEOM 23
GEOM 24
GEOM 25
GEOM 26
GEOM 27
GEOM 28
GEOM 29
GEOM 30
GEOM 31
GEOM 32
GEOM 33
GEOM 34
GEOM 35
GEOM 36
GEOM 37
GEOM 38
GEOM 39
GEOM 40
GEOM 41
GEOM 42
GEOM 43
GEOM 44
GEOM 45
GEOM 46
GEOM 47
GEOM 48
GEOM 49
GEOM 50
GEOM 51
GEOM 52
GEOM 53
GEOM 54
GEOM 55
GEOM 56
GEOM 57
GEOM 58
GEOM 59
GEOM 60
GEOM 61
GEOM 62
GEOM 63
GEOM 64
GEOM 65
GEOM 66
GEOM 67
GEOM 68
GEOM 69
GEOM 70
GEOM 71
GEOM 72
GEOM 73
GEOM 74

ORDT=DZ/OI
ICONST(11)=100\*ICONST(11)
ICONST(12)=100\*ICONST(12)
CONTINUE
RETURN
103 FORMAT(10,4)NEGATIVE SIGMA-BAR-1 IN EIGENM INDICATES
104 FORMAT(10,4)NEGATIVE SIGMA-BAR-2 IN EIGENM INDICATES
END
SUBROUTINE GEOM(RNDSZ,ANG,RZ,ORDZ,ZSTA,M,R9)
DIMENSION ZSTA(20),ORD(200),RZ(200)
COMMON /NBOED/ XBO(100),YBOD(100),NBOD
C.....FUNCTION DEFINITIONS
F(A,B)=EXP(-ABS(A-RNDSZ)/H)
F(A,B)=5\*A\*(SIN(12+\*B)-2.\*SQRT(1-(A)-E1(A)-SIN(B)\*B2))
E(A,B)=ABS(A\*(A+\*SIN(18)\*COS(B)+SORT(A\*\*B-1.)/(A\*\*B+COS(18)\*B-1.))
C.....M=EO J=O EQUATORIAL PLANE FOR A MAGNETIC PLANET
C.....M=EO J=O EQUATORIAL PLANE FOR A MAGNETIC PLANET
C.....M=EO J=O EQUATORIAL PLANE FOR A MAGNETIC PLANET
IF(M.EQ.0)GO TO 10
IF(M.LT.0) GO TO 20
IF (M.LT.0) GO TO 30
C.....THIS DETERMINES THE BODY SHAPE OF A NONMAGNETIC PLANET
C
IMAX=200
PI=3.1415926535898
RADI=150/PI
DELTA=ANG/FLOAT(IMAX)
M1=990
C.....PERFORM AN INTEGRATION FROM 0 TO 170 DEGREES
ZSTA(1)=1.0
RZ(1)=R9C
XX=THETA/RAOI
DROZ(1)=F(R,XX)/R1
J=2
IMAXM1=IMAX-1
DO 5 I=1,IMAXM1
XX=THETA/RAOI
R=PI\*DELTA/RAOI\*(F(R,XX)
THETA=THETA+DELTA
XX=THETA/RAOI
R=PI\*DELTA/RAOI\*(F(R,XX)
DROZ(I)=F(R,XX)
5 CONTINUE
ZSTA(J)=1+K\*CDOS(110,--THETA)/RAOI
DPOZ(J)=R\*SIN(110--THETA)/RAOI
DROZ(J)=(-ORDI\*H\*CS(XXX)+R\*SIN(XXX))/(-ORDT+\*SIN(XXX))-R\*CDOS(XXX)
J=J+1
10 CONTINUE
ZSTA(J)=1+XOOS(NBOD)
DRZ(J)=YEGEN(NBOD)
PZURN.
END

GEOM 2
GEOM 3
GEOM 4
GEOM 5
GEOM 6
GEOM 7
GEOM 8
GEOM 9
GEOM 10
GEOM 11
GEOM 12
GEOM 13
GEOM 14
GEOM 15
GEOM 16
GEOM 17
GEOM 18
GEOM 19
GEOM 20
GEOM 21
GEOM 22
GEOM 23
GEOM 24
GEOM 25
GEOM 26
GEOM 27
GEOM 28
GEOM 29
GEOM 30
GEOM 31
GEOM 32
GEOM 33
GEOM 34
GEOM 35
GEOM 36
GEOM 37
GEOM 38
GEOM 39
GEOM 40
GEOM 41
GEOM 42
GEOM 43
GEOM 44
GEOM 45
GEOM 46
GEOM 47
GEOM 48
GEOM 49
GEOM 50
GEOM 51
GEOM 52
GEOM 53
GEOM 54
GEOM 55
GEOM 56
GEOM 57
GEOM 58
GEOM 59
GEOM 60
GEOM 61
GEOM 62
GEOM 63
GEOM 64
GEOM 65
GEOM 66
GEOM 67
GEOM 68
GEOM 69
GEOM 70
GEOM 71
GEOM 72
GEOM 73
GEOM 74

SUBROUTINE GEOM(KS)
LEVEL=2
TEMP=1.0
LARGE=1.0
FC(1)=2.0
FC(2)=4.0
FC(3)=8.0
FC(4)=16.0
FC(5)=32.0
FC(6)=64.0
FC(7)=128.0
FC(8)=256.0
FC(9)=512.0
FC(10)=1024.0
FC(11)=2048.0
FC(12)=4096.0
FC(13)=8192.0
FC(14)=16384.0
FC(15)=32768.0
FC(16)=65536.0
FC(17)=131072.0
FC(18)=262144.0
FC(19)=524288.0
FC(20)=1048576.0
FC(21)=2097152.0
FC(22)=4194304.0
FC(23)=8388608.0
FC(24)=16777216.0
FC(25)=33554432.0
FC(26)=67108864.0
FC(27)=134217728.0
FC(28)=268435456.0
FC(29)=536870912.0
FC(30)=1073741824.0
FC(31)=2147483648.0
FC(32)=4294967296.0
FC(33)=8589934592.0
FC(34)=17179869184.0
FC(35)=34359738368.0
FC(36)=68719476736.0
FC(37)=137438953472.0
FC(38)=274877906944.0
FC(39)=549755813888.0
FC(40)=1099511627776.0
FC(41)=2199023255552.0
FC(42)=4398046511104.0
FC(43)=8796093022208.0
FC(44)=17592186044416.0
FC(45)=35184372088832.0
FC(46)=70368744177664.0
FC(47)=140737488355328.0
FC(48)=281474976710656.0
FC(49)=562949953421312.0
FC(50)=1125899906842624.0
FC(51)=2251799813685248.0
FC(52)=4503599627370496.0
FC(53)=9007199254740992.0
FC(54)=18014398509481984.0
FC(55)=36028797018963968.0
FC(56)=72057594037927936.0
FC(57)=144115188075855872.0
FC(58)=288230376151711744.0
FC(59)=576460752303423488.0
FC(60)=1152921504606846976.0
FC(61)=2305843009213693952.0
FC(62)=4611686018427387904.0
FC(63)=9223372036854775808.0
FC(64)=18446744073709551616.0
FC(65)=36893488147419103232.0
FC(66)=73786976294838206464.0
FC(67)=147573952589676412928.0
FC(68)=295147905179352825856.0
FC(69)=590295810358705651712.0
FC(70)=1180591620717411303424.0
FC(71)=2361183241434822606848.0
FC(72)=4722366482869645213696.0
FC(73)=9444732965739290427392.0
FC(74)=18889465931478580854784.0

GEOM 2
GEOM 3
GEOM 4
GEOM 5
GEOM 6
GEOM 7
GEOM 8
GEOM 9
GEOM 10
GEOM 11
GEOM 12
GEOM 13
GEOM 14
GEOM 15
GEOM 16
GEOM 17
GEOM 18
GEOM 19
GEOM 20
GEOM 21
GEOM 22
GEOM 23
GEOM 24
GEOM 25
GEOM 26
GEOM 27
GEOM 28
GEOM 29
GEOM 30
GEOM 31
GEOM 32
GEOM 33
GEOM 34
GEOM 35
GEOM 36
GEOM 37
GEOM 38
GEOM 39
GEOM 40
GEOM 41
GEOM 42
GEOM 43
GEOM 44
GEOM 45
GEOM 46
GEOM 47
GEOM 48
GEOM 49
GEOM 50
GEOM 51
GEOM 52
GEOM 53
GEOM 54
GEOM 55
GEOM 56
GEOM 57
GEOM 58
GEOM 59
GEOM 60
GEOM 61
GEOM 62
GEOM 63
GEOM 64
GEOM 65
GEOM 66
GEOM 67
GEOM 68
GEOM 69
GEOM 70
GEOM 71
GEOM 72
GEOM 73
GEOM 74

USE CYLINDRICAL BODY FOR HARD ALT. 0.01
ZSTA(1)=1.0
ZSTA(2)=1.0
ZSTA(3)=1.0
ZSTA(4)=1.0
ZSTA(5)=1.0
ZSTA(6)=1.0
ZSTA(7)=1.0
ZSTA(8)=1.0
ZSTA(9)=1.0
ZSTA(10)=1.0
ZSTA(11)=1.0
ZSTA(12)=1.0
ZSTA(13)=1.0
ZSTA(14)=1.0
ZSTA(15)=1.0
ZSTA(16)=1.0
ZSTA(17)=1.0
ZSTA(18)=1.0
ZSTA(19)=1.0
ZSTA(20)=1.0
ZSTA(21)=1.0
ZSTA(22)=1.0
ZSTA(23)=1.0
ZSTA(24)=1.0
ZSTA(25)=1.0
ZSTA(26)=1.0
ZSTA(27)=1.0
ZSTA(28)=1.0
ZSTA(29)=1.0
ZSTA(30)=1.0
ZSTA(31)=1.0
ZSTA(32)=1.0
ZSTA(33)=1.0
ZSTA(34)=1.0
ZSTA(35)=1.0
ZSTA(36)=1.0
ZSTA(37)=1.0
ZSTA(38)=1.0
ZSTA(39)=1.0
ZSTA(40)=1.0
ZSTA(41)=1.0
ZSTA(42)=1.0
ZSTA(43)=1.0
ZSTA(44)=1.0
ZSTA(45)=1.0
ZSTA(46)=1.0
ZSTA(47)=1.0
ZSTA(48)=1.0
ZSTA(49)=1.0
ZSTA(50)=1.0
ZSTA(51)=1.0
ZSTA(52)=1.0
ZSTA(53)=1.0
ZSTA(54)=1.0
ZSTA(55)=1.0
ZSTA(56)=1.0
ZSTA(57)=1.0
ZSTA(58)=1.0
ZSTA(59)=1.0
ZSTA(60)=1.0
ZSTA(61)=1.0
ZSTA(62)=1.0
ZSTA(63)=1.0
ZSTA(64)=1.0
ZSTA(65)=1.0
ZSTA(66)=1.0
ZSTA(67)=1.0
ZSTA(68)=1.0
ZSTA(69)=1.0
ZSTA(70)=1.0
ZSTA(71)=1.0
ZSTA(72)=1.0
ZSTA(73)=1.0
ZSTA(74)=1.0





```

INITA 121
INITA 122
INITA 123
INITA 124
INITA 125
INITA 126
INITA 127
INITA 128
INITA 129
INITA 130
INITA 131
INITA 132
INITA 133
INITA 134
INITA 135
INITA 136
INITA 137
INITA 138
INITA 139
INITA 140
INITA 141
INITA 142
INITA 143
INITA 144
INITA 145
INITA 146
INITA 147
INITA 148
INITA 149
INITA 150
INITA 151
INITA 152
INITA 153
INITA 154
INITA 155
INITA 156
INITA 157
INITA 158
INITA 159
INITA 160
INITA 161
INITA 162
INITA 163
INITA 164
INITA 165

CONST(2)=COS(ALPH)
UINF=QINF*CONST(2)
DO 3 K=2,NPHI1
  PHI=PHI(P(K))
  VINF(K)=QINF*CONST(1)*COS(PHI)
  WINF(K)=QINF*CONST(1)*SIN(PHI)
CONTINUE
DO 26 J=3,NTZ
  DO 28 K=3,NPHI
    P(J,K)=P90(J-2,K-2)
    RHQ(J,K)=RHQ90(J-2,K-2)
    U(J,K)=U90(J-2,K-2)
    V(J,K)=V90(J-2,K-2)
    W(J,K)=W90(J-2,K-2)
  28 CONTINUE
DO 29 K=3,NPHI
  PS(K)=P50(K-2)
  RSZ(K)=RSZ90(K-2)
  RSPHI(K)=RSPHI90(K-2)
  29 CONTINUE
DO 25 K=3,2
  ZINT=ZLC
  M=6-K
  I=NPHI+K
  N=NPHI-K
  PS(K)=RS(M)
  FS(I)=RS(N)
  RSZ(K)=RSZ(M)
  RSPHI(K)=RSPHI(M)
  25 CONTINUE
C*****WRITE TAPE - INITIAL DATA AND BODY SHAPE
ZM=P(3,3)/ABS(RHD(3,3))*GAMMA
ZM=ABS(ZM)
DO 3P K=3,NPHI
  SK=P(3,K)/ABS(RHD(3,K))*SAGMA
  SK=ABS(SK)
  3P CONTINUE
S(12)=S(4)
SINPHI(1)=SINPHI
CALL GEMBLP(HLP,NPHI,Z,RB,RBZ,KBPH,IPRNT)
RETURN
END

SUREQUINE (UCONK1)
LEVEL 2, LITLAP(3), P(2,60,MO)
COMMON(LANG,TAPE(4,2,4,41),E2(4,2,4,41),
* FC(4,2,4,41),H0(4,2,4,41),
LEVEL 2, RHD,P,UV,ROB,ROBZ,VINF,ROBPH,ROBZ,
* BCT,DTDZ,DFOR,ACT,ICONST,GAM,CONST,RRCOND,RS,
* RSPHI
COMMON /PVAR8/RHD(2,4,41), P(2,4,4,41), U(2,4,4,41), W(2,4,
* ),
RSH(4,1), KOSZ(4,1), VINF(4,1),
* KOPPH(4,1), RBZ(4,1),
* OTDPH(2,4,4,1), GCI(4,1),
* ICONST(5,5), NREGDN,
* RSZ(4,1), RSPHI(4,1),
* COPMON /IDVAR/RK=ZTA(4,1),PHI(4,1),DTIL(4,1),
* COMNU/SVAP/TAPE,
* ZENC, PI, ALPHA, GAMMA, SIGMA,
* TAPE2, DISKJ, ALPH, DISKZ,
* DZPK4, ZM, TMU,
* TML, RZ, BZ, NPHI, NIT,
* NPHI, NPHI1, NPHI2, NPHI3,
* NT, NIT, NT2, NTA,
* PHIF, METHUB, LAG, NRC,
* QINF,GASCUS,NK,AL,NPLNCH,
* INT,GET,DISKX,DISKZ,TAPE2,
* COMNU/RK/DI/WR,RS,CSMS,OR,
* COMNU /ACONT/NFECA(1,1)
* COMNU/CLLSTR/RJA(1,2,4),
* CLMCON /LUCJ/NTEST(3,1),
* 60 TO (5,5)Z=PI
CONTINUE
DO 3 J=3,NTZ
  3J X=PI(1)
C**CUDF,CONSUMVATIVE,VARLABELS

```

```

INITA 37
INITA 38
INITA 39
INITA 40
INITA 41
INITA 42
INITA 43
INITA 44
INITA 45
INITA 46
INITA 47
INITA 48
INITA 49
INITA 50
INITA 51
INITA 52
INITA 53
INITA 54
INITA 55
INITA 56
INITA 57
INITA 58
INITA 59
INITA 60
INITA 61
INITA 62
INITA 63
INITA 64
INITA 65
INITA 66
INITA 67
INITA 68
INITA 69
INITA 70
INITA 71
INITA 72
INITA 73
INITA 74
INITA 75
INITA 76
INITA 77
INITA 78
INITA 79
INITA 80
INITA 81
INITA 82
INITA 83
INITA 84
INITA 85
INITA 86
INITA 87
INITA 88
INITA 89
INITA 90
INITA 91
INITA 92
INITA 93
INITA 94
INITA 95
INITA 96
INITA 97
INITA 98
INITA 99
INITA 100
INITA 101
INITA 102
INITA 103
INITA 104
INITA 105
INITA 106
INITA 107
INITA 108
INITA 109
INITA 110
INITA 111
INITA 112
INITA 113
INITA 114
INITA 115
INITA 116
INITA 117
INITA 118
INITA 119
INITA 120

DETA=PHIF/FLOAT(NPHI)
DPMI=DETA
DT=1.0/FLOAT(NT-1)
DI=D(1,DI)
DIDPA=DI/DTA
GAM(1)=GAMMA-1.0*0.5
GAP(2)=GAM(1)/GAMA
NITER=75
PALE=0.0
R=COT
R=OC
IF(R<=0.0) GO TO 15
IF(C=5)KALOG((1.0+(EXP(RK))-1.0)/PHIFD(180.01/
* (1.0-EXP(-RK)))-PHIFD(180.01))
Y0Z=Y0I/(W*PHIFD/RADI)
15 CONTINUE
DO 35 I1=2,NPHI1
  Z1=I1-3
  ETAL(I1)=Z1*DETA
  IF(RK<0.0) GO TO 40
  PHIF(I1)=ETAL(I1)
  DIL(I1)=1.0
  DILF(I1)=C*0
  GO TO 35
40 CONTINUE
Y0Z=RRK*ETAL(I1)/PI-T5)
SHETA=SINH(Y93)
CHETA=COSH(Y93)
PHIF(I1)=PHIFD/ADI*(1.0+SHETA/Y0I)
DILF(I1)=Y0Z*PI/CHETA
DILF(I1)=Y0Z*W*SHETA/CHETA**2
CONTINUE
PHIF(2)=PHIF(4)
PHIF(NPHI1)=PHIF(NPHI)
DIL(2)=DIL(4)
DIL(NPHI1)=DIL(NPHI)
DILF(2)=DILF(4)
DILF(NPHI1)=DILF(NPHI)
DILF(3)=C*0
DILF(NPHI)=C
DIL(NPHI)=C
DIL(NPHI)=C
SINHJ=SINH(KJ)
DO 36 I1=2,NTZ
  Z1=I1-3
  TP(I1)=Z1*DI
  IF(R<0.0) GO TO 41
  DT=F*TP(I1)
  SOT=SINH(OT)
  COT=COSH(OT)
  XI(I1)=SOT/SINHJ
  TRI(I1)=SINHJ/(R*J*GOT)
  TRIL(I1)=SINHJ*SOTI/COT**2
  GO TO 42
  XI(I1)=TP(I1)
  TRI(I1)=1-C
  TAL(I1)=0.0
  CONTINUE
  NCON=2
  NTOSD5=0
  ZB5=9999.0
  ZELD=9999.0
  ITPR18=9999
  ITPR1F=4984
  CONST(9)=45
  ICONST(4)=1.1
  TAP(1)=1
  TAP(2)=2
  DISK1=1
  DISK2=3
C**CALCULATE FREE STREAM QUANTITIES
C
GAM(3)=GAMPA/GAMMA-5.0)
GAM(4)=1.0/(GAMMA-1-C)
AA=1.0+GAM(1)*XNACH**2
BB=AA-1.0
PINF=1.0/AA**CAR(3)
*HCIN=1.0/AA**GAM(4)
QINF=SQRT(PB/AA)
CONST(1)=SIN(ALPH)

```

```

DO 20 N=1,4
  O(N,J,K)=F(N)
  F(N,J,K)=F(N)
  G(N,J,K)=G(N)
  H(N,J,K)=H(N)
CONTINUE
GO TO 3
C++SIT CONSERVATIVE VARIABLES AT N+1 TILDE
DO 5 N=1,4
  T(F(J+Q,N+1,2)) GO TO 30
C++KESIT ETMP AT BODY AND SACK
30 ETMP(N,J,K)=(N)
CONTINUE
FC(N,J,K)=F(N)
GC(N,J,K)=G(N)
HC(N,J,K)=H(N)
CONTINUE
5 CONTINUE
RETURN
2 CONTINUE
C++CCLES CONSERVATIVE VARIABLES--PERFECT GAS
AA=1/G-CAR(2)
DO 1 K=3,NPHI
  DD 1 J=3,NPZ
  A=ETMP(J,K)
  B=LIMP(J,K)
  C=ETMP(J,K)
  D=ETMP(J,K)
  PE=9/A
  VIJ,K)=C/A
  VIJ,K)=D/A
  PL=B5+2*4*AA*CC
  IF (ED) 7,8,9
CONTINUE
7 DD=G*O
CONTINUE
8 VIJ,K)=(B5+SRT(DD))/(2*G*AA)
PHD(J,K)=A/VIJ,K)
VIJ,K)=H(C-VIJ,K)**2-VIJ,K)**2+2)
CONTINUE
1 RETURN
END
SUPROUTINE OUTPIM
LEVEL 2,ETMP,50,FJ,G,H
CERN,JN,LARGE,ETMP(4,24,41),ED(4,24,41),
  F(4,24,41),GC(4,24,41),HC(4,24,41)
LEVEL 2, KH0,P,UV,W,ROB,ROBZ,VIN,VIN,ARUBPH,RR,KBZ,RRBPH,DTDP4,
  BCT,DTDZ,DTDR,ACT,ICUNST,GA,CUNST,NRELGUN,RS,MSZ,NKSPHI,KSTRSZL,
  KSPHIT
COMMON /PVAR3/R=DT(2,41), P(2,4,41), U(2,4,41), V(2,4,41)
  R0(41), ROBZ(41), VINF(41), WINF(41)
  DRP(41), RBZ(41), RBZ(41), RBZ(41), RBPH(41)
  GTP(2,4,41), PCT(41), DT(2,4,41), DTOK(41), ACT(41)
  ICUNST(50), GAR(25), CONST(53), ANLEGON, NS(41)
  KST(41), KSPHIT(41), RST(41), RST(41), RST(41), RSPHIT(41)
  COMMON /IDVAKB/KK,ETA(41),PHI(41),DTIL(41),DTILE(41),DTA,TP(24)
  COMMON/SVAB/TS,Z, PHI, DT, Z
  ZENG, PI, ALPHA, GAMMA, SIGMA, AMACH, TAPEL
  TAPEZ, DISKA, ALPH, DISKZ, SIGM, NPKN, DZOT
  GZUPH, ZH, THM0, THLD, TML, NPHI, TTM
  THL, RZ, BZ, NPHI, NIT, KPHI, NITER
  NPHI, NP41, NP42, NP43, NP44, NP45, NP46, NP47, NP48, NP49, NP50, NP51, NP52, NP53, NP54, NP55, NP56, NP57, NP58, NP59, NP60, NP61, NP62, NP63, NP64, NP65, NP66, NP67, NP68, NP69, NP70, NP71, NP72, NP73, NP74, NP75, NP76, NP77, NP78, NP79, NP80, NP81, NP82, NP83, NP84, NP85, NP86, NP87, NP88, NP89, NP90, NP91, NP92, NP93, NP94, NP95, NP96, NP97, NP98, NP99, NP100, NP101, NP102, NP103, NP104, NP105, NP106, NP107, NP108, NP109, NP110, NP111, NP112, NP113, NP114, NP115, NP116, NP117, NP118, NP119, NP120, NP121, NP122, NP123, NP124, NP125, NP126, NP127, NP128, NP129, NP130, NP131, NP132, NP133, NP134, NP135, NP136, NP137, NP138, NP139, NP140, NP141, NP142, NP143, NP144, NP145, NP146, NP147, NP148, NP149, NP150
  PHF, METHUD, LAG, NMC, PINF, KNOIN, VINF
  GAIN, GASON, NRE4, NPNUNCH
  IALGFR, DISK, DISKZ, TAPEZ
  COMMON/NTRO/ST(41),Z(41),Z(41),ITPRIB,ITPRF,NCAS,NTDOS
  COMMON/CLUS/TRA,NJA(12),TXI(24),TXIT(24)
  COMMON/DNST/XPLOT,NBLUN,NZEND,NZADD
  COMMON/CON/RYCON,YCON(20),KCON,RCUN(20),XC(20),LOC,YC(20),IG(1)
  F(20),G(20),H(20),I(20)
  COMMON /BLCN/ THETA(20),RP(20,25)
  COMMON/VCOMP/ V(12),Z(20),VY(20),VJ(20)
  COMMON /SHOCKS/ ORSDX(100),ADST(50)
  IF (NZNED) 0, C) WRITE(6,610)
  NZEND=NZENE+1

```



SHOCKM 58 M=C-K  
SHOCKM 59 I=NPHI\*K  
SHOCKM 60 N=NPHI-K  
SHOCKM 61 RSZ(K)=PSZT(M)  
SHOCKM 62 RSZ(L)=RSZT(N)  
SHOCKM 63 RSPH(K)=RSPH(M)  
SHOCKM 64 RSPH(L)=RSPH(N)  
SHOCKM 65 CONTINUE  
SHOCKM 66 RETURN  
SHOCKM 67 CONTINUE  
SHOCKM 68 C..SHOCK CORR=LCIOR  
SHOCKM 69 DO F K=3,NFMI  
SHOCKM 70 K5(K)=RSK(K)\*5\*(RSZ(K)+RSZT(K))\*DZ  
SHOCKM 71 DO 9 K=1,2  
SHOCKM 72 M=C-K  
SHOCKM 73 I=NPHI\*K  
SHOCKM 74 N=NPHI-K  
SHOCKM 75 R5(K)=R5(M)  
SHOCKM 76 RS(L)=RS(L)  
SHOCKM 77 CONTINUE  
SHOCKM 78 DO 10 K=3,NPHI  
SHOCKM 79 R5P(M)=R5(K)\*1\*(RS(K)+RSZ(K))/2\*(D\*DETA)\*DTIL(K)  
SHOCKM 80 PS=P(L)\*Z(K)  
SHOCKM 81 FSPAT=R5/PLNF  
SHOCKM 82 ULT=ULTILU(P5KAT)  
SHOCKM 83 PHRAT=R5D5(P5RAT)  
SHOCKM 84 P5L=P5(K)  
SHOCKM 85 RSPH=RSPH(K)  
SHOCKM 86 FSPH=RSPH(K)  
SHOCKM 87 FAC(L)=VINF(K)-WINF(K)\*RSPH  
SHOCKM 88 FAC(L)=VINF(K)+WINF(K)\*RSPH  
SHOCKM 89 IFFACTZ=LT. 5.0\*ULT--UIT  
SHOCKM 90 RSZL=DRSDZ(ULT,RSPH,FAC(L),FAC(L))  
SHOCKM 91 F5Z(K)=R5ZL  
SHOCKM 92 ABART=ABAR(VINF(K),WINF(K),PSZL,RSPH,RHRAT)  
SHOCKM 93 USF=USVINF(K),ABART,RSZL  
SHOCKM 94 WSF=WSVINF(K),ABART,RSZL  
SHOCKM 95 PHO(INL)=Q5J  
SHOCKM 96 R5P=KRPAT\*PHOIN  
SHOCKM 97 PHO(INL)=R5P  
SHOCKM 98 VINFZ(K)=VSF  
SHOCKM 99 W(INL)=K1=VSF  
SHOCKM 100 CONTINUE  
SHOCKM 101 DO 11 K=1,2  
SHOCKM 102 I=NPHI\*K  
SHOCKM 103 N=NPHI-K  
SHOCKM 104 RSZ(K)=PSZ(M)  
SHOCKM 105 R5Z(L)=R5Z(N)  
SHOCKM 106 RSPH(K)=RSPH(M)  
SHOCKM 107 RSPH(L)=RSPH(N)  
SHOCKM 108 CONTINUE  
SHOCKM 109 RETURN  
SHOCKM 110  
SHOCKM 111 END  
SHOCKM 112

SETDAT 98  
SETDAT 99  
SETDAT 100  
SETDAT 101  
SETDAT 102  
SETDAT 103

SHOCKM 2  
SHOCKM 3  
SHOCKM 4  
SHOCKM 5  
SHOCKM 6  
SHOCKM 7  
SHOCKM 8  
SHOCKM 9  
SHOCKM 10  
SHOCKM 11  
SHOCKM 12  
SHOCKM 13  
SHOCKM 14  
SHOCKM 15  
SHOCKM 16  
SHOCKM 17  
SHOCKM 18  
SHOCKM 19  
SHOCKM 20  
SHOCKM 21  
SHOCKM 22  
SHOCKM 23  
SHOCKM 24  
SHOCKM 25  
SHOCKM 26  
SHOCKM 27  
SHOCKM 28  
SHOCKM 29  
SHOCKM 30  
SHOCKM 31  
SHOCKM 32  
SHOCKM 33  
SHOCKM 34  
SHOCKM 35  
SHOCKM 36  
SHOCKM 37  
SHOCKM 38  
SHOCKM 39  
SHOCKM 40  
SHOCKM 41  
SHOCKM 42  
SHOCKM 43  
SHOCKM 44  
SHOCKM 45  
SHOCKM 46  
SHOCKM 47  
SHOCKM 48  
SHOCKM 49  
SHOCKM 50  
SHOCKM 51  
SHOCKM 52  
SHOCKM 53  
SHOCKM 54  
SHOCKM 55  
SHOCKM 56  
SHOCKM 57

SHOCKM 2  
SHOCKM 3  
SHOCKM 4  
SHOCKM 5  
SHOCKM 6  
SHOCKM 7  
SHOCKM 8  
SHOCKM 9  
SHOCKM 10  
SHOCKM 11  
SHOCKM 12  
SHOCKM 13  
SHOCKM 14  
SHOCKM 15  
SHOCKM 16  
SHOCKM 17  
SHOCKM 18  
SHOCKM 19  
SHOCKM 20  
SHOCKM 21  
SHOCKM 22  
SHOCKM 23  
SHOCKM 24  
SHOCKM 25  
SHOCKM 26  
SHOCKM 27  
SHOCKM 28  
SHOCKM 29  
SHOCKM 30  
SHOCKM 31  
SHOCKM 32  
SHOCKM 33  
SHOCKM 34  
SHOCKM 35  
SHOCKM 36  
SHOCKM 37  
SHOCKM 38  
SHOCKM 39  
SHOCKM 40  
SHOCKM 41  
SHOCKM 42  
SHOCKM 43  
SHOCKM 44  
SHOCKM 45  
SHOCKM 46  
SHOCKM 47  
SHOCKM 48  
SHOCKM 49  
SHOCKM 50  
SHOCKM 51  
SHOCKM 52  
SHOCKM 53  
SHOCKM 54  
SHOCKM 55  
SHOCKM 56  
SHOCKM 57

SHOCKM 2  
SHOCKM 3  
SHOCKM 4  
SHOCKM 5  
SHOCKM 6  
SHOCKM 7  
SHOCKM 8  
SHOCKM 9  
SHOCKM 10  
SHOCKM 11  
SHOCKM 12  
SHOCKM 13  
SHOCKM 14  
SHOCKM 15  
SHOCKM 16  
SHOCKM 17  
SHOCKM 18  
SHOCKM 19  
SHOCKM 20  
SHOCKM 21  
SHOCKM 22  
SHOCKM 23  
SHOCKM 24  
SHOCKM 25  
SHOCKM 26  
SHOCKM 27  
SHOCKM 28  
SHOCKM 29  
SHOCKM 30  
SHOCKM 31  
SHOCKM 32  
SHOCKM 33  
SHOCKM 34  
SHOCKM 35  
SHOCKM 36  
SHOCKM 37  
SHOCKM 38  
SHOCKM 39  
SHOCKM 40  
SHOCKM 41  
SHOCKM 42  
SHOCKM 43  
SHOCKM 44  
SHOCKM 45  
SHOCKM 46  
SHOCKM 47  
SHOCKM 48  
SHOCKM 49  
SHOCKM 50  
SHOCKM 51  
SHOCKM 52  
SHOCKM 53  
SHOCKM 54  
SHOCKM 55  
SHOCKM 56  
SHOCKM 57

SHOCKM 2  
SHOCKM 3  
SHOCKM 4  
SHOCKM 5  
SHOCKM 6  
SHOCKM 7  
SHOCKM 8  
SHOCKM 9  
SHOCKM 10  
SHOCKM 11  
SHOCKM 12  
SHOCKM 13  
SHOCKM 14  
SHOCKM 15  
SHOCKM 16  
SHOCKM 17  
SHOCKM 18  
SHOCKM 19  
SHOCKM 20  
SHOCKM 21  
SHOCKM 22  
SHOCKM 23  
SHOCKM 24  
SHOCKM 25  
SHOCKM 26  
SHOCKM 27  
SHOCKM 28  
SHOCKM 29  
SHOCKM 30  
SHOCKM 31  
SHOCKM 32  
SHOCKM 33  
SHOCKM 34  
SHOCKM 35  
SHOCKM 36  
SHOCKM 37  
SHOCKM 38  
SHOCKM 39  
SHOCKM 40  
SHOCKM 41  
SHOCKM 42  
SHOCKM 43  
SHOCKM 44  
SHOCKM 45  
SHOCKM 46  
SHOCKM 47  
SHOCKM 48  
SHOCKM 49  
SHOCKM 50  
SHOCKM 51  
SHOCKM 52  
SHOCKM 53  
SHOCKM 54  
SHOCKM 55  
SHOCKM 56  
SHOCKM 57

SHOCKM 2  
SHOCKM 3  
SHOCKM 4  
SHOCKM 5  
SHOCKM 6  
SHOCKM 7  
SHOCKM 8  
SHOCKM 9  
SHOCKM 10  
SHOCKM 11  
SHOCKM 12  
SHOCKM 13  
SHOCKM 14  
SHOCKM 15  
SHOCKM 16  
SHOCKM 17  
SHOCKM 18  
SHOCKM 19  
SHOCKM 20  
SHOCKM 21  
SHOCKM 22  
SHOCKM 23  
SHOCKM 24  
SHOCKM 25  
SHOCKM 26  
SHOCKM 27  
SHOCKM 28  
SHOCKM 29  
SHOCKM 30  
SHOCKM 31  
SHOCKM 32  
SHOCKM 33  
SHOCKM 34  
SHOCKM 35  
SHOCKM 36  
SHOCKM 37  
SHOCKM 38  
SHOCKM 39  
SHOCKM 40  
SHOCKM 41  
SHOCKM 42  
SHOCKM 43  
SHOCKM 44  
SHOCKM 45  
SHOCKM 46  
SHOCKM 47  
SHOCKM 48  
SHOCKM 49  
SHOCKM 50  
SHOCKM 51  
SHOCKM 52  
SHOCKM 53  
SHOCKM 54  
SHOCKM 55  
SHOCKM 56  
SHOCKM 57

SHOCKM 2  
SHOCKM 3  
SHOCKM 4  
SHOCKM 5  
SHOCKM 6  
SHOCKM 7  
SHOCKM 8  
SHOCKM 9  
SHOCKM 10  
SHOCKM 11  
SHOCKM 12  
SHOCKM 13  
SHOCKM 14  
SHOCKM 15  
SHOCKM 16  
SHOCKM 17  
SHOCKM 18  
SHOCKM 19  
SHOCKM 20  
SHOCKM 21  
SHOCKM 22  
SHOCKM 23  
SHOCKM 24  
SHOCKM 25  
SHOCKM 26  
SHOCKM 27  
SHOCKM 28  
SHOCKM 29  
SHOCKM 30  
SHOCKM 31  
SHOCKM 32  
SHOCKM 33  
SHOCKM 34  
SHOCKM 35  
SHOCKM 36  
SHOCKM 37  
SHOCKM 38  
SHOCKM 39  
SHOCKM 40  
SHOCKM 41  
SHOCKM 42  
SHOCKM 43  
SHOCKM 44  
SHOCKM 45  
SHOCKM 46  
SHOCKM 47  
SHOCKM 48  
SHOCKM 49  
SHOCKM 50  
SHOCKM 51  
SHOCKM 52  
SHOCKM 53  
SHOCKM 54  
SHOCKM 55  
SHOCKM 56  
SHOCKM 57

SHOCKM 2  
SHOCKM 3  
SHOCKM 4  
SHOCKM 5  
SHOCKM 6  
SHOCKM 7  
SHOCKM 8  
SHOCKM 9  
SHOCKM 10  
SHOCKM 11  
SHOCKM 12  
SHOCKM 13  
SHOCKM 14  
SHOCKM 15  
SHOCKM 16  
SHOCKM 17  
SHOCKM 18  
SHOCKM 19  
SHOCKM 20  
SHOCKM 21  
SHOCKM 22  
SHOCKM 23  
SHOCKM 24  
SHOCKM 25  
SHOCKM 26  
SHOCKM 27  
SHOCKM 28  
SHOCKM 29  
SHOCKM 30  
SHOCKM 31  
SHOCKM 32  
SHOCKM 33  
SHOCKM 34  
SHOCKM 35  
SHOCKM 36  
SHOCKM 37  
SHOCKM 38  
SHOCKM 39  
SHOCKM 40  
SHOCKM 41  
SHOCKM 42  
SHOCKM 43  
SHOCKM 44  
SHOCKM 45  
SHOCKM 46  
SHOCKM 47  
SHOCKM 48  
SHOCKM 49  
SHOCKM 50  
SHOCKM 51  
SHOCKM 52  
SHOCKM 53  
SHOCKM 54  
SHOCKM 55  
SHOCKM 56  
SHOCKM 57

SHOCKM 2  
SHOCKM 3  
SHOCKM 4  
SHOCKM 5  
SHOCKM 6  
SHOCKM 7  
SHOCKM 8  
SHOCKM 9  
SHOCKM 10  
SHOCKM 11  
SHOCKM 12  
SHOCKM 13  
SHOCKM 14  
SHOCKM 15  
SHOCKM 16  
SHOCKM 17  
SHOCKM 18  
SHOCKM 19  
SHOCKM 20  
SHOCKM 21  
SHOCKM 22  
SHOCKM 23  
SHOCKM 24  
SHOCKM 25  
SHOCKM 26  
SHOCKM 27  
SHOCKM 28  
SHOCKM 29  
SHOCKM 30  
SHOCKM 31  
SHOCKM 32  
SHOCKM 33  
SHOCKM 34  
SHOCKM 35  
SHOCKM 36  
SHOCKM 37  
SHOCKM 38  
SHOCKM 39  
SHOCKM 40  
SHOCKM 41  
SHOCKM 42  
SHOCKM 43  
SHOCKM 44  
SHOCKM 45  
SHOCKM 46  
SHOCKM 47  
SHOCKM 48  
SHOCKM 49  
SHOCKM 50  
SHOCKM 51  
SHOCKM 52  
SHOCKM 53  
SHOCKM 54  
SHOCKM 55  
SHOCKM 56  
SHOCKM 57

## REFERENCES

1. Spreiter, J. R. and Jones, W. P.: On the Effect of a Weak Interplanetary Magnetic Field on the Interaction Between the Solar Wind and the Geomagnetic Field. *Jour. Geophys. Res.*, vol. 68, 1963, pp. 3555-3564.
2. Spreiter, J. R., Alksne, A. Y., and Summers, A. L.: Hydromagnetic Flow Around the Magnetopause. *Plan. & Space Sci.*, vol. 14, 1966, pp. 223-253.
3. Spreiter, J. R., Alksne, A. Y., and Summers, A. L.: External Aerodynamics of the Magnetosphere. Physics of the Magnetosphere (Ed. R. L. Carovillano, J. F. McClay, and H. R. Radoski), D. Reidel Pub. Co., 1968, pp. 304-378 (also NASA TN 4482, 1968).
4. Spreiter, J. R. and Alksne, A. Y.: Plasma Flow Around the Magnetosphere. *Rev. Geophys.*, vol. 7, 1969, pp. 11-50.
5. Spreiter, J. R., Summers, A. L., and Rizzi, A. W.: Solar Wind Flow Past Nonmagnetic Planets - Venus and Mars. *Plan. & Space Sci.*, vol. 18, 1970, pp. 1281-1289.
6. Spreiter, J. R. and Alksne, A. Y.: Solar Wind Flow Past Objects in the Solar System. *Ann. Rev. Fluid Mech.*, vol. 2, pp. 313-354 (Ed. W. R. Sears, M. D. Van Dyke, and W. G. Vincenti), Annual Review, Inc., Palo Alto, CA, 1970.
7. Spreiter, J. R., March, C. M., Summers, A.: Hydromagnetic Aspects of Solar Wind Flow Past the Moon. *Cosmic Electrodynamics*, vol. 1, no. 1, 1970, pp. 5-50.
8. Spreiter, J. R. and Rizzi, A. W.: Aligned Magneto-hydrodynamics Solution for Solar Wind Flow Past the Earth's Magnetosphere. *Acta Astronautica*, vol. 1, 1974, pp. 15-35.
9. Briggs, B. R. and Spreiter, J. R.: Theoretical Determination of the Boundary and Distortion of the Geomagnetic Field in a Steady Solar Wind. NASA TR R-178, 1963.
10. Chapman, S. and Ferraro, V. C. A.: An Outline of a Theory of Magnetic Storms. *Terrest. Magnetism Atmospheric Elec.*, vol. 36, 1931, pp. 77-97, 171-186.
11. Midgley, J. E. and Davis, Jr., L.: Calculation by a Moment Technique of the Perturbation of the Geomagnetic Field by the Solar Wind. *Jour. Geophys. Res.*, vol. 68, 1963, pp. 5111-5123.
12. Mead, G. D. and Beard, D. B.: Shape of the Geomagnetic Field Solar Wind Boundary. *Jour. Geophys. Res.*, vol. 69, 1964, pp. 1169-1179.
13. Olsen, W. P.: The Shape of the Titled Magnetopause. *Jour. Geophys. Res.*, Vol. 74, 1969, pp. 5642-5651.

14. Beard, D. B.: The Interaction of the Terrestrial Magnetic Field with the Solar Corpuscular Radiation. Jour. Geophy. Res., vol. 65, 1960, pp. 3559-3568.
15. Spreiter, J. R. and Briggs, B. R.: Theoretical Determination of the Form of the Hollow Produced in the Solar Corpuscular Stream by Interaction with the Magnetic Dipole Field of the Earth. NASA TR R-120, 1961.
16. Spreiter, J. R. and Briggs, B. R.: Theoretical Determination of the Form of the Boundary of the Solar Corpuscular Stream Produced by Interaction with the Magnetic Dipole Field of the Earth. Jour. Geophys. Res., vol. 67, no. 1, Jan. 1962, pp. 37-51.
17. Spreiter, J. R. and Briggs, B. R.: On the Choice of Condition to Apply at the Boundary of the Geomagnetic Field in the Steady-State Chapman-Ferraro Problem. Jour. Geophys. Res., vol. 67, no. 7, Jul. 1962, pp. 2983-2985.
18. Davis, Jr., L. and Beard, D. B.: A Correction to the Approximate Condition for Locating the Boundary Between a Magnetic Field and a Plasma. Jour. Geophys. Res., vol. 67, 1962, pp. 4505-4507.
19. Spreiter, J. R. and Summers, A. L.: On Conditions Near the Neutral Points on the Magnetosphere Boundary. Plan. & Space Sci., vol. 15, 1967, pp. 787-798.
20. Kuhn, G. D., Goodwin, F. K., and Perkins, Jr., S. C.: User's Manual for Space-Shuttle Computer Programs. NEAR TR 110, Apr. 1976.
21. Chaussee, D. S., Stahara, S. S., and Spreiter, J. R.: Application of an Axisymmetric Implicit Blunt Body Procedure: Computation of Solar Wind Flows Past Terrestrial Planets. AIAA Paper No. 77-700, Jun. 1977.
22. Beam, R. M. and Warming, R. F.: An Implicit Finite-Difference Algorithm for Hyperbolic Systems in Conservation-Law Form. J. Comp. Phys., vol. 22, no. 1, Sep. 1976.
23. Kutler, P., Reinhardt, W. A., and Warming, R. F.: Multi-Shocked, Three-Dimensional Supersonic Flow Fields with Real Gas Effects. AIAA Journal, vol. 11, May 1973, pp. 657-664.
24. Kutler, P., Reinhardt, W. A., and Warming, R. F.: Numerical Computations of Multi-Shocked Three-Dimensional Supersonic Flow Fields with Real Gas Effects. AIAA Paper No. 72-702, Jun. 1972.
25. Chaussee, D. S., Holtz, T., and Kutler, P.: Inviscid Supersonic/Hypersonic Body Flow Fields and Aerodynamics from Shock-Capturing Technique Calculations. AIAA Paper No. 75-837, Jun. 1975.
26. MacCormack, R. W.: The Effect of Viscosity in Hypervelocity Impact Cratering. AIAA Paper No. 69-354, 1969.
27. Alksne, A. Y. and Webster, D. L.: Magnetic and Electric Fields in the Magnetosheath. Plan. & Space Sci., vol. 18, 1970, pp. 1203-1212.

28. Grad, H.: Reducible Problems in Magneto-Fluid Dynamics Steady Flows. Rev. Mod. Phys., vol. 32, 1960, pp. 830-847.
29. Imai, I.: On Flows of Conducting Fluids Past Bodies. Rev. Mod. Phys., vol. 32, 1960, pp. 992-999.
30. Inouye, M. and Lomax, H.: Comparison of Experimental and Numerical Results for the Flow of a Perfect Gas About Blunt-Nosed Bodies. NASA TD-1426, Sep. 1962.





$\beta$	MAGNETO PAUSE		IONO PAUSE		IONO PAUSE		IONO PAUSE	
	Equatorial Trace		$H/R_0 = 0.01$		$H/R_0 = 0.1$		$H/R_0 = 0.2$	
	$x/D$	$Y_m/D$	$x/R_0$	$Y_1/R_0$	$x/R_0$	$Y_1/R_0$	$x/R_0$	$Y_1/R_0$
78°	0.2580	1.2138	0.2134	1.0041	0.2419	1.1382	0.2614	1.2298
82°	0.1772	1.2610	0.1435	1.0212	0.1650	1.1737	0.1796	1.2777
86°	0.0913	1.3060	0.0723	1.0345	0.0843	1.2062	0.0925	1.3232
90°	0.0	1.3491	0.0	1.0442	0.0	1.2356	0.0	1.3661
94°	-0.0972	1.3900	-0.0735	1.0507	-0.0882	1.2620	-0.0983	1.4065
98°	-0.2008	1.4289	-0.1482	1.0547	-0.1806	1.2854	-0.2029	1.4441
102°	-0.3115	1.4656	-0.2246	1.0568	-0.2776	1.3058	-0.3143	1.4788
106°	-0.4302	1.5002	-0.3033	1.0577	-0.3795	1.3233	-0.4332	1.5106
110°	-0.5578	1.5327	-0.3851	1.0580	-0.4870	1.3380	-0.5603	1.5394
114°	-0.6959	1.5630	-0.4711	1.0581	-0.6011	1.3501	-0.6968	1.5651
118°	-0.8461	1.5913	-0.5626	1.0581	-0.7230	1.3598	-0.8442	1.5877
122°	-0.0107	1.6175	-0.6612	1.0581	-0.8543	1.3672	-1.0043	1.6072
126°	-1.1927	1.6416	-0.7688	1.0581	-0.9973	1.3727	-1.1797	1.6237
130°	-1.3961	1.6638	-0.8879	1.0581	-1.1550	1.3765	-1.3737	1.6371
134°	-1.6262	1.6840	-1.0218	1.0581	-1.3317	1.3790	-1.5911	1.6476
138°	-1.8905	1.7022	-1.1752	1.0581	-1.5332	1.3805	-1.8387	1.6555
142°	-2.1997	1.7186	-1.3544	1.0581	-1.7679	1.3812	-2.1261	1.6611
146°	-2.5696	1.7332	-1.5688	1.0581	-2.0483	1.3816	-2.4679	1.6646
150°	-3.0242	1.7460	-1.8328	1.0581	-2.3932	1.3817	-2.8866	1.6666
154°	-3.6026	1.7571	-2.1695	1.0581	-2.8330	1.3817	-3.4189	1.6675
							$x/R_0$	$Y_1/R_0$
							$x/R_0$	$Y_1/R_0$
							$x/R_0$	$Y_1/R_0$
							$x/R_0$	$Y_1/R_0$
							$x/R_0$	$Y_1/R_0$
							$x/R_0$	$Y_1/R_0$
							$x/R_0$	$Y_1/R_0$
							$x/R_0$	$Y_1/R_0$
							$x/R_0$	$Y_1/R_0$
							$x/R_0$	$Y_1/R_0$
							$x/R_0$	$Y_1/R_0$
							$x/R_0$	$Y_1/R_0$

Table 1 (Continued)

$\beta$	MAGNETOPAUSE		IONOPAUSE		IONOPAUSE		IONOPAUSE			
	$x/D$	$y_m/D$	$x/R_0$	$y_i/R_0$	$x/R_0$	$y_i/R_0$	$x/R_0$	$y_i/R_0$		
	Equatorial Trace		$H/R_0 = 0.01$		$H/R_0 = 0.1$		$H/R_0 = 0.2$		$H/R_0 = 0.5$	
$158^\circ$	-4.3723	1.7665	-2.6190	1.0581	-3.4199	1.3817	-4.1281	1.6678	-5.9779	2.4152
$162^\circ$	-5.4608	1.7743	-3.2567	1.0582	-4.2526	1.3817	-5.1333	1.6679	-7.4439	2.4187
$166^\circ$	-7.1412	1.7805	-4.2440	1.0582	-5.5419	1.3817	-6.6897	1.6679	-9.7048	2.4197
$170^\circ$	-10.1239	1.7851	-6.0011	1.0582	-7.8363	1.3818	-9.4594	1.6679	-13.7235	2.4198
$174^\circ$	-17.0135	1.7882	-10.0678	1.0582	-13.1466	1.3818	-15.8695	1.6680	-23.0232	2.4198

Table 1 (Concluded)

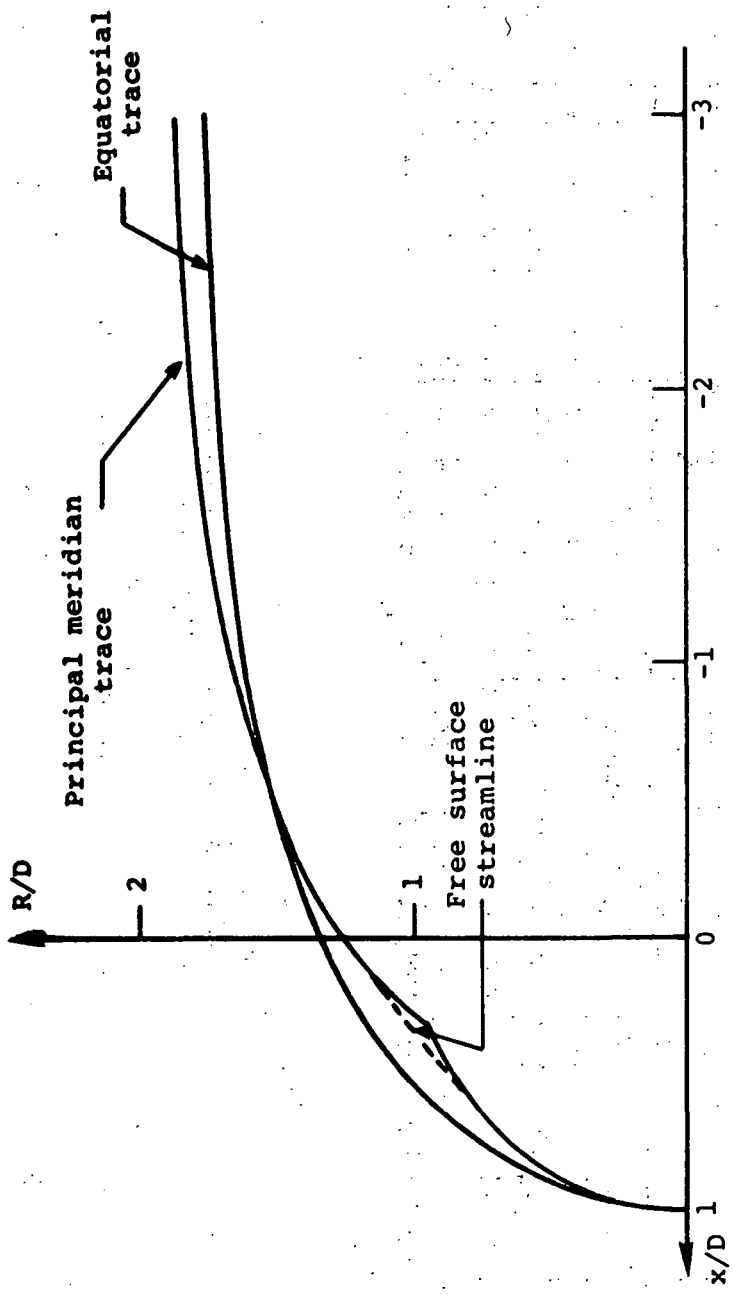


Figure 1. - Comparison of the equatorial and principal meridian traces of the magnetosphere boundary as provided by the simplified theory of equation 16.

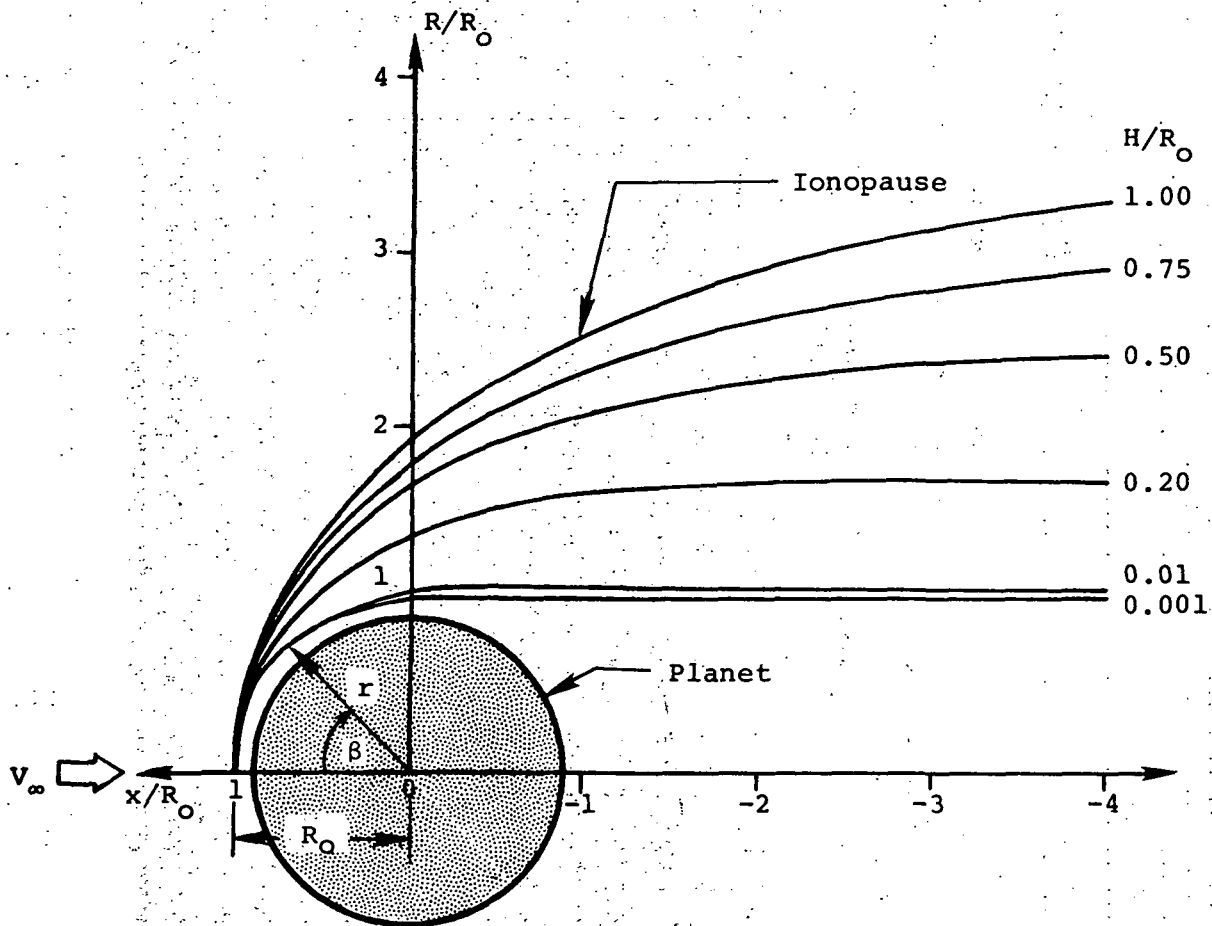


Figure 2. - Illustration of ionopause shapes for various values of the ionosphere scale height to shock standoff distance ratio  $H/R_0$ .

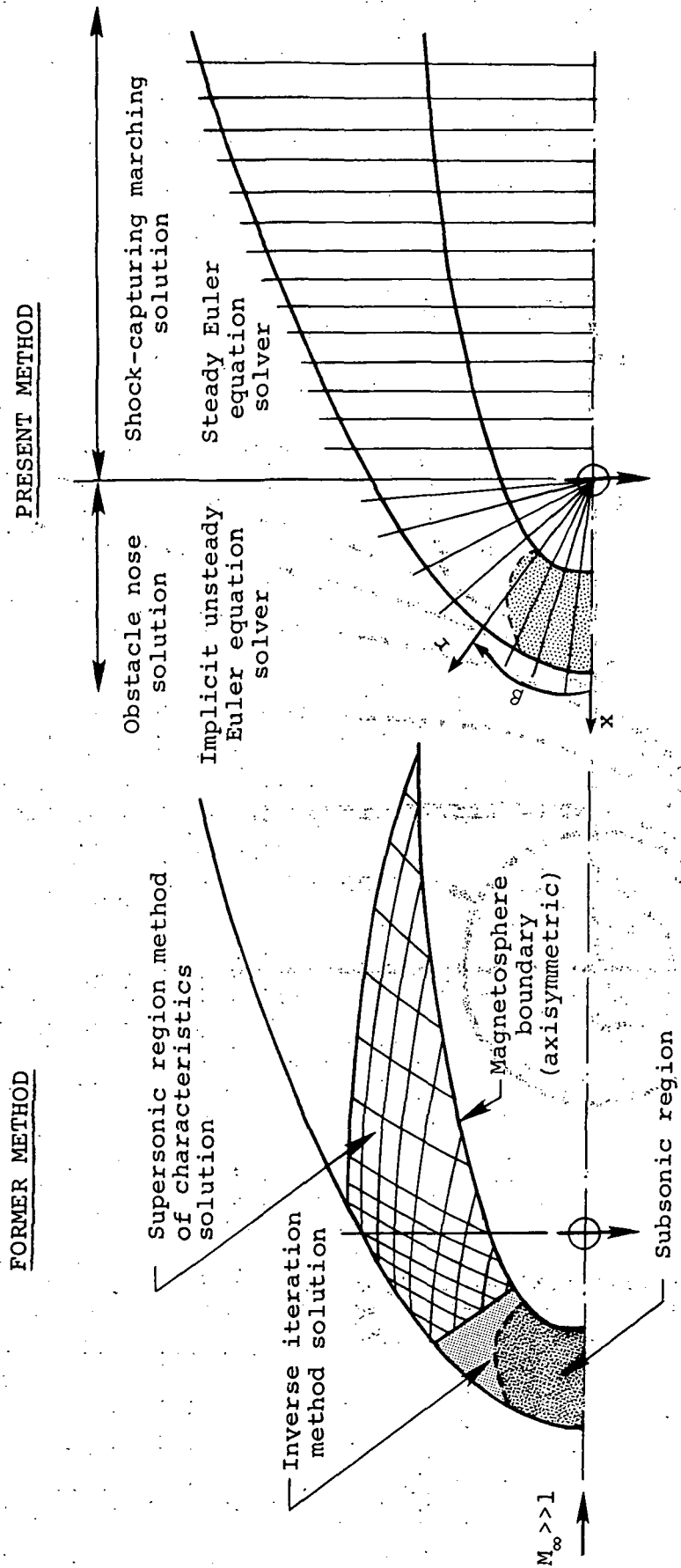


Figure 3 - Comparison of former and present computational procedures for determining the gasdynamic flow properties of solar wind-magneto/ionopause interactions.

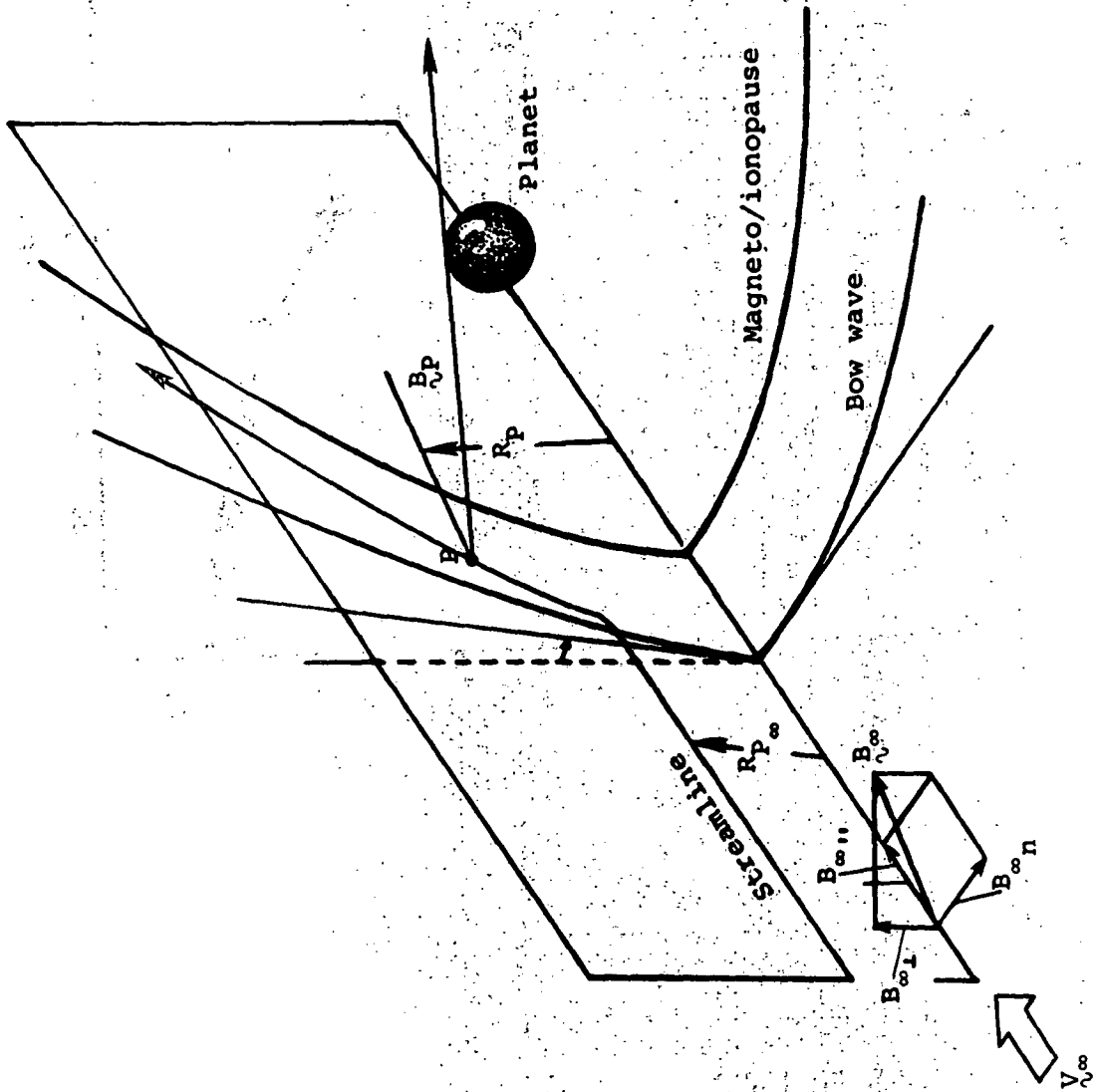
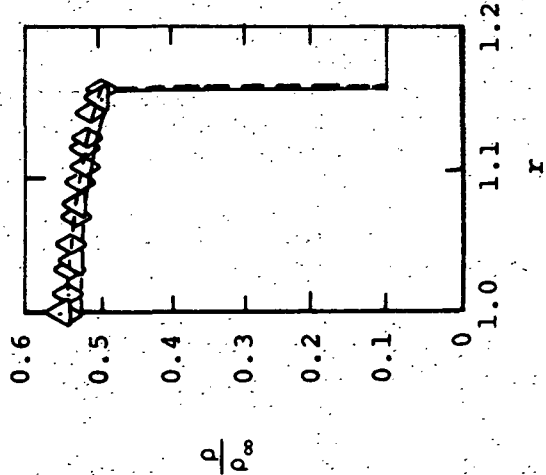
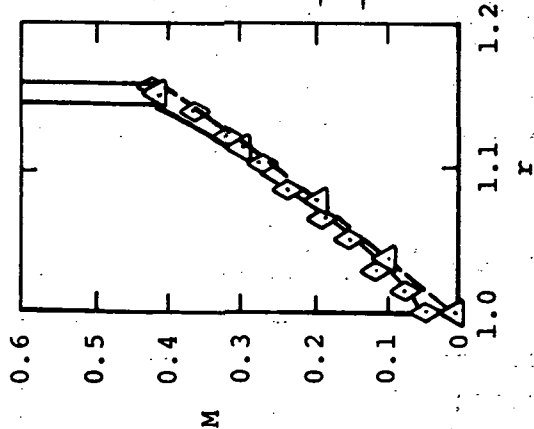


Figure 4. - Illustration of the components of the three-dimensional magnetic field.



$\gamma = 1.4$   $M_\infty = 4.926$

SPHERE

- ◇ Implicit
- Experiment (Xerikos & Anderson)
- Finite volume
- Explicit (Moretti)
- △ Explicit (Barnwell)
- Explicit (Chaussee)

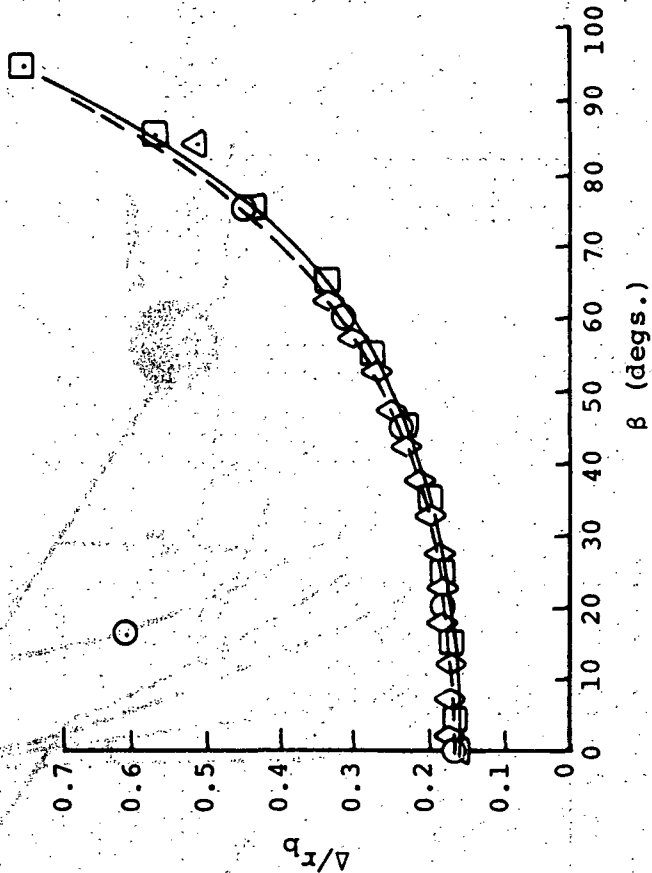
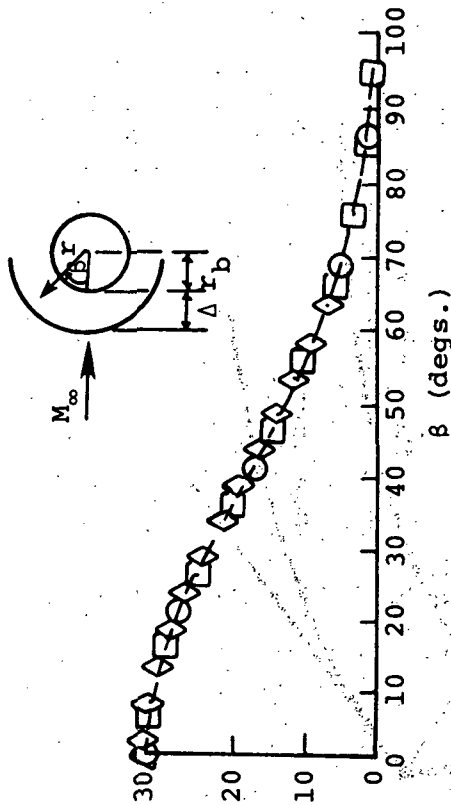
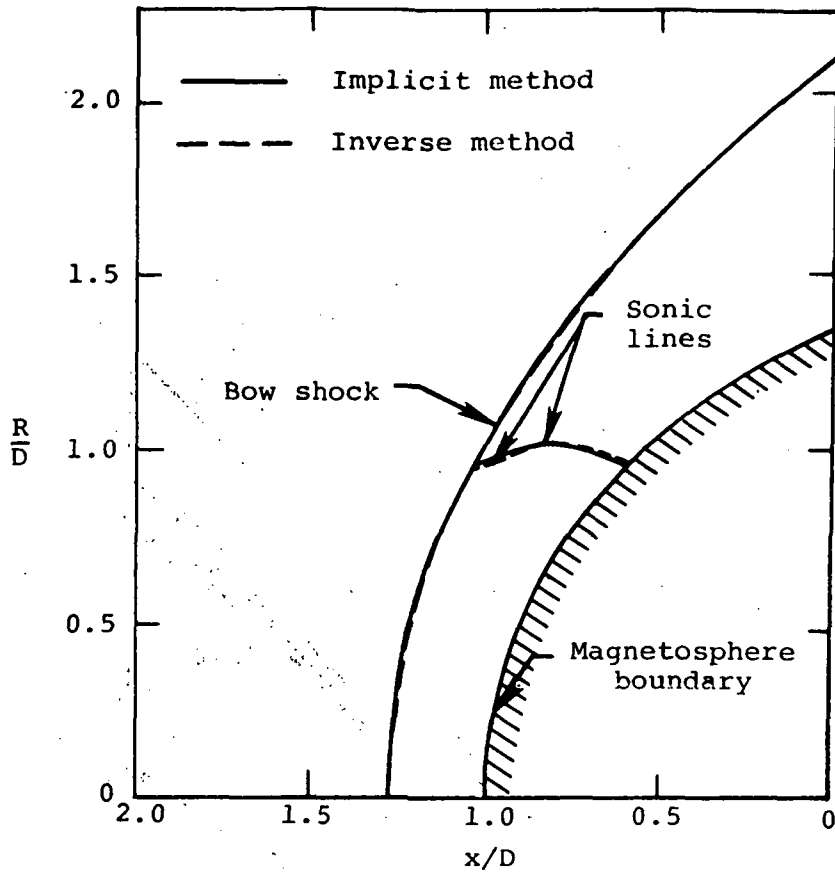
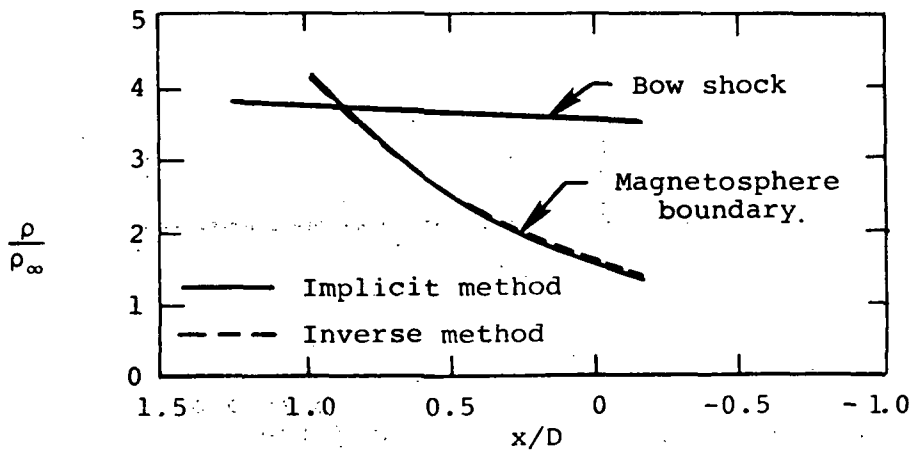


Figure 5. - Comparison of flow properties predicted by the present implicit method with other techniques and experiment for supersonic flow past a sphere;  $M_\infty = 4.926$ ,  $\gamma = 1.4$ .





(a) Shock shape and sonic line location.



(b) Density distribution.

Figure 6. - Comparison of implicit and inverse methods for shock shape and sonic line location, and density distribution along bow shock and magnetosphere boundary for  $M_\infty = 8$ ,  $\gamma = 5/3$  flow past the rotated equatorial trace of the magnetopause.

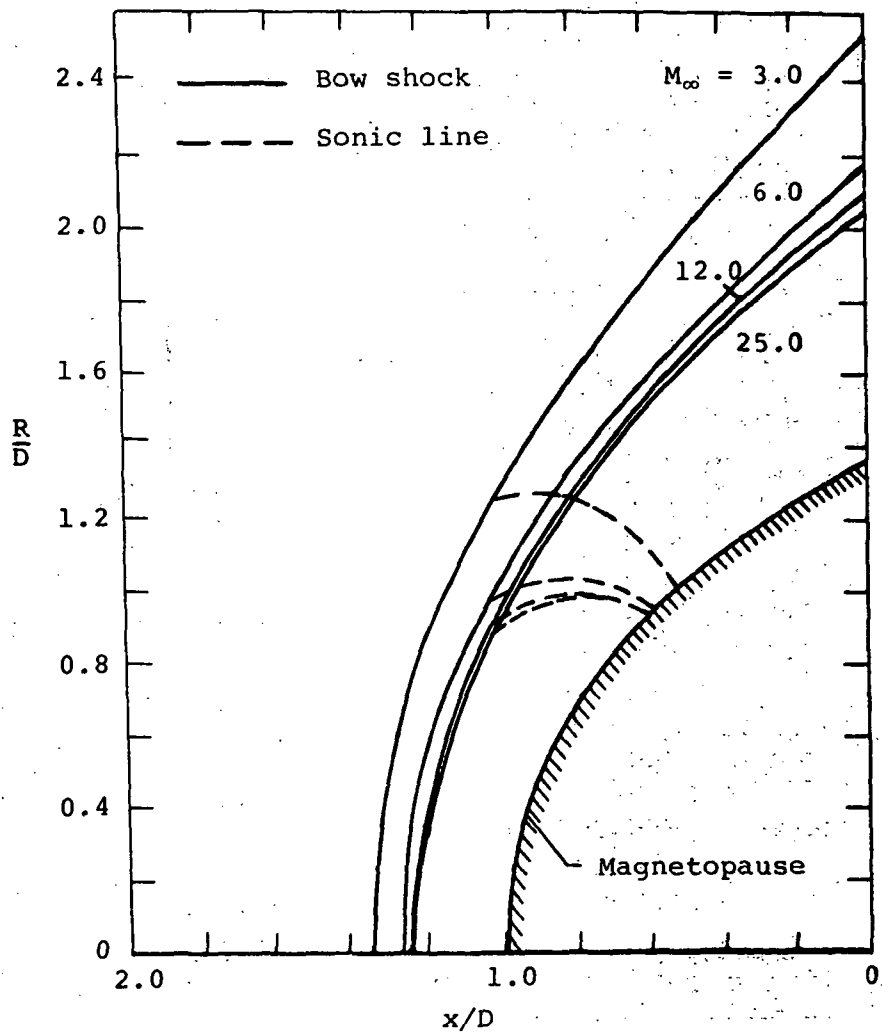


Figure 7. - Bow wave and sonic line locations for various supersonic flows past the rotated equatorial trace of the magnetopause with  $\gamma = 5/3$ .

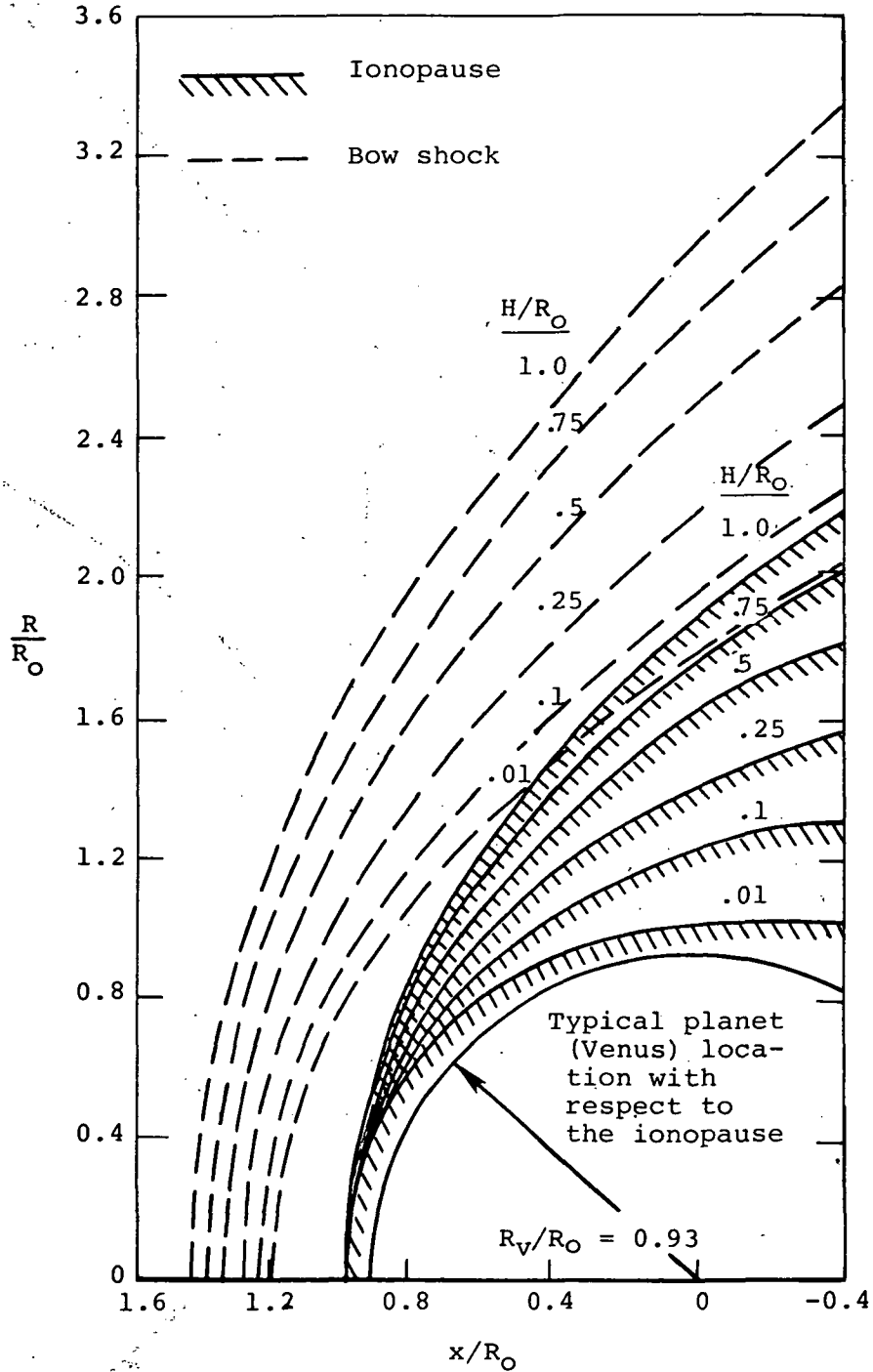


Figure 8. - Bow shock location for solar wind flow with  $M_\infty = 8$ ,  $\gamma = 5/3$  past various ionopause shapes.

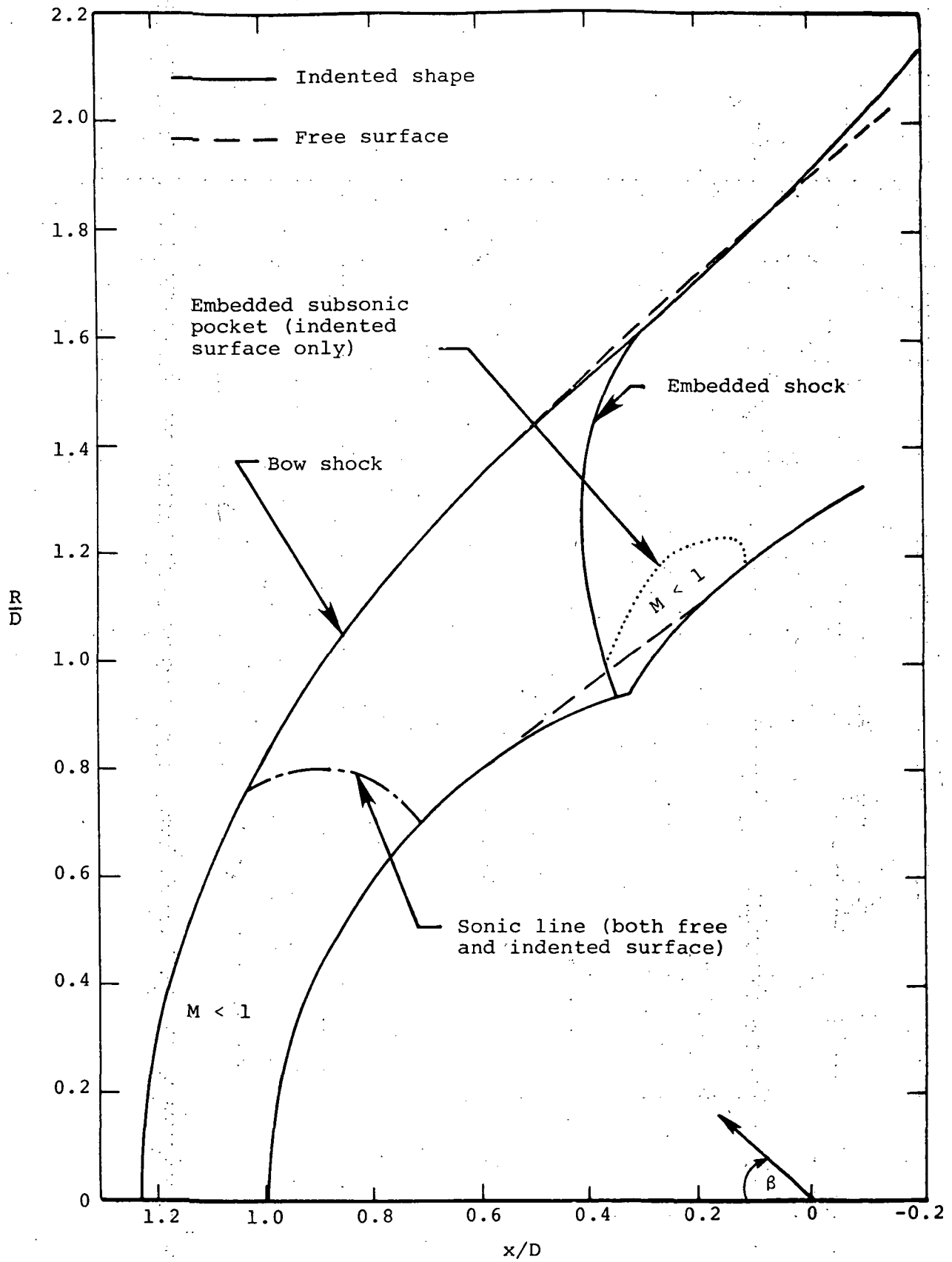


Figure 9. - Bow shock and embedded shock locations for solar wind flow with  $M_\infty = 5$ ,  $\gamma = 5/3$  past the rotated principal meridian of the magnetosphere.

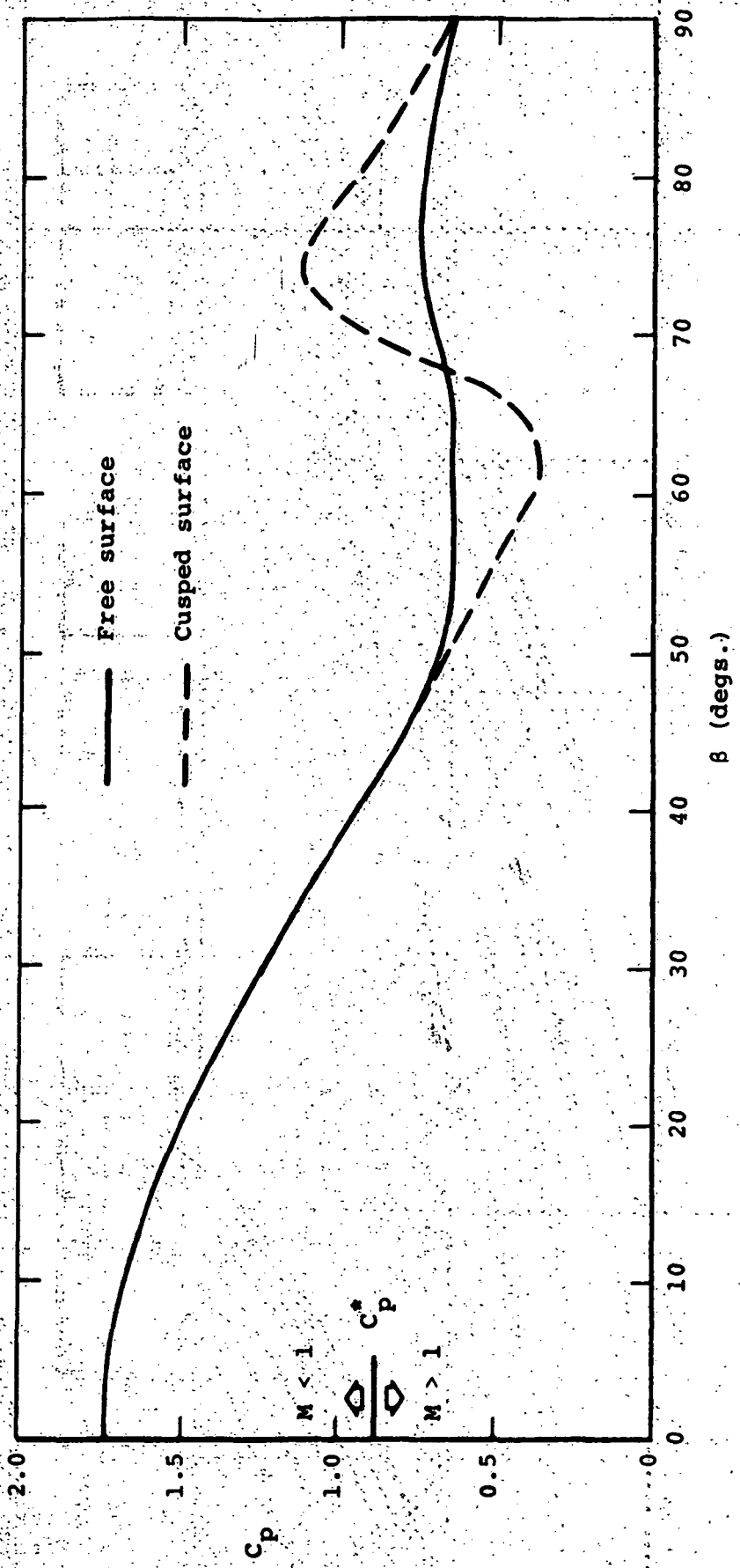
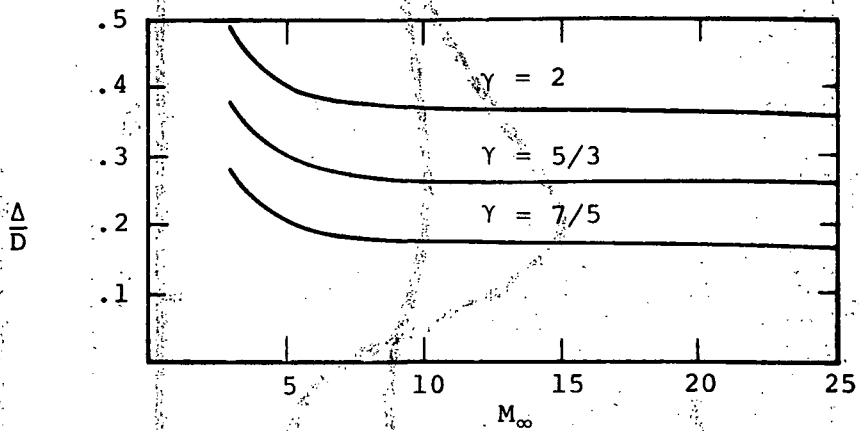
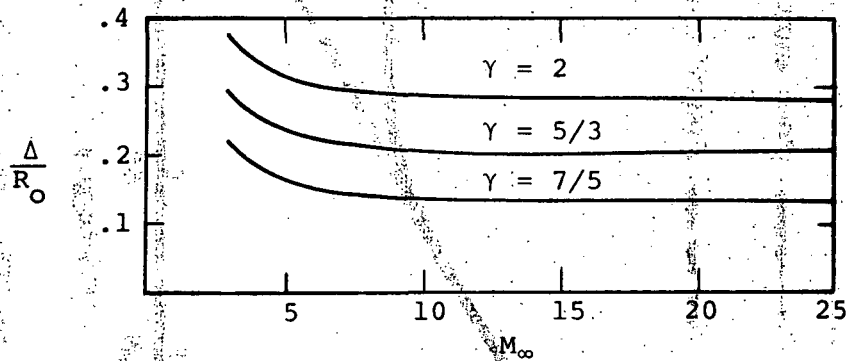


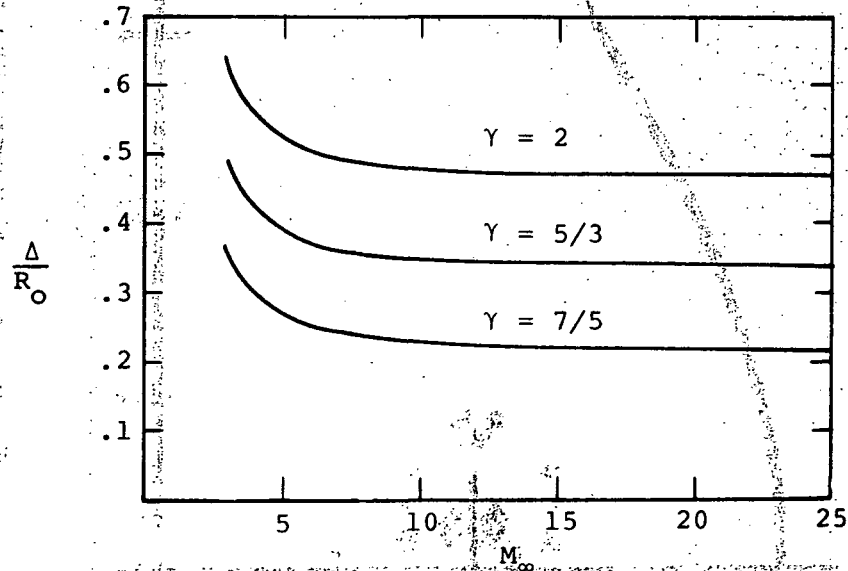
Figure 10. - Magnetopause pressure coefficients for the principal meridian magnetopause shapes shown in figure 9.



(a) Magnetopause equatorial trace



(b) Ionopause trace -  $H/R_0 = .01$



(c) Ionopause trace -  $H/R_0 = .5$

Figure 11. - Variation of shock stand-off distance with oncoming Mach number and ratio of specific heats for various magneto/ionopause traces as determined by the present implicit procedure.

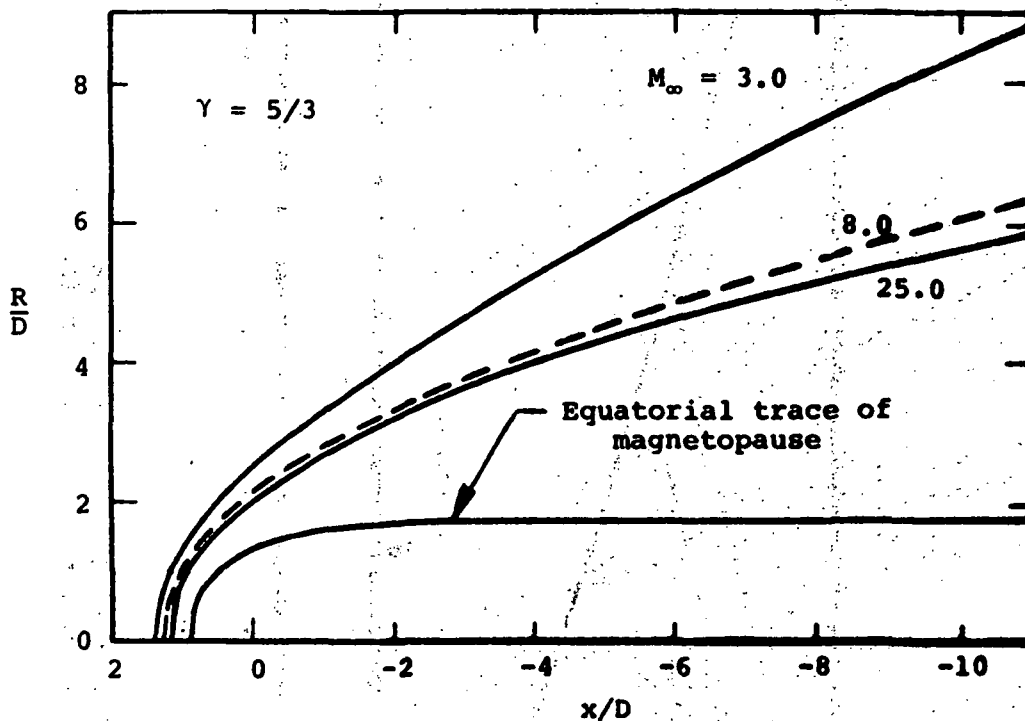


Figure 12. - Shock shapes for various supersonic flows past the rotated equatorial trace of the magnetopause; combined near (blunt body) and far (marching) solutions.

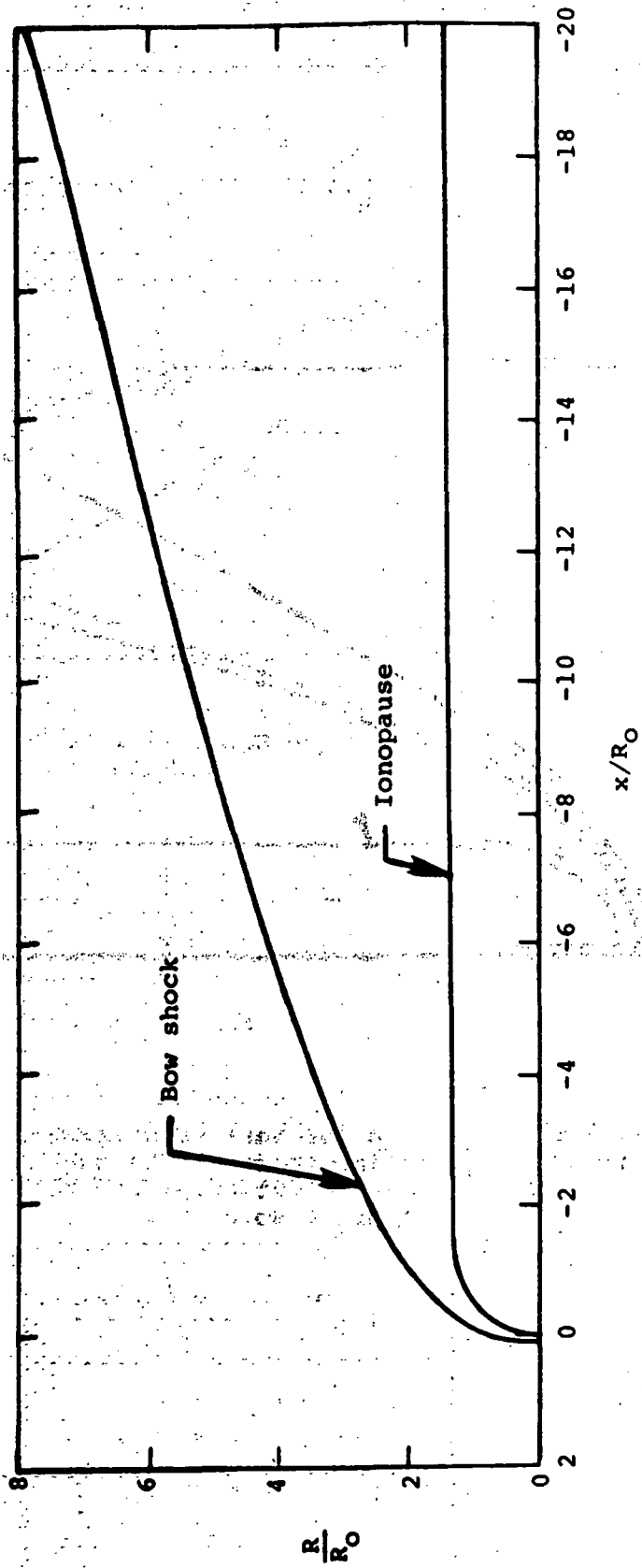
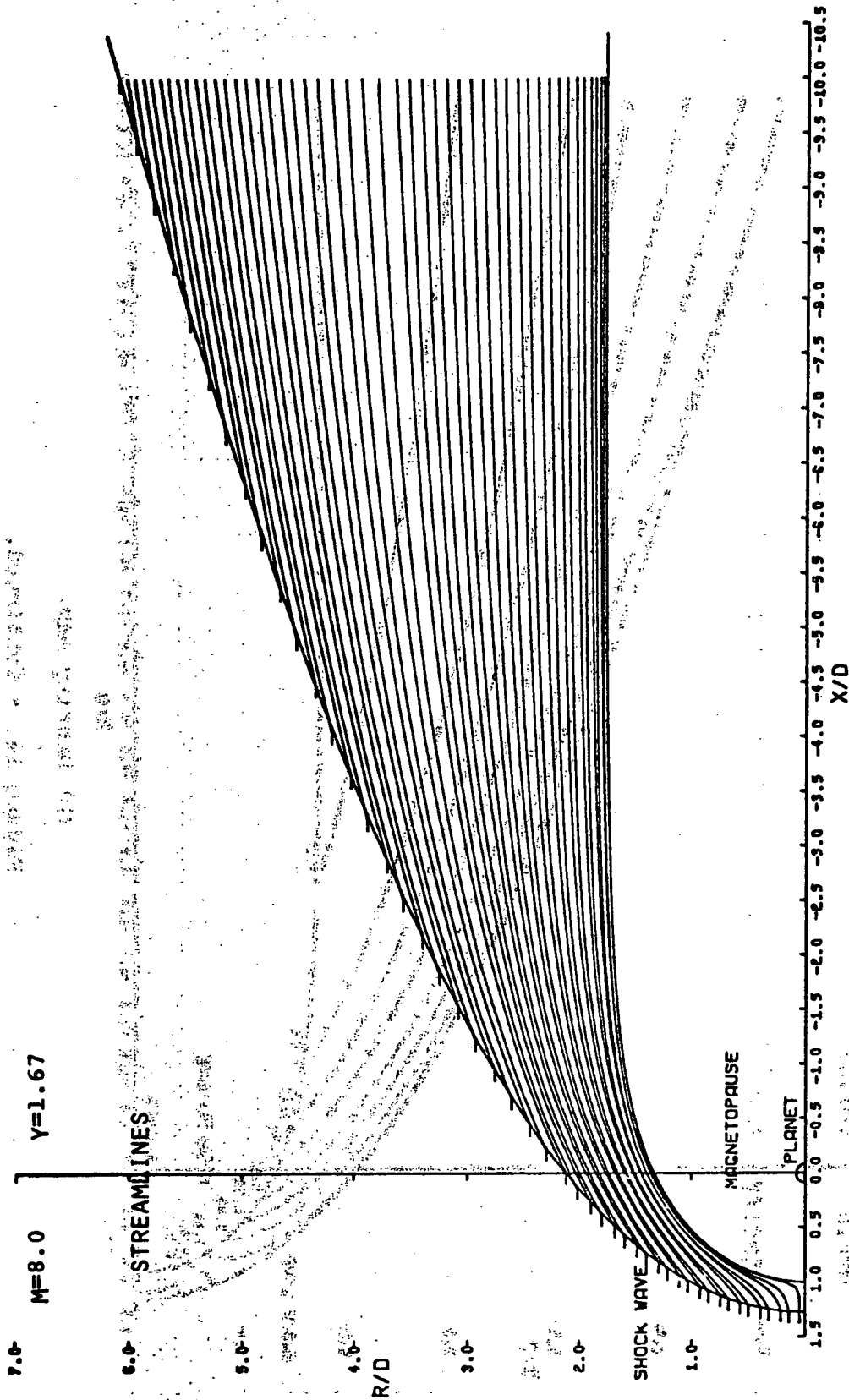


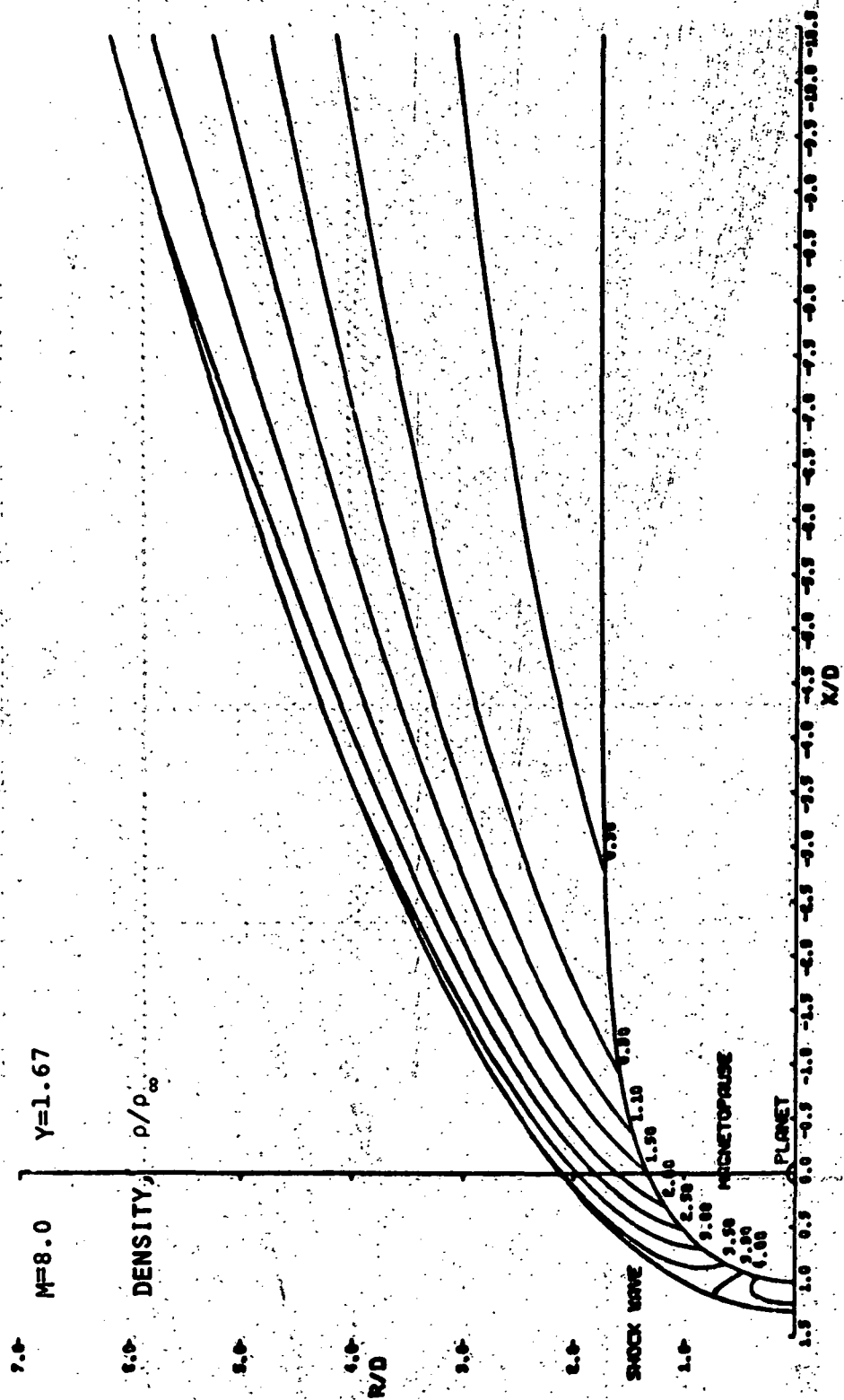
Figure 13. - Shock shape for  $M_\infty = 8$ ,  $\gamma = 5/3$  flow past an ionopause shape with  $H/R_0 = 0.1$ ; combined near (blunt body) and far (marching) field solutions.





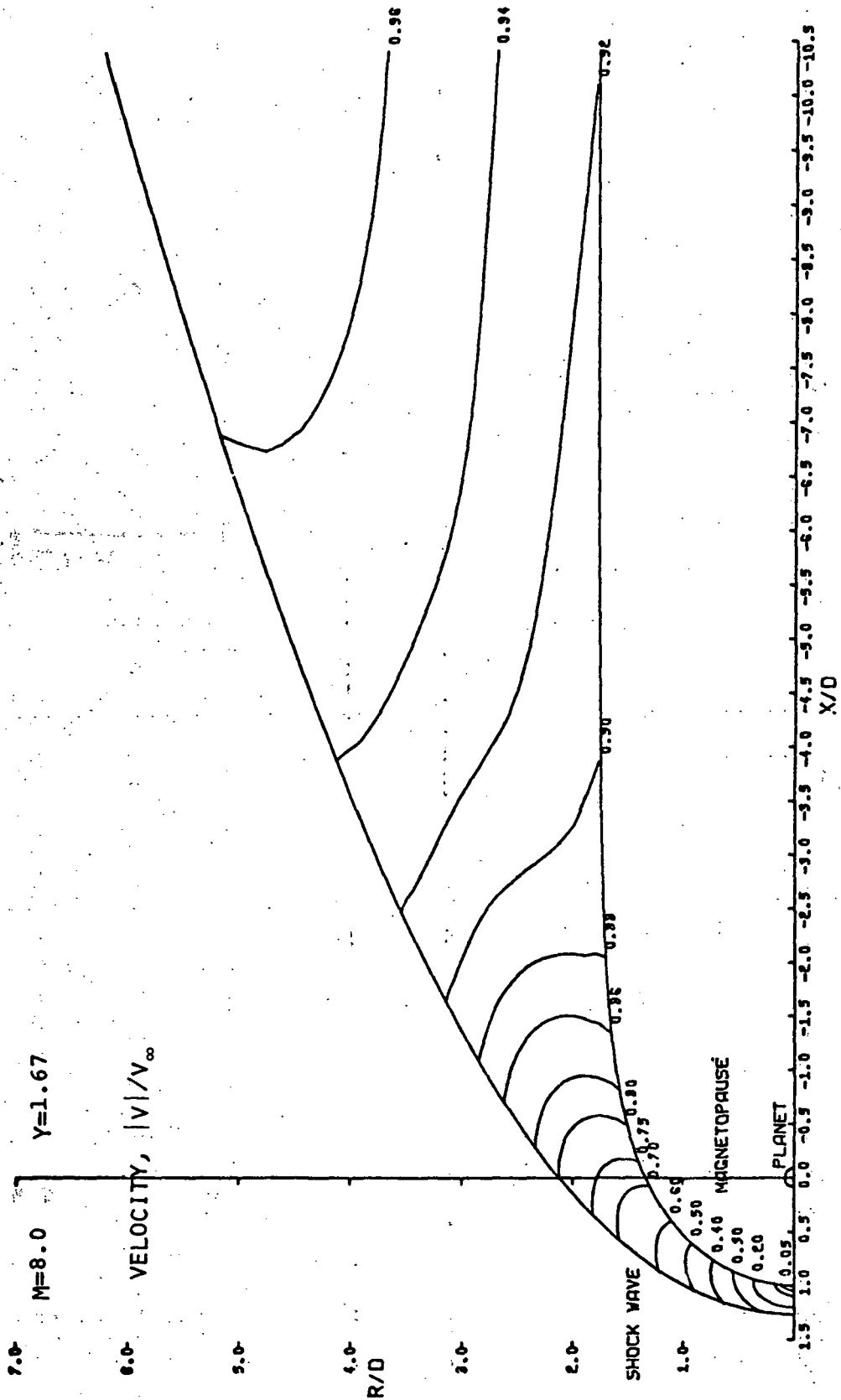
(a) Streamline Map.

Figure 14. - Streamline, density, and velocity maps for  $M_{\infty} = 8.0$ ,  $\gamma = 5/3$  flow past the rotated equatorial trace of the magnetopause; combined blunt body and marching flow field.



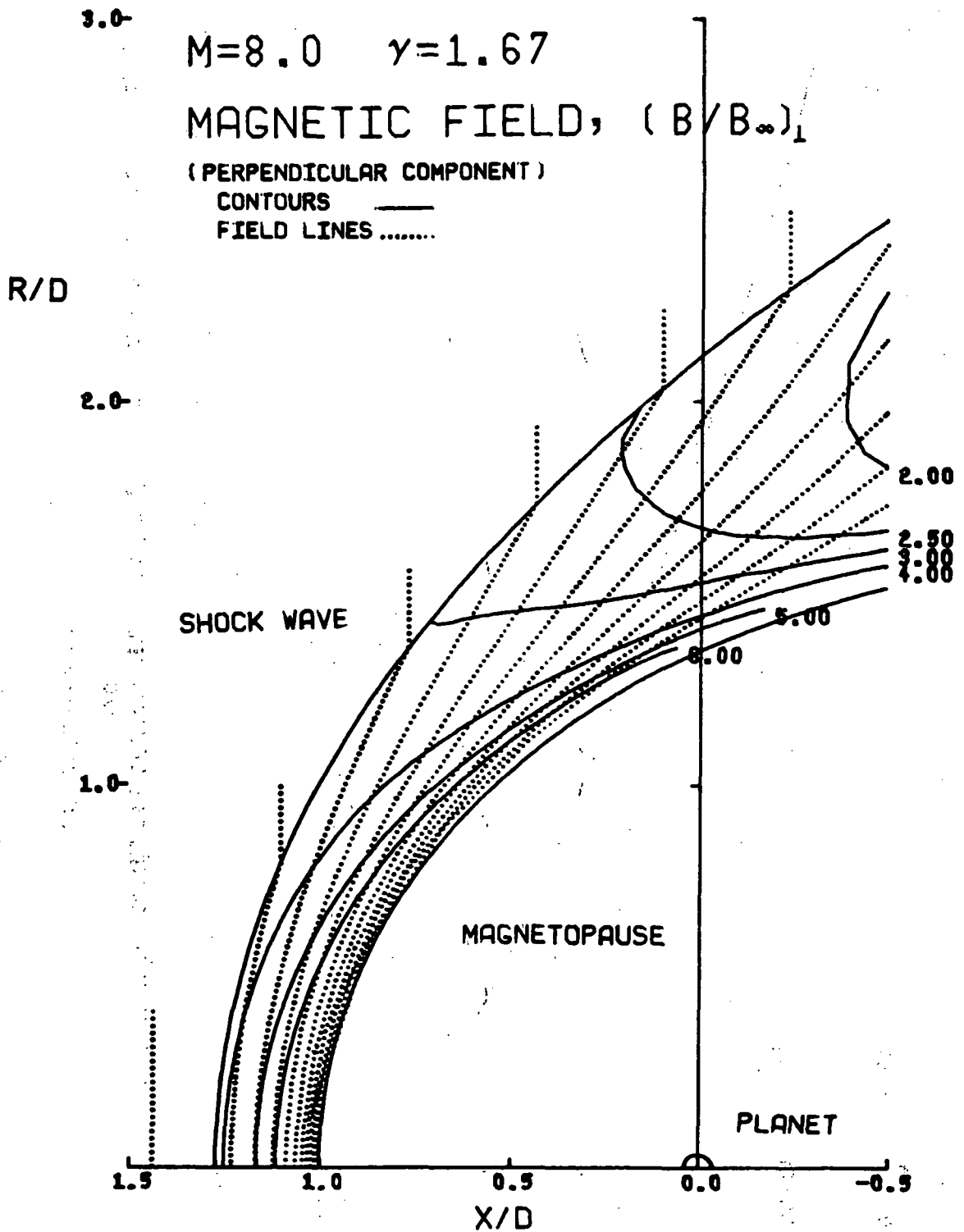
(b) Density map.

Figure 14. - Continued.



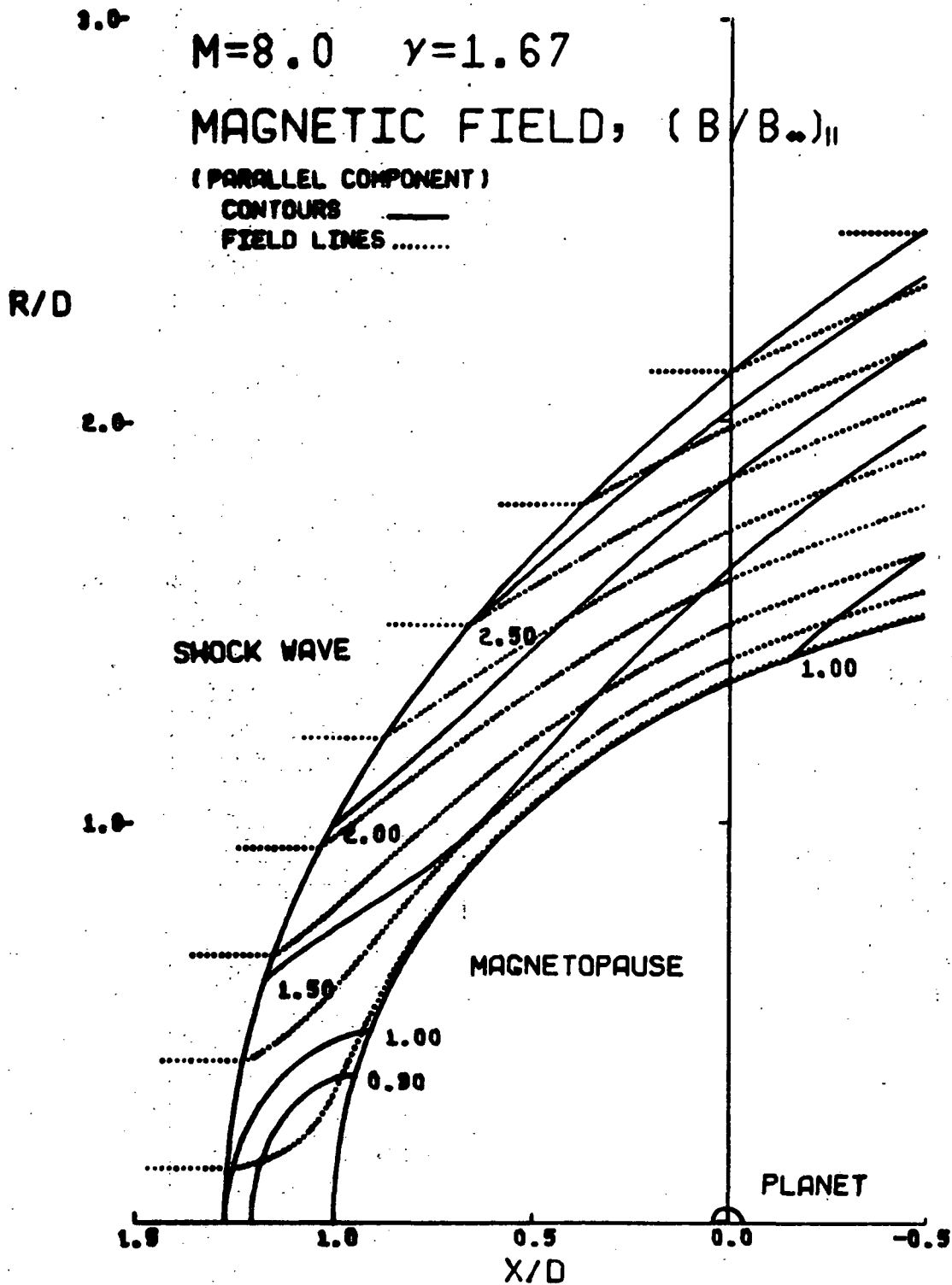
(c) Velocity map.

Figure 14. - Concluded.



(a) Perpendicular component  $(B/B_\infty)_\perp$

Figure 15. - Contours and field line locations of the in-plane magnetic field components  $(B/B_\infty)_\perp$  and  $(B/B_\infty)_\parallel$  for  $M_\infty = 8$  and  $\gamma = 5/3$  flow past the rotated equatorial trace of the magnetopause.



(b) Parallel component  $(B/B_\infty)_\parallel$

Figure 15. - Concluded.

National Aeronautics and  
Space Administration

Washington, D.C.  
20546

Official Business

Penalty for Private Use, \$300

THIRD-CLASS BULK RATE

Postage and Fees Paid  
National Aeronautics and  
Space Administration  
NASA-451



**NASA**

POSTMASTER: If Undeliverable (Section 158  
Postal Manual) Do Not Return

---